

---

---

BIOMECHANICAL STUDY OF THE  
MECHANICAL AND STRUCTURAL  
PROPERTIES OF ADHERENT CELLS

---

---

A THESIS SUBMITTED TO THE UNIVERSITY OF SHEFFIELD IN PARTIAL  
FULFILMENT OF THE REQUIREMENTS FOR THE DEGREE OF

DOCTOR IN PHILOSOPHY

MECHANICAL ENGINEERING  
UNIVERSITY OF SHEFFIELD  
MAY 2013

SARA BARRETO, M.Sc.

SUPERVISOR

PROF. DAMIEN LACROIX

CO-SUPERVISOR

DR. CÉCILE M. PERRAULT

*External examiner:*

Dr. J. Patrick MCGARRY

*Internal examiner:*

Dr. Gwendolen REILLY



## Acknowledgements

I would like to thank those who contributed to the achievement of this thesis for my doctorate degree.

First and foremost I would like to acknowledge my supervisor, Damien, for his continuous support and guidance during the course of this research work. Also for the dedication to my work and for giving me the opportunity to take part in a new direction on modelling cell mechanics research, previously unexplored within the group. I am also grateful for Damien's encouragement for participating in so many different conferences, collaborations, summer schools and networking around the world that made my PhD program one of the best experiences one can have.

My deepest gratitude to Cécile for co-supervising my work and for her scientific and personal advice in many situations. I am also grateful to Cécile for sharing her passion for the experimental work and for the dynamics in participating in different scientific activities.

I will be forever grateful to Dan for his enthusiasm to motivate me, for showing me I can always explore new fields on this journey of science and for co-supporting my research in his lab at Berkeley.

I would like to thank the institutions and members that welcomed me during my PhD program: the Institute for Bioengineering of Catalonia, directed by Prof. Josep Planell, and the Technical University of Catalonia (UPC) where I first started and spent most of my PhD; the Fletcher Lab and the University of California at Berkeley, where I did an internship and learned experimental cell mechanics; and finally the University of Sheffield and the Insigneo group, where I finished my PhD.

I am grateful to all the members of the previous Biomechanics and mechanobiology group for the good environment conducive for research, especially

to Clara for her patience and friendship, Andrea for his continuous Abaqus advice, computational support and humor, Andy for his kindness, Jerome for his professionalism and criticism that helped to improve my work, and Aura for the positive energy.

I would like to thank all the members of Fletcher Lab for their welcoming receptions and for engaging intellectual discussions with very interesting points of view on cell mechanics and in "how to make science". A special thank to Casper for being there during the long hours of good and bad experiments with the AFM and for sharing not only his knowledge but also his Danish dark humor.

I am grateful to all the members of the research group in Sheffield and Insigneo. I am especially thankful to Hanifeh in research, for the encouragement during the period of writing the thesis, as well as for her unconditional friendship.

Friends are always a very important part of my life and I am thankful for the understanding and support of my lifelong friends.

Lastly, I am incredibly thankful for the support of my family. Especially to *mãe*, *pai* and João, always with uplifting words and acts of encouragement. You are the best of me.

To my *avó*. Thank you for your smile, thank you for your laugh and for your tears every time I left. Thank you for your words that I will never forget. Thank you for your never-ending love.

**I gratefully acknowledge the financial support from Fundação para a Ciência e Tecnologia (FCT) Portugal under Grant No.**

**[SFRH/BD/47264/2008]**

## Publications and presentations resulting from this study

### *Scientific journals*

S. Barreto, C. H. Clausen, C. M. Perrault, D. A. Fletcher, D. Lacroix, *A multi-structural single cell model of force-induced interactions of cytoskeletal components*, DOI: 10.1016/J. Biomaterials, 2013, 04.022

### *Oral presentations in conferences*

H. Khayyeri, S.Barreto, D. Lacroix, *A computational investigation of the mechanism behind cell mechanosensation*, Bioengineering in Ireland19, Co. Meath - Irland,18-19 January, 2013

S. Barreto, C. M. Perrault, D. A. Fletcher, D.Lacroix, *Prestress controls forces of adherent cells and it is dependent on the extracellular tissue stiffness*, 8th European Solid Mechanics Conference, Graz - Austria, 9-13 July 2012

S. Barreto, C. M. Perrault, D. Lacroix, *Effect of the cytoskeleton fibers and substrate rigidity on adherent cells*, 18th Congress of the European Society of Biomechanics (ESB2012), Lisbon - Portugal, 1-4 July 2012

S. Barreto, C. M. Perrault, D. A. Fletcher, D. Lacroix, *Computational prediction of external and internal cell forces-regulation by the individual fibers of the cytoskeleton*, Computer Methods in Biomechanics and Biomedical Engineering, Berlin - Germany, April 2012

S. Barreto, C. M. Perrault, D. Lacroix, *Contribution of individual CSK elements for the elastic response of cell*, I Reunión del capítulo español de la Sociedad Europea de Biomecánica, Zaragoza - Spain, 10 November 2011

S. Barreto, C. M. Perrault, D. Lacroix, *Modelling the mechanical response of a single cell in magnetic twisting cytometry: contribution of the cytoskeleton filaments*, 6th World Congress on Biomechanics, Singapore, 1-6 August 2010

S. Barreto, C. M. Perrault, D. Lacroix, *Modelling the mechanical response of a single cell in magnetic twisting cytometry*, 3rd IBEC Symposium on Bio-engineering and Nanomedicine, Barcelona - Spain, 1 -2 June 2010

***Poster presentations in conferences***

S. Barreto, C.H. Clausen, C.M. Perrault, D.A. Fletcher and D. Lacroix, *A multi-structural mechanical model of the cytoskeleton - changes in cellular mechanical properties following cortical and deep cytoskeleton components disruption*, 2012 Annual Meeting of The American Society for Cell Biology, San Francisco - USA, 15-19 December 2012

S. Barreto, C. M. Perrault, D. Lacroix, *Modeling the interaction of actin bundles and microtubules during stretching*, Cell Mech, Amsterdam - Holand, 17-19 October 2011

## Abstract

A cell is a biological complex system and its understanding requires a combination of various approaches including biomechanics. Like engineering materials, cells deform when external forces act on them. There is evidence that many normal and diseased conditions of cells are dependent on, or regulated by the way cells mechanically interact with the environment.

A major interest in cell mechanics is the regulation of cellular function by mechanical forces, which is determined by the composition and structures of cells. While the exact structural mechanisms involved in force transmission inside the cells are not well understood, computational cell modelling can yield important insights. This may contribute to build up a structure-function relationship of different adherent cell types. One approach to studying the mechanosensing processes is to understand the mechanical properties of cells' constitutive components individually.

For this purpose, a representative 3D finite element model of a single adherent cell was developed based on the internal structures of the cytoskeleton that provide the cells with their mechanical properties. The results indicate which cytoskeleton components are targeted to respond to specific loading conditions, such as compression and stretching. More specifically, actin cortex and microtubules are targeted to respond to compressive loads, while actin bundles and microtubules are major components in maintaining cell forces during stretching.

This approach clarifies the effects of cytoskeletal heterogeneity and regional variations on the interpretation of force-deformation measurements. With a sensitivity study of the material properties of the different cellular components, the model shows how these properties differ to define cell rigidity across different cell types. Cell force is mainly affected by changes in cortex

thickness, cortex Young's modulus and rigidity of the cytoplasm. Changes in rigidity of actin bundles and number of microtubules influence cell response to shear loads, while the number of actin bundles deeper in the interior of the cell, affect cell response to compression.

The time dependent responses observed following a power-law are remarkably similar to those reported for a variety of measurements with atomic force microscopy, suggesting this model is a consensus description of the fundamental principles defining cell mechanics. Simulations of the dynamic response of a single cell suggest that the origin of different force-relaxation times is linked to the structural architecture of the cell. The results also suggest that it is important to consider the viscoelastic properties of the cortex, other than the cytoplasm, to properly define the time-dependent response of the cell to compressive loads.

The FE single-cell model includes the three parameters defining the fundamental principles defining cell mechanics: rigidity, prestress and time-dependence deformation following a power-law behaviour. This thesis contributes to understand the mechanical interaction and properties across different cell components, responsible for cell behaviour, that will ultimately lead to functional adaptation or pathological conditions.

# Contents

<b>List of Figures</b>	<b>i</b>
<b>List of Tables</b>	<b>v</b>
<b>Nomenclature</b>	<b>vi</b>
<b>1 Introduction</b>	<b>1</b>
1.1 General background . . . . .	1
1.2 Mechanobiology - The motivation . . . . .	4
1.3 Modelling cell mechanics . . . . .	8
1.4 Author's thesis . . . . .	10
<b>2 Literature Review</b>	<b>13</b>
2.1 Introduction . . . . .	13
2.2 The cell and cytoskeletal structures . . . . .	14
2.3 Cell mechanical behaviour . . . . .	22
2.3.1 Methods for measuring cell mechanics . . . . .	22
2.3.2 Active methods . . . . .	25
2.3.3 Power-law rheology . . . . .	30
2.3.4 Stiffness, prestress and power-law . . . . .	36
2.3.5 Stiffening and fluidisation . . . . .	38

2.3.6	Cytoskeleton disruption . . . . .	40
2.4	Models to describe cell behaviour . . . . .	43
2.4.1	Models for suspended cells . . . . .	44
2.4.2	Models of cytoskeletal networks . . . . .	45
2.4.3	Finite element models . . . . .	50
2.4.4	Models for CSK dynamics . . . . .	55
2.5	Conclusions . . . . .	59
<b>3</b>	<b>Finite element model for a single adherent cell</b>	<b>62</b>
3.1	Introduction . . . . .	62
3.2	Material and methods . . . . .	66
3.2.1	Finite element single-cell model . . . . .	66
3.2.2	Material properties . . . . .	69
3.2.3	Loads and boundary conditions . . . . .	74
3.2.4	Finite element simulations . . . . .	76
3.3	Results . . . . .	77
3.3.1	Mesh-independence of the results . . . . .	77
3.3.2	Prediction of cell deformation . . . . .	79
3.3.3	Distribution of forces in the cell . . . . .	81
3.3.4	Cell contractility . . . . .	81
3.3.5	Sensitivity study . . . . .	86
3.4	Discussion . . . . .	88
3.4.1	The cell model concept . . . . .	88
3.4.2	Prestress in actin bundles . . . . .	91
3.4.3	Relationship between deformation, force and focal ad- hesions . . . . .	92
3.4.4	How cells sense and respond to different mechanical stimuli . . . . .	96

3.4.5	Main conclusions . . . . .	97
<b>4</b>	<b>Effect of cytoskeletal disruption on force transmission</b>	<b>99</b>
4.1	Introduction . . . . .	99
4.2	Material and methods . . . . .	102
4.2.1	Numerical approach . . . . .	102
4.2.2	Cell culture and drug treatment . . . . .	103
4.2.3	Indentation experiments with atomic force microscopy . . . . .	104
4.2.4	Data analysis for Young's modulus measurement . . . . .	105
4.2.5	Immunofluorescence staining and imaging . . . . .	107
4.2.6	Numerical predictions for small indentations . . . . .	109
4.3	Results . . . . .	109
4.3.1	Corroboration of the numerical results with AFM . . . . .	109
4.3.2	Role of the components of the CSK . . . . .	112
4.3.3	In the range of small forces . . . . .	114
4.3.4	Force-induced changes in U2OS actin structure . . . . .	114
4.3.5	AFM measurements and imaging of living cells . . . . .	117
4.3.6	Comparison between numerical results and AFM measurements . . . . .	122
4.4	Discussion . . . . .	123
4.4.1	Force-induced changes in the actin structure of living cells . . . . .	123
4.4.2	Mechanical stimuli regulate CSK components' activation to resist external forces . . . . .	124
4.4.3	Mechanical role of actin cortex, and other actin and microtubules networks in compression . . . . .	125
4.4.4	Mechanical role of actin cortex and deep actin and microtubules networks in stretching . . . . .	130

4.4.5	Main conclusions . . . . .	131
<b>5</b>	<b>Sensitivity analysis to explain cell mechanics variability</b>	<b>133</b>
5.1	Introduction . . . . .	133
5.2	Methods . . . . .	136
5.2.1	Parametrical analysis of the cellular components . . . . .	136
5.2.2	Measuring mechanical parameters in living cells . . . . .	137
5.3	Results . . . . .	139
5.3.1	Numerical analysis of the properties of the cellular components . . . . .	139
5.3.2	Relationship between rigidity and spreading area of cells	144
5.4	Discussion . . . . .	148
5.4.1	Main conclusions . . . . .	153
<b>6</b>	<b>Computational investigation of power-law behaviour in adherent cells</b>	<b>155</b>
6.1	Introduction . . . . .	155
6.2	Materials and methods . . . . .	158
6.2.1	Power-law behaviour . . . . .	158
6.2.2	Numerical implementation of viscoelasticity . . . . .	159
6.2.3	Force-relaxation and equilibration time analysis . . . . .	159
6.3	Results . . . . .	161
6.3.1	Finite element analysis of whole cell strain and force-relaxation curves . . . . .	161
6.3.2	Effect of loading and instantaneous modulus on viscoelastic response . . . . .	164
6.3.3	Distance-dependence force propagation . . . . .	166
6.4	Discussion . . . . .	171

6.4.1	The parameters affecting power-law behaviour in the finite element analysis . . . . .	171
6.4.2	Viscoelastic properties for different indentation positions	175
6.4.3	Main conclusions . . . . .	176
<b>7</b>	<b>Discussion</b>	<b>178</b>
7.1	General discussion . . . . .	178
7.2	Limitations . . . . .	182
7.2.1	Computational limitations . . . . .	182
7.2.2	Experimental limitations . . . . .	186
<b>8</b>	<b>Conclusive remarks</b>	<b>189</b>
8.1	Main results and contributions . . . . .	189
8.2	Future prospects . . . . .	192
	<b>Bibliography</b>	<b>196</b>
	<b>Appendices</b>	<b>225</b>
<b>A</b>	<b>Subroutine to calculate prestress</b>	<b>225</b>
<b>B</b>	<b>Subroutine to calculate major principal strains</b>	<b>227</b>

# List of Figures

2.1	Structure of an eukaryotic cell (Alberts et al., 2002).	15
2.2	Muscle contraction	19
2.3	Experimental techniques and related biological events for the different force and displacement ranges (adapted from Sunyer (2008)).	23
2.4	Experimental techniques to probe cell and molecular mechanics (Vaziri & Gopinath, 2008).	24
2.5	Power-law creep response (Kollmannsberger & Fabry, 2011).	33
2.6	The creep response of a cell: a time course of cell deformation produced by a constant applied stress (Stamenović, 2006).	37
2.7	Cell rheology is related with prestress (Stamenovic et al., 2004).	39
2.8	A comparison of the frequency dependence of several cell rheology experiments (Hoffman & Crocker, 2009).	41
2.9	Tensegrity structures.	48
2.10	FE models based on tensegrity.	54
3.1	FE model of a single cell.	66
3.2	Confocal images of microtubules staining of human mesenchymal stem cells.	69

3.3	Projections of actin bundles and microtubules distribution in the cell model with respect to the nucleus. . . . .	70
3.4	Methods to calculate tension in actin bundles of endothelial cells from their level of pre-existing strain, using glass needle manipulation (Deguchi et al, 2005). . . . .	72
3.5	Stress-strain relationship defining the mechanical behaviour of actin bundles with and without prestrained conditions. . . . .	73
3.6	Loading conditions applied to the model cell for the simulations of compression followed by stretching. . . . .	74
3.7	Different bead positions for indentation on the top of the cell. . . . .	77
3.8	Mesh-independence of the results using continuum hexahedral elements. . . . .	78
3.9	Deformation of the different cellular components. . . . .	80
3.10	Distribution of forces in the bottom part of the cell. . . . .	82
3.11	Effect of prestress on cell response. . . . .	83
3.12	Variation of prestrain in the actin bundles and the effect on cell contractility for compression and stretching. . . . .	84
3.13	Effect of variation of indentation depth on cell forces. . . . .	85
3.14	Effect of variation of amplitude of stretching on cell forces. . . . .	86
3.15	Cell force considering different indentation positions. . . . .	87
4.1	Phase-contrast image of the cantilever used in the AFM to indent the cells, using a bead on the top of the nucleus of each living single-cell. . . . .	106
4.2	Corroboration of the model comparing numerical and AFM force-indentation curves . . . . .	110
4.3	Statistical analysis of FE predictions and AFM force-indentation measurements for U2OS and 3T3 cells. . . . .	111

4.4	Contribution of each component of the cytoskeleton for the different stimuli, and effect of interaction between the elements of the cytoskeleton. . . . .	113
4.5	Cytoskeleton disruption for different small indentations. . . . .	115
4.6	Fluorescence images of U2OS GFP-actin structure before and after AFM indentation. . . . .	116
4.7	Young's modulus of 3T3 and U2OS cells before and after CSK disruption, calculated from AFM force measurements. . . . .	118
4.8	Actin structure of U2OS GFP-actin cells. . . . .	119
4.9	Fluorescence images of actin structures of NIH-3T3 fibroblasts	120
4.10	Overall Young's modulus and force obtained numerically and with AFM for cells with the same rigidity. . . . .	121
4.11	Mechanical role of actin filaments, microtubules and intermediates filaments on living adherent endothelial cells, (Wang, 1998). . . . .	131
5.1	Parametrical study of the mechanical properties of the continuum elements of the cell (cytoplasm and nucleus) for the effect in the overall reaction force of the cell. . . . .	140
5.2	Structural and spatial variation of actin bundles and microtubules. . . . .	142
5.3	Parametrical study of the mechanical properties of the continuum elements of the cell (cytoplasm and nucleus) for the effect in the overall cell reaction force. . . . .	143
5.4	Confidence ellipse of the correlation between Young's modulus and spreading area of NIH 3T3 cells. . . . .	145
5.5	Confidence ellipse of the correlation between Young's modulus and spreading area of U2OS cells. . . . .	146

5.6	Measurements of peripheral actin thickness from microscopic images of living 3T3 and U2OS cells. . . . .	147
6.1	Cross-sectional view of strain distribution in the cell over time.	162
6.2	Force-relaxation curves considering different PL exponents $\beta$ .	163
6.3	The effect of prestress in the force-relaxation curve considering $\beta = 0.2$ . . . . .	164
6.4	Force-relaxation curves considering variation of instantaneous moduli and indentation depths for PL exponent $\beta = 0.2$ . . . .	165
6.5	Cell forces for different PL exponents considering $t = 1$ s (which corresponds to the time for maximum indentation), and $t = 15$ s (which corresponds to the time of relaxation after indentation). . . . .	167
6.6	Force-relaxation curves for different bead positions. . . . .	168
6.7	Comparing force-relaxation curves for two bead positions considering different material properties of the cell components. .	170
6.8	Force-relaxation curves obtained at different loads, varying from 0.5 to 4nN, applied on the nuclear region of an MCF-7 cell by <a href="#">Moreno-Flores et al. (2010)</a> . . . . .	174

# List of Tables

3.1	Cell mesh properties in Abaqus . . . . .	67
3.2	Material properties . . . . .	71
5.1	Material properties affecting cell response . . . . .	144
6.1	Prony-series parameters for fitting power-law rheology model using Equation 6.1 . . . . .	160
6.2	Decrease in force after 15 s of compression . . . . .	163

# Nomenclature

<i>3D</i>	three-dimensional
<i>ABPs</i>	actin-binding proteins
<i>AFM</i>	atomic force microscopy
<i>Cyto – D</i>	cytochalasin-D
<i>CSK</i>	cytoskeleton
<i>DAPI</i>	4',6-diamidino-2-phenylindole fluorophore
<i>ECM</i>	extracellular matrix
<i>FAs</i>	focal adhesions
<i>FE</i>	finite element
<i>FITC</i>	fluorescein isothiocyanate
<i>GFP</i>	green fluorescent protein
<i>GWLC</i>	glassy worm-like chain model
<i>HASM</i>	human airway smooth muscle
<i>PL</i>	power-law
<i>MT</i>	microtubules
<i>MTC</i>	magnetic twisting cytometry
<i>Noc</i>	nocodazole
<i>SGMs</i>	soft glassy materials
<i>SGR</i>	soft glass rheology

*TRITC* tetramethyl rhodamine

*WLC* worm-like chain model

## INTRODUCTION

---

### 1.1 General background

History has often been defined based on the properties of materials of choice for a given era such as Stone, Bronze, Iron and Steel ages. The advancement of human civilisation was entangled with the characterisation of these materials, especially on the basis of their mechanical properties. Mechanics of materials is one of the oldest forms of engineering and applied sciences.

The living cell, a universe unto itself, can be seen as the most complex form of a material. Cells were first observed in the late 1600s by Antoni van Leeuwenhoek, a fabric merchant that polished glass to create single-lens microscopes capable to reveal the pores of a thin slice of cork, moving bacteria and a pattern of bands in muscle fibres ([Fletcher, 2010](#)). Observing living cells and their interactions with the surroundings was the first step to open the door into a new world that captures the interactions of cells with forces from the surrounding environments.

Within multicellular organisms, cells are constantly exposed to mechanical stresses, such as compression due to cells moving through tissues; tension transmitted through deformation of adherent cells or extracellular matrix (ECM); or shear stress, due to air or blood flow. Interestingly, cells respond

to these forces adjusting their shape, function and behaviour. Although cells have been mainly studied chemically, the concept of cell mechanics - physical forces existing within cells - and especially its relation to cell physiology, grew rapidly with the industrialisation during the nineteenth century (Seifriz, 1937; Thompson, 1917).

The industrial revolution was the basis for the understanding and development of several theories and experimental approaches such as indentation, beam bending or Kelvin, Maxwell and Hertz models, to test the mechanical and structural properties of materials. These theories were used for the development of new boats, bridges and buildings (Thompson, 1917). This new technological knowledge contributed to the first experimental analysis of cell and tissue mechanics using a variety of techniques based upon these macro-scale engineering mechanics. These theories are still currently applied for nano-scale testing and modelling of a diversity of biological materials, as it will be presented.

Cells were initially thought to be small compartments containing homogeneous gels, elastic, viscoelastic or plastic fluids. Later, the development of microscopic techniques, including dark field illumination, oil immersion lenses, high-quality glass optics and optical microscopy, as well as the advances in sample preparation, contributed to the observation of the nucleus, membrane filamentous structures and other cytoplasmic components of cells. These self-contained systems of a compartmentalised structural physiology enable cells to interact with other cells and with the external environment. During these interactions, cell physiology requires coordination of a complex biochemical and a diverse biomechanical environment. An interest on how the molecular structures and entire cells mechanically organise, to respond to physical forces from the environment, has been growing since then.

However, the active nature of cells, at the spatial and temporal domains, is still a challenge for researchers to reveal the complex nature of this structure. Sometimes forces acting on cells are local and temporal, whereas other times they are global and sustained (Fletcher, 2010). Precise quantitative mechanical measurements on single living cells became possible with the development of modern techniques in recent decades, such as magnetic tweezers, laser tweezers, atomic force microscopy (AFM), cell poking, microplates, and cell stretchers.

As the experimental findings on the mechanical properties of the cell become more complex, many theoretical models have been developed to describe cellular mechanics as either an elastic or viscoelastic continuum, a combination of discrete mechanical elements or a combination of viscoelastic fluid within a dense meshwork (Bao & Suresh, 2003; Huang et al., 2004; Ingber et al., 2000; Kasza et al., 2007). With these new theoretical and experimental tools, it is now possible to measure the mechanical properties of cells and alter the mechanical environment to predict their response to a specific type of force. This brought the opportunity to initiate and control biological pathways and predict the biological responses of cells that are associated with mechanical interactions. By complementing novel experimental techniques with robust computational approaches capable of modelling mechanical response at varying scales provides new avenues to understand cell mechanics and mechanobiology.

Therefore, studying the mechanics of human cells is important for two main reasons. Firstly, cells are continuously exposed to physical stresses and strains. These can arise from external physical forces acting on the body, or physiological environmental conditions occurring within the body, which can help determine health and function of the human body (Lim et al., 2006).

This triggered the curiosity of studying if forces work as important signals that relate with cell functionality. Secondly, biomechanical investigation can provide quantitative data on the changes in the physical properties of cells through the progression of certain human diseases. This has been driven by an increasing body of evidence suggesting that mechanical properties of cells, as well as their ability to sense and respond to mechanical signalling, are intricately linked to a myriad of biological functions ([Chicurel et al., 1998](#); [Hoffman & Crocker, 2009](#); [Zhu et al., 2000](#)).

## 1.2 Mechanobiology - The motivation

*“The mechanisms by which mechanical forces lead to eventual biochemical and molecular responses remain undefined, and unraveling this mystery will undoubtedly provide new insight into strengthening bone, growing cartilage, improving cardiac contractility, and constructing tissues for artificial organs.”* ([Huang et al., 2004](#))

To perform their specialised functions, cells must express genetic information, synthesise, modify, sort, store and transport biomolecules. Cells also convert different forms of energy, transduce signals, maintain internal structures and respond to external environments. Living cells possess structural and physical properties established by one or more components in the interior of the cell, that enable them to withstand the physiological environment and mechanical stimuli occurring in the body. This coupling between mechanical forces and biological processes is referred to as mechanobiology.

The response of cells to applied forces is divided into two parts: the first is a mechanical response consisting on the deformation of the cell's load-

bearing structures (Gardel et al., 2006; Janmey & Weitz, 2004; Kasza et al., 2007); and the second is the biochemical signalling response, which potentially leads to most force-induced phenotypic changes (Geiger & Bershadsky, 2002). This mechanism by which cells transform mechanical signals into biological responses is known as mechanotransduction. While the biochemistry of cells has been studied for many years, research on the molecular principles underlying cell mechanics and mechanotransduction is still taking place for the ultimate goal of understanding cells physiology. Therefore, deciphering the relationship between cellular activities and the structure of living cells is a key step towards understanding and predicting cell functions with direct implications for understanding human health and disease.

The structural components of the cell - the cytoskeleton (CSK) - are of protein origin and represent over 80% of cellular protein of some eukaryotic cells (Ramaekers & Bosman, 2004). The cytoskeleton is composed of hundreds of associated proteins organised into three major classes of filamentous proteins known as actin filaments, microtubules and intermediate filaments. These proteins form a highly complex network that provide a structural and dynamic natural organisation to the cell. The CSK is involved in the maintenance of cell shape and integrity and in generating movements of the whole cell, and of the intercellular components. Biochemical, and more recently, mechanical research of cytoskeletal properties have emerged and revolutionised the field of cell biology, with the accelerating awareness of complex interplay between cytoskeletal components and many cellular processes (Ramaekers & Bosman, 2004). Today many of these cellular processes, such as cell growth, differentiation, apoptosis, motility, signal transduction and gene expression are known to be driven by, and dependent upon, a mechanically intact cytoskeleton to maintain cell shape and structural integrity

(Galbraith & Sheetz, 1998; Geiger & Bershadsky, 2002; Ingber, 1993; Maniotis et al., 1997).

The structure of eukaryotic cells is controlled by a dynamic balance of mechanical forces. These forces are generated from intrinsic molecular components along with actively generated forces from cell-cell contact and cell-substrate adhesion, which are transmitted to the nucleus (Wang & Ingber, 1994) through the cytoskeleton. This balance of the mechanical forces leads to CSK remodelling and allows the cells to adapt to, and withstand new environments, to maintain their physiology. Loss of force transmission between the extracellular matrix, the cytoskeleton and the interior of the nucleus is implicated in loss of tissue homeostasis and is a hallmark of many mechanobiological diseases, including muscular dystrophies, cancer progression and metastases, and loss of hearing (Pajerowski et al., 2007; Tapley & Starr, 2013; Wang et al., 2009).

As an attempt to understand mechanotransduction for cell physiology, earlier studies were concentrated in cells of tissues with obvious structural roles, such as bone, cartilage, and skin where mechanical loading appears to be essential in maintaining normal function. Nonetheless, even cells from less mechanically dynamic tissues are exposed to force or tension generated locally by cell-cell or cell-ECM interactions, responding to physical stimuli that may reflect *in vivo* functions. In these cases, the force generated depends on the stiffness of the tissue in which the cells are embedded (Engler et al., 2006; Takai et al., 2005). The physical principles of cell mechanics and studies on the possible relationship between tissue elasticity and disease, have shown that specific cell properties are an important factor for differentiation of stem cells into specific tissues (Engler et al., 2006; Ingber, 2003a). Further development of mechanical concepts and hypotheses for stem cell

differentiation into different skeletal cells is an important step in the tissue engineering, cell therapy and regenerative medicine fields.

Application of mechanical forces on cells has shown to induce chemo-mechanical responses that can be related to control or alter gene expression and differentiation pathways (Charras & Horton, 2002a; Hamill & Martinac, 2001; Hoey et al., 2012; Huang et al., 2004). Clearly, a major challenge is defining precisely how mechanical forces result in biochemical signals. Experimental findings to date suggest that cells use many pathways, although a specific pathway may be dominant in a given circumstance, depending on cell type and mechanical loading condition (Huang et al., 2004). To fully understand changes in cell function one must first understand the fundamental mechanics of the cell.

*In vitro* cell culture studies are performed for the investigation of the effect of mechanical loading in cell deformations, cell-matrix interactions, motility, adhesion, reorganisation of the cytoskeleton, force transmission and gene expressions. Computational models are another way of experimentation that can be used to analyse mechanical responses that have been implicated at the cellular and molecular level in terms of complex biological processes on tissue and organ levels. The importance of mechano-computational studies can be appreciated for determining mechanical parameters of cells such as, stiffness, Young's modulus and rigidity, which is a useful start to understand cellular processes that involve mechanical changes. To appreciate the mechanical operation of a whole cell, one must understand how its components behave both in isolation and as a composite structure. It is important to understand individual behaviour of cellular components as it is equally important to assemble the components and observe how the cell functions as a whole. A given structural element plays more than one role in the cell and

may act cooperatively with other elements to produce a desired physical response. Knowing how mechanical perturbations propagate across the cell is necessary to understand the spatial coordination of cellular processes. Once researchers have a better understanding on how a specific force actuates on each structural component of a cell, they will be able to relate this with a specific biological response. In the author's opinion, understanding the relationship between forces, intracellular structures and cell function requires meaningful quantification of these coupled variables using a multi-structural cell model of the static and dynamic mechanical response of all the relevant load-bearing structures in the cell and their interconnection.

### 1.3 Modelling cell mechanics

*"By which mechanism do cells resist shape deformation and maintain their structural stability?"* is still the central question in cell mechanics. Computational analysis offers a higher degree of complexity that includes molecular, cellular, tissue and organ levels for a better understanding of force transmission processes by which mechanical conditions influence an integrated biological system. Integrating experimental and computational approaches can make the engineering of cells with enhanced functional properties possible.

Finite element (FE) analysis is a quantitative scientific computational technique used to simulate mechanics and biophysics at different scales. With FE models, one can define loads and boundary conditions applied onto a structure with defined material properties. FE analysis has been applied with success to modelling and determining the strain distributions within tissues and organs, including studies of mechanotransduction to predict fracture healing in bone (Byrne et al., 2011; Lacroix & Prendergast, 2002) and

cartilage (Guilak & Mow, 2000). Moreover, FE analysis has been used to model single cell structural mechanics: the idea that the cortical membrane that surrounds the cytoplasm of the cell was the main component responsible for cell structural stability, led to simple homogenous models for cell mechanics (Charras & Horton, 2002b; Guilak & Mow, 2000; McCreadie & J, 1997).

Furthermore, the potential inhomogeneities in material properties of cells were included in this type of analysis by considering that the cytoskeleton plays a role in transmitting and distributing mechanical stresses within cells as well as in their conversion into a chemical response. Structurally based models of cells including CSK mechanics have been proposed to predict cellular material properties from the cytoskeletal structure (Cañadas et al., 2002; De Santis et al., 2011; Ingber, 1993; Stamenović et al., 1996), the rearrangement of the cytoskeleton (Dowling et al., 2013; Picart et al., 2000), or the evolution of the cell shape in response to stretching (Drury & Dembo, 1999). However, current theories for CSK mechanics in response to stress lack the ability to explain the role for cross-link mechanics between the different cytoskeletal fibres and do not corroborate experimental observations in different time scales. In the author's opinion, a new structural cell model explaining the fundamental principles in cell mechanics and coupling multiple phenomena is needed: the inclusion of CSK together with cortical shell mechanics and the components of mechanical interest; multi-scale behaviour integrating filament and continuum components; and a model that will bring the possibility to predict static/passive and dynamic/active behaviour of the cytoskeleton (interaction between CSK fibres and time-dependent responses).

## 1.4 Author's thesis

*In vitro* experiments showed that cytoskeleton components play a very important role in cell mechanobiology, but the relationship between cell mechanics and cytoskeleton properties still needs to be better understood. Experimental investigation of cell mechanics is not always performed in controlled mechanical environments and experiments in different time scales have reported a large variability in response of cells to mechanical loading. The objective of this thesis is to investigate and model the mechanisms that determine the mechanical behaviour of the structural cellular components, force propagation and the dynamic resistance to deformation due to applied forces.

This work aims to adopt a computational approach to investigate the architecture and mechanics of cells with emphasis placed on the mechanical analysis of the different cytoskeletal filaments, whole cell contractility and propagation of forces at different time scales. The challenge of creating a multi-structural cell model with experimental validation is considered to decipher the complexity of cellular mechanical properties. The author aims to demonstrate the power and contribution of computational mechanical simulations to improve the fundamental understanding of cell biophysics and biology, and outline the potential of future advancements in mechanobiology for physiology and disease.

The general aims are investigated throughout the chapters, which address several aspects as follows:

- In chapter 2, a literature review of the main concepts for cell mechanics is presented. This includes a description of the biological cell concepts in biomechanics, the fundamental physical and mechanistic principles describing rheology of cells and the current source of variability in cell

mechanics experiments. Also, a brief review on the most impactful experimental methods and key computational and phenomenological models regarding CSK mechanical properties.

- In chapter 3, a new concept of a multi-structural cell model is presented for predictions of the mechanics of living cells and its structural components during two loading conditions, compression and stretching. The emphasis of the analysis with the FE model is placed on the fact that CSK structures are essential for generating and maintaining cell forces. Results are discussed in terms of the forces, deformation and inherent cell contractility that are observed upon compression and stretching.
- In chapter 4, simulations of experimental studies using AFM and magnetic twisting cytometry (MTC), combined with CSK-disrupting drugs are performed. The biophysical and biomechanical differences in the observed cellular responses from diverse single-cell stimulation techniques is analysed based on the role of individual CSK components that were modelled independently from each other. Atomic force microscopy experiments in two cell types, U2OS osteosarcoma cells and NIH-3T3 fibroblasts are performed to corroborate the model predictions.
- Chapter 5 presents a sensitivity study to evaluate how changes in material properties of the cellular components affect model predictions in terms of cell forces. This study investigates if the relationship between material properties and spatial distribution of specific components CSK is sufficient to define the mechanical properties of a cell type, to investigate the variability in cell mechanics.
- In chapter 6, the material properties of the model cell are redefined to include the dynamic response of the cell to compressive loads over

time. These material properties follow a weak power-law (PL), which is considered a fundamental principal in defining the cell response to external applied forces. Viscoelastic properties are analysed in terms of force-relaxation curves and discussed for different indentation position and for cell components.

- Chapter 7 is dedicated to the general discussion and limitations of the proposed computational cell model. Finally, this thesis ends with conclusive remarks in chapter 8, where the main results and contributions of this thesis to cell mechanics, as well as future prospects, will be summarised.

---

## LITERATURE REVIEW

---

### 2.1 Introduction

Quantitative description of forces and deformations applied to, and generated by cells has challenged scientists for the past two decades. To explain the behaviour of cells when exposed to mechanical forces, experimental techniques along with computational approaches have been developed to mechanically describe the CSK of living cells.

However, experimental research in cell mechanics is performed across different cell types and using different assumptions to fit and interpret the results for different theories. Due to a large number of experimental techniques, the degree of variability among different cells, cytoskeleton dynamics, irregular geometries and complex mechanical properties ([Lim et al., 2006](#)), reliable interpreting and comparing experimental measurements on living cells has been notoriously difficult. Understanding the set of cell mechanical properties that can be reproduced consistently is crucial for developing computational models, since the performance of computer simulations is evaluated in relation to experimental observations. Well-developed computational models that can predict cell responses corresponding to experimental findings are powerful tools for cell mechanics investigation.

In this literature review, a consensus description of the biological concepts in cell mechanics will be given. Also, a review on the most impactful experimental methods and key computational and phenomenological models regarding CSK rheology will be presented. Comments on their applicability in interpreting, as well as predicting, the mechanics of living cells and its structural components will be made. Finally, some conclusions will be drawn regarding the technical challenges to overcome to develop computational methods for cell mechanics in relation to the objectives of this thesis.

## 2.2 The cell and cytoskeletal structures

Eukaryotic cells are highly complex structures consisting of a large number of different components (Figure 2.1). Cell mechanics is central for many biological cell functions. Mechanically, eukaryotic cells are stabilised by the cytoskeleton, a contractile filamentous network that spans the entire cell body. The ability of a cell to perform its function is mainly maintained by the structural stiffness and rheology of the cytoskeleton and its active mechanical interaction with the external environment. The shape, mechanical strength and integrity of cells, as well as the ability to contract, move and divide or merge, is established by the remarkable range of configurations the cytoskeleton adopts. This is accomplished by the dynamic polymerisation and depolymerisation of its components, which is a highly versatile remodelling process that is far from thermodynamic equilibrium. The CSK is therefore an important mechanoreceptor responsible for the structural integrity and stiffness of a cell.

In the human body, several thousand different proteins form the cytoskeleton (Kollmannsberger & Fabry, 2011). The main components of the cy-

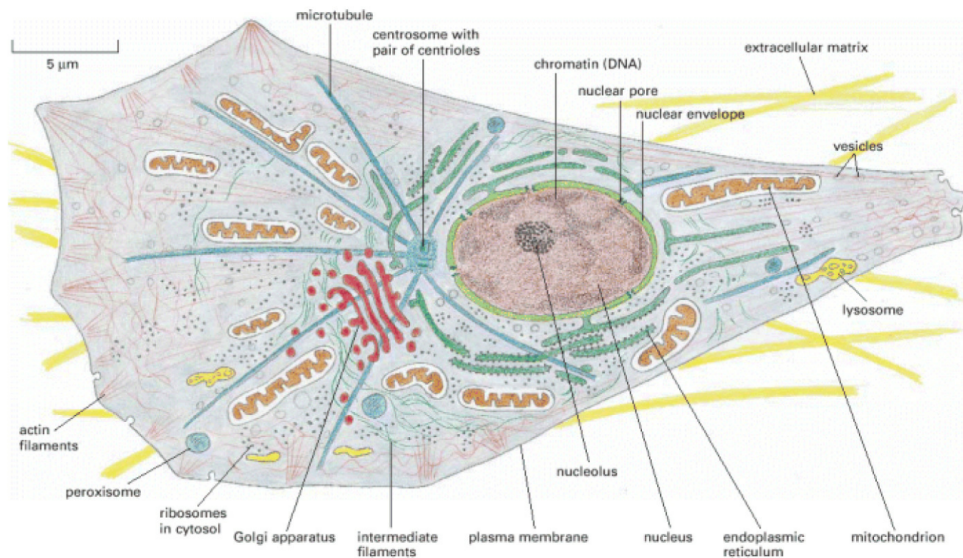


Figure 2.1: Structure of an eukaryotic cell (Alberts et al., 2002).

toskeleton are three families of proteins, which assemble to form three main types of filaments: actin filaments, intermediate filaments and microtubules. This network of proteins fills the space between organelles in the cytoplasm of living cells. Although the specific components are highly variable and diverse, the three types determine the structural integrity to maintain a particular shape necessary to accomplish a specific function. In this way, the CSK determines the mechanical characteristics of cell deformation needed for regulating a variety of cellular processes, such as mechanotransduction, migration, and cell functionality or apoptosis.

The most important differences between the three filaments of the cytoskeleton are their mechanical stiffness, the dynamics of assembly, their polarity, and the type of proteins which they associate with.

Microtubules (MT) are hollow cylindrical structures assembled from dimers of the proteins  $\alpha$ -tubulin and  $\beta$ -tubulin, which have approximately 24 nm in diameter. This tubular structure provides a high bending stiffness to the

microtubules because it makes them more resistant to bending compared to solid cylinders with the same amount of material per unit length. Microtubules exhibit the largest deformability of the three polymers (Suresh, 2007).

Microtubules have the most complex assembly and disassembly dynamic behaviour, stable growing and rapid shrinking, which is called the dynamic instability of the microtubules. Microtubules typically have one end attached to a single microtubule organising centre, called centrosome. Microtubules are long and straight in a star formation, disposed from the centrosome, near the cell nucleus, to the cell periphery. This network is often associated with molecular motors kinesins and dyneins, which are proteins designed to travel along the microtubules to help in the transport of nutrients and other proteins. In addition, microtubules play a major role during cell division, where they are involved in the segregation of replicated chromosomes through the formation of the mitotic spindles, which are complex cytoskeletal machinery.

Actin exists in cells in the form of a globular monomeric protein G-actin, and in form of a filamentous protein F-actin, originated from the polymerisation of G-actin into a twisted strand with a diameter in the range of 7-10 nm. F-actin is a polarised structure with a barbed end and a pointed end, where the filament grows slowly or disassembles respectively, in a process called treadmilling. The actin is continually assembled and disassembled in response to the local activity of signalling systems that determine their position and activity. For this reason, F-actin growth and organisation changes as function of cell activity, as it will be presented.

F-actin can be organised into different actin networks through the action of actin-binding proteins (ABPs), which promote the formation of highly organised structures in comparison to a single actin filament. Depending on

the type and concentration of ABPs, mechanically different, but functionally important, actin networks appear in cells, including linear bundles as stress fibres and three dimensional lattice network as the cell cortex.

For example, F-actin forms lamellipodia and filopodia during cell migration. It also appears in cells in the form of actin bundles defined between two points, that are crucial for cell adhesion to a substrate via the focal adhesion (FAs). FAs establish the contact between cytoskeleton and the tissue that support cells, the extracellular matrix (ECM). The ECM together with the microtubules counterbalance the contractile forces built up by the myosin motors and actin bundles, leading to a constant prestress in the CSK (Stamenović et al., 2002; Wang et al., 2002). In highly contractile cells, when the actin and myosin filaments align and span through the entire cell, they become called stress fibers. Cells generate force through fibrous bundles of myosin acting on actin microfilaments in the cytoskeleton (Huxley, 2004). In muscle cells, the actin-myosin bundles are known as myofibrils, while in nonmuscle cells, they are known as stress fibers. Together, the actin and the molecular motor myosin in the stress fibres, enable the cell contraction and resistance to high forces.

Myosin moves in a stepwise, walking cycle along actin microfilaments. During each contraction, myosin exerts pulling forces of 3-4 pN on actin filaments of opposite polarities to shorten the total length of the fibrous bundle (Brenner, 2006). The ends of many of these microfilaments are linked to focal adhesions (FAs), which attach cells to the ECM through integrin receptors or to adherent junctions (AJs), which are intercellular patches of cadherins for cell-cell interactions. Consequently, myosin-generated contraction leads to the development of isometric tension or prestress, which extends SFs beyond their unloaded lengths.

Similar to that which occurs in the skeletal muscle fibre, composed of thin actin filaments and thick filaments of myosin, this system interlocks and overlaps in a way to produce length change and tension development, which generates cell contractility. Actin and myosin are linked by cross-bridges made from extensions of the myosin molecules at regular intervals, see Figure 2.2 A. Neither the thick nor thin bands change in length when the muscle contracts. Only the degree of overlap between thick and thin filaments changes. Huxley (1957) proposed the *Sliding Filament Model*, suggesting that muscle contraction results as the cross-bridges linking the actin and myosin molecules pull the filaments over one another (Huxley, 1957). Hill (1938) hypothesised a specific relationship between the force generated by a muscle and the speed at which a stimulated muscle contracts under a given load, which is expressed, for each sarcomere in a muscle, as the characteristic equation:

$$(v + b)(F + a) = b(F_0 + a) \quad (2.1)$$

where  $F$  is the force generated by the muscle,  $v$  is the velocity of shortening to which a muscle contracts,  $F_0$  is the maximum (isometric) force exerted by the muscle, and  $a$  and  $b$  are constants. Hill's equation shows that the maximum speed of contraction of the muscle (where  $F = 0$ ) is given by:

$$v_{max} = \frac{bF_0}{a} \quad (2.2)$$

This relationship between  $F$  and  $v$  is hyperbolic Hill (1938) therefore, the higher the load applied to the muscle, the lower the contraction velocity (Figure 2.2 B). Similarly, the higher the contraction velocity, the lower the tension in the muscle. In other words, as the load increases, the muscle cannot lift the load as far.

Hill (1938) estimated that  $ab = g_1/f_1$  where  $f_1$  is the rate constant (attachments per second) for cross-bridge connection as actin and myosin molecules

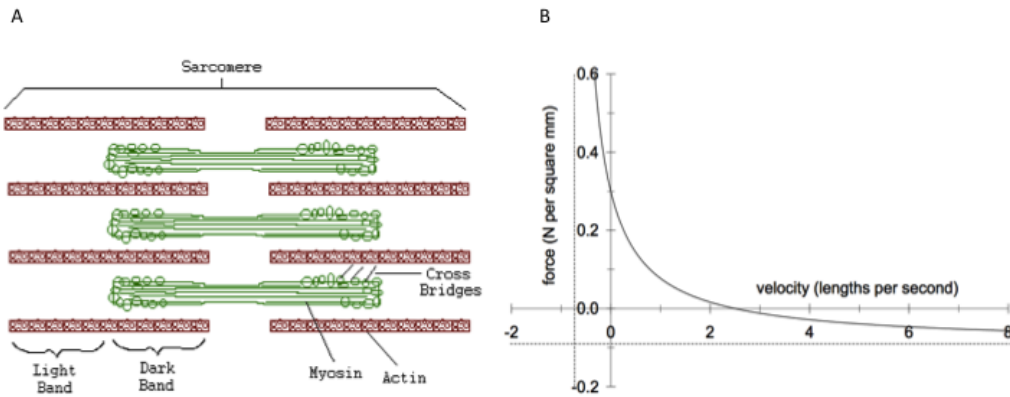


Figure 2.2: Muscle contraction. (A) Thin filaments of actin and thick filaments of myosin form the muscle fibers. These thick and thin filaments are linked at regular intervals by cross-bridges made from extensions of the myosin molecules. (B) hypothesised specific relationships between the force generated by a muscle and the speed at which a stimulated muscle contracts, under a given load (adapted from [www.tiem.utk.edu](http://www.tiem.utk.edu)).

combine to form cross-bridges. The rate constant  $g_1$  is the rate (detachments per second) for cross-bridge detachment. The muscle tension decreases as the shortening velocity increases, which has been attributed to the fact that there is a loss in tension as the cross-bridges in the contractile element that then, reform in a shortened condition.

Gordon et al. (1966) collected data relating the degree of overlap between actin and myosin filaments to the tension in a muscle: the striation spacing gives the degree of overlap. At 4 mm, the actin and myosin filaments do not overlap. Consequently the tension in the muscle is very low. As striation spacing decreases, the degree of overlap increases. Correspondingly, the degree of tension in the muscle increases. When the striation spacing is less than 2.0, the degree of overlap between actin and myosin filaments is too

high for them to function optimally. Consequently, the tension in the muscle decreases. This experimental investigation further demonstrated that tension in muscles depends on the degree of overlap between myosin and actin filaments, supporting Hill's equation by experimental data, substantiating the idea that the force generated by a muscle is related to the rate of cross-bridge detachment. Furthermore, both supported Huxley's *Sliding Filament Model*: sarcomeres contract, and the force generated by a muscle increases, as the thick and thin filaments increase in their degree of overlap.

Other than actin bundles, in all animal cells, F-actin organises into a thin layer adjacent to the cell membrane known as the actin cortex, where the content of actin is higher than in the interior of most of the cells. This layer of actin helps to anchor transmembrane proteins to proteins of the cytoplasm for cell adhesion. For each cellular process, the actin has a distinct molecular composition and structure, which suggests that the mechanical properties of these networks may be tuned for a specific aspect of cellular physiology (Deguchi et al., 2006).

F-actin is capable of sustaining much higher stresses and withstands deformation better than both intermediate filaments and microtubules (Suresh, 2007). Recent rheological studies on reconstituted actin networks showed that the concentration of ABPs affects the rigidity of these actin structures that can vary from a few kPa to GPa (Mofrad, 2009).

Intermediate filaments are made of intermediate filament proteins, which constitute a large and heterogeneous family distributed for six known classes with more than fifty different members. These proteins are tissue-specific, and examples include: keratin in epithelial cells; vimentin in mesenchymal cells, internexin in neuronal cells; and desmin in muscle cells (Kollmannsberger & Fabry, 2011). They are rope-like fibres with a diameter of around

10 nm, without polarity and therefore, they cannot support directional movement of molecular motors as microtubules and actin filaments.

The mechanobiology of the intermediate filaments is not so well understood as those of actin filaments and microtubules. It is known that intermediate filaments are the least stiff and more deformable of the three types of cytoskeletal components. For this reason, intermediate filaments also resist tensile forces much more effectively than compressive forces (Fletcher & Mullins, 2010). Intermediate filaments are more stable than any other cytoskeletal filament, although they alter their configuration under the right circumstances. Because of this stability, they provide a network of support to the cell. For example, in airway epithelial cells, the keratin intermediate filaments form a network that helps cells to resist shear stresses (Flitney et al., 2009). Intermediate filaments form the nuclear lamina just beneath the inner nuclear membrane that stabilises the nucleus and thus, contributes to its integrity. They start to contribute to the overall mechanical response of the cell during large cell deformation (Janmey et al., 1991), when intermediate filaments become fully extended and stretched (Wang & Stamenović, 2000).

Although distinct in their properties, these three components of the cytoskeleton are highly connected to each other, to the nucleus, and to the cell membrane. The organisation in terms of architecture of these filaments is central to the cytoskeleton response to either external or internal mechanical changes. Although their individual contribution to cell mechanical behaviour cannot easily be separated in living cells, several *in vitro* studies to isolate CSK components from cells have been performed to investigate CSK mechanics (Brangwynne et al., 2006; Deguchi et al., 2006; Deguchi & Sato, 2009; Hawkins et al., 2010).

## 2.3 Cell mechanical behaviour

### 2.3.1 Methods for measuring cell mechanics

A variety of experimental techniques, that often involve a mechanical perturbation to the cells in the form of imposed force or deformation, has been developed for observation of static and dynamic responses of the cell. A mechanical characterisation of the structural architecture of the CSK, in terms of stress, strain and deformation can bring useful knowledge to its dynamic behaviour. Precise quantitative mechanical measurements on single living cells became possible with the development of microrheological techniques in the recent decades, such as MTC, AFM, laser tweezers, cell stretchers, microplates, etc (Figure 2.3).

Since the first measurements, reported values of Young's modulus, stiffness, force and deformation measured by different techniques vary by more than one order of magnitude. This scatter in the available data increases when different cell types are compared. Nonetheless, measurements of stiffness seems to be in a close range of  $10^2$  to  $10^3$  Pa, depending on the type of cell and experimental approach used (Karcher et al., 2003). These reported values of whole cell stiffness are approximately six orders of magnitude softer than some of the cytoskeletal proteins. The low volume fraction of the fibres and the dynamics of the networks reduces the overall cell stiffness further.

Cells are subjected to static and dynamic forces in their physiological environment. Therefore, it is of particular interest to describe the behaviour of cells in different time scales that cover both an immediate response to forces but also its propagation over different times. The microrheological techniques impose forces as small as in the range of  $10^{-15}$  to  $10^{-6}$  N and displacements from  $10^{-10}$  to  $10^{-2}$  m, to probe the force interactions between individual

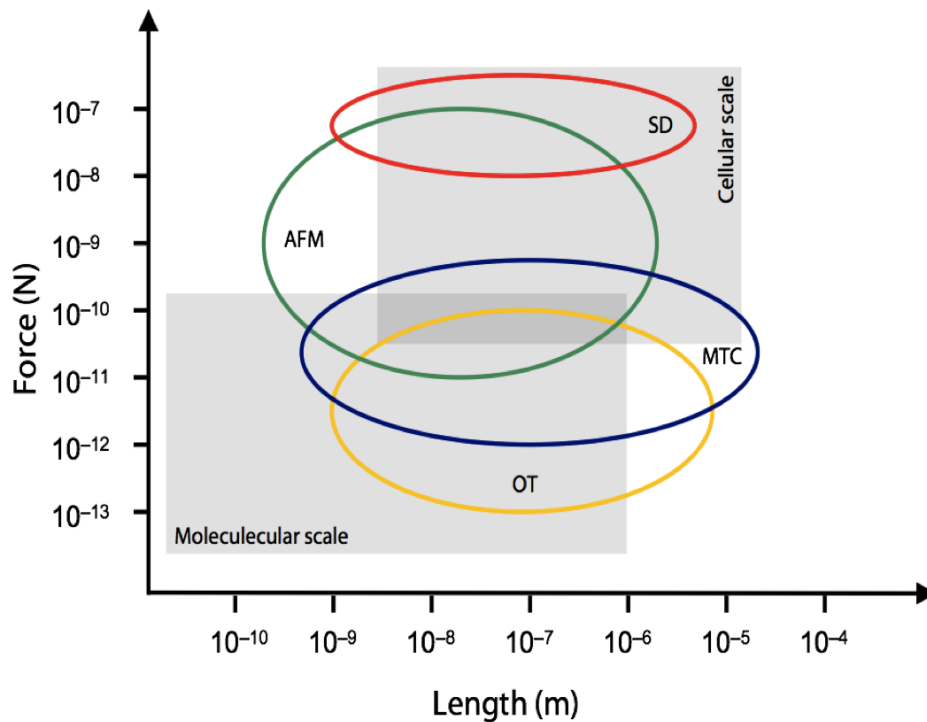


Figure 2.3: Experimental techniques and related biological events for the different force and displacement ranges (adapted from [Sunyer \(2008\)](#)). Atomic force microscopy (AFM), magnetic twisting cytometry (MTC), optical tweezers (OT) and substrate deformation (SD).

molecules inside the cell, as well as the mechanical response of the entire cell. In this sense, the different techniques are complementary to each other, and each technique is suited for a different force range and length scale (Figure 2.3), covering different time scales. This is important to consider since the complexity of the cell cytoskeleton, heterogeneity, active remodelling and signal transduction mechanisms are all dominant in understanding cellular behaviour.

The microrheological tools can be broadly classified into two categories: the passive measurement methods, that examine the motion of particles in-

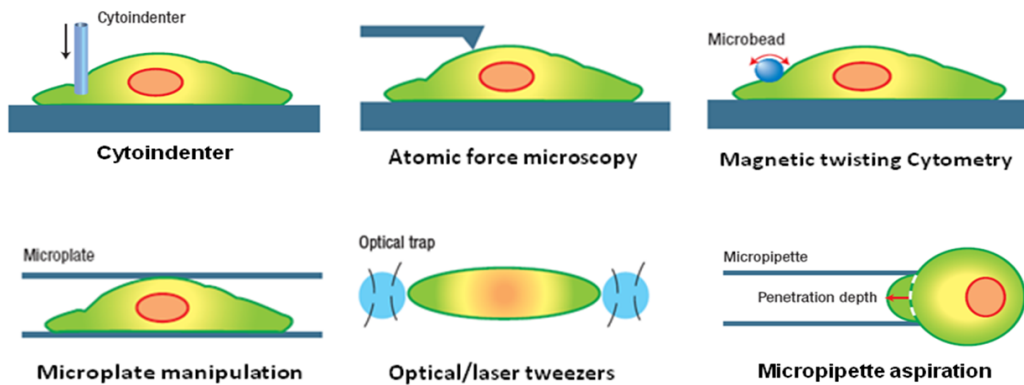


Figure 2.4: Experimental techniques to probe cell and molecular mechanics (Vaziri & Gopinath, 2008).

roduced in the cells due to thermal fluctuations; and active methods, which involve direct application of forces. Mainly, the active methods fall into two other categories of experiments: those that apply a mechanical stimulus to a localised portion of the cell, such as AFM, MTC, and cytoindentation; and those where a mechanical stimulus is applied to the entire cell, such as laser/optical tweezers, microplate manipulation, micropipette aspiration and substrate deformation (see Figure 2.4). Such rheological methods at small scales provided new prospects for the characterisation of local inhomogeneities in cells.

Passive microrheology techniques do not apply external forces. It rather monitors microbeads embedded into the cytoskeleton using either video recordings and particle tracking or laser beam interferometry, as reviewed in Mofrad (2009). Later, particle tracking was combined with fluorescence microscopy to measure cytoskeletal rheology using fluorescent microspheres as tracer particles (Jonas et al., 2008). Inside the cells, the beads are either forced through the cellular matrix or engulfed by phagocytic cells.

However, measurements from the inside can damage the cell and affect

the natural conditions of the cell interior by inducing changes in the CSK architecture due to its rapid remodelling for adaptation to new environments. Passive methods also have the risk of being confounded by any non-Brownian tracer motion such as intracellular trafficking or cell crawling. For that reason, techniques with application of external forces, typically localised at the site of the interrogation, are believed to be more prominent.

### 2.3.2 Active methods

Forces can be applied to adherent cells, which are normally embedded in the ECM or adhered to a substrate, or to non-adherent cells, such as blood cells.

Micropipette aspiration is the most common technique to study the mechanical tension in the cellular membrane of non-adherent cells by applying a suction within the micropipette to apply pulling forces on monocytes, red blood cells, leukocytes and erythrocytes (Drury & Dembo, 1999; Hochmuth, 2000). This technique was also very useful for the first measurements obtained on isolated nucleus for mechanical characterisation of this cellular component. The nucleus was measured to be about nine-times stiffer than the cytoplasm in endothelial cells (Maniotis et al., 1997), ten-times in neutrophil (Dong et al., 1991) and about four-times stiffer in chondrocytes (Guilak & Mow, 2000).

Other techniques are more suitable to measure mechanical properties in adherent cells. Once attached, these adherent cells generate internal tensile forces through actomyosin interactions and exert tractions on the underlying substrate or ECM. Cell traction forces are crucial to many biological processes such as inflammation, wound healing, angiogenesis, and metastasis.

Traction force microscopy is one of the most efficient and reliable techniques that has been used to determine how much force is exerted by the cell

onto an extracellular substrate, and how the external forces affect the global contractile state of the cell. The measurement of these forces is done through plating cells onto flexible substrates and recording the distortions caused by those forces (1-100 nN) on the substrate (Beningo & Wang, 2002; Sniadecki et al., 2006).

Traction forces of locomotive fibroblasts and other cell types were first observed as wrinkles in a thin, flexible film of silicone rubber (Harris et al., 1980). To better assess film distortions and allow measurements of traction forces, small beads, of known elastic moduli, were embedded into silicone films for the quantification of film distortion during cell migration (Lee et al., 1994). Also, fluorescent microbeads were embedded into polyacrylamide gels, which could be crosslinked to different degrees in order to change the stiffness of the elastic substrate for the range of traction forces generated by a particular cell type (Dembo & Wang, 1999). Arrays of fluorescent beads imprinted onto elastomeric substrates afforded even greater precision than randomly seeded beads for the measurement of traction forces at individual FAs (Balaban et al., 2001).

Another approach to this method is to use micro and nanofabricated pillars of known size and elasticity to determine traction forces microscopically. Tan et al. (2003) have developed a microfabricated system that uses an array of vertical cantilevers to measure the traction forces at multiple locations on a cell. During attachment, spreading, migration or contraction cells, on the top surface of an array of flexible microposts, exert traction forces that bend several posts. The deflections of the posts occurred independently of neighboring posts and, therefore, directly reported the subcellular distribution of traction forces. This technique demonstrated that cell area positively correlates with average traction force per post and that cell morphology regulates

the magnitude of traction force generated by cells (Tan et al., 2003). Force increased with size of adhesions for adhesions larger than  $1 \mu\text{m}^2$ , whereas no such correlation existed for smaller adhesions. Cells that were prevented from spreading and flattening against the substrate did not contract in response to stimulation by serum or lysophosphatidic acid, whereas spread cells did. Furthermore, Sniadecki et al. (2007) developed a system to apply external forces to the cells using cobalt nanowires embedded inside the microposts to measure traction forces before and after force stimulation in order to monitor cellular response to forces. Sniadecki et al. (2007) found that applying a step force led to an increase in local focal adhesion size at the site of application but not at nearby nonmagnetic posts, with a decrease in cell contractility at discrete locations along the cell periphery. Together, these data reveal an important dynamic biological relationship between external and internal forces and demonstrate the utility of this microfabricated system to explore this interaction.

In particular two other experimental techniques will be in focus in this literature review, the AFM and MTC since they will be used to corroborate the computational tool developed in this thesis.

Atomic force microscopy, invented by Binnig et al. (1986), is one of the most valuable tools for measuring forces and displacements on both molecular and cellular scales, at the nanoscale level. This technique consists of a cantilever, typically made of silicon or silicon nitrate, with a tip at the end to probe or image the surface of the sample. When the tip interacts with a sample, the cantilever deflects. This deflection can be measured by sensing the position of a laser beam that reflects off the cantilever to a quadrant photodiode, whose output signal is collected by a differential amplifier. Angular displacement of cantilever results in one photodiode collecting more

light than the other photodiode, producing an output signal proportional to the deflection of the cantilever. At the same time, a piezoelectric crystal precisely moves the cantilever in the three dimensions with nanometer accuracy in a feedback loop, that guarantees the measuring of a constant deflection over time.

There are three general types of AFM measurements and imaging: contact mode; tapping mode and non-contact mode. In the contact mode, the AFM simultaneously scans the movement of the tip on the surface of the sample and measures its deflection. The deflection time-course is then converted into a topographical image of the surface profile. Only AFM enables the three-dimensional (3D) profile of cell surfaces to be acquired at high resolution together with their material property distribution (Mahaffy et al., 2000; Radmacher, 1997). In the tapping mode, the tip of the cantilever makes intermittent contact with the surface. AFM measurements can be carried out on either living cells or intact molecules in an aqueous environment, instead of being fixed and in a vacuum. The trade-off of AFM is that an incorrect choice of tip for the required resolution can lead to image artifacts. Small forces cause less deflection of the cantilever, whereas large forces, obtained with a larger tip size to measure soft materials, can damage the sample. For example, when using a sharp tip, the spatial inhomogeneity of the cells, such as the presence of the stress fibres and microtubules, makes the interpretation of the results difficult. Because of this inconvenience, a more quantitative AFM technique, using polystyrene beads with a controlled radius attached to the tip of the cantilever, was developed to create a well-defined probe geometry (Chaudhuri et al., 2009; Mahaffy et al., 2004).

The AFM is typically used in conjunction with an optical microscope for real-time visualisation. The interpretation of force-indentation measurements

has usually been done to fit the Hertz model for the different contact tips with elastic samples. This method allows the calculation of the Young's modulus of the cell (Rosenbluth et al., 2006). This is limited to the assumption that the sample is a homogeneous, semi-infinite elastic body, which leads to an oversimplification of estimated Young's modulus. The lowest force that can be exerted is limited by the thermal noise of the AFM cantilever in liquid, and is around 20 pN (Eghiaian & Schaap, 2011).

This technique has been further developed to consider a broad range of studies in cell mechanics, including both physiological and non-physiological conditions. To directly observe cellular deformation and to correlate changes in the shape of cells and stress fibres formation with force-induced measurements, Chaudhuri et al. (2009) combined AFM with a side-view fluorescent imaging path along the axis of loading. This has also been used to study the mechanics and contraction dynamics of single platelets and implications in clot stiffening (Lam et al., 2011). AFM can also investigate the effects of cell microenvironment rigidity, that has been identified as an important signal influencing several biological processes (Bao & Suresh, 2003). This important input signal was normally investigated by culturing cells in deformable substrates using polyacrylamide hydrogels (Pelham & Wang, 1999) or micro-fabricated posts (Tan et al., 2003), which are limited to single static rigidity for each experiment. For this purposes, Webster et al. (2011) developed a method to control the stiffness of the AFM cantilever, called "stiffness clamp", where a precise feedback control of the cantilever deflection is used to investigate cellular response to changes in rigidity of the external environment. With AFM in "stiffness clamp" mode, it is possible to test more than one stiffness for experiment in a control manner. With these advancements, it is now possible to distinguish cell response to force, deformation and stiffness.

Forces limits in AFM, below 20 pN, are better controlled with MTC, optical traps and optical stretchers. With minimum forces, small indentations, below  $0.2 \mu\text{m}$  can be applied with these techniques. This variation of force and indentation becomes important to understand how the amount of small deformation imposed to a cell affects its mechanical response.

In the MTC, a microbead is coated with fibronectin or some other suitable molecule, which binds to integrins on the cell surface providing a direct link between bead and cell. The bead is then subjected to a force or torque due to the application of a magnetic field. Paramagnetic beads are used when pulling forces are applied to the cell (Bausch et al., 2001; Karcher et al., 2003), whereas ferromagnetic beads are used when torsional forces are applied to cells (Fabry et al., 2001). The diameter is typically in the range of 1 to  $5 \mu\text{m}$ .

Mechanical anisotropy is also found in cells using MTC experiments, which is related to the CSK structure, more precisely due to presence of stress fibers in cells (Hu et al., 2003, 2004). Experimental work with MTC showed the interest of this approach for the study of mechanotransduction pathways. An example would include the changes in the endothelin-1 gene expression when actin cytoskeleton was disrupted with cytochalasin-D, and when cell prestress was modified using an inhibitor of the myosin ATPase, which interfered with the actomyosin-based cytoskeleton contractility during MTC experiments (Wang & Ingber, 1994). The mechanical contribution of various cell components, including cytoplasm, cortex and nucleus, was also investigated with MTC (Laurent et al., 2003).

### 2.3.3 Power-law rheology

Recent experimental investigations have revealed a set of cell mechanical properties that is reproduced consistently for different probing techniques and

cell types (Hoffman et al., 2006; Pullarkat et al., 2007; Trepats et al., 2008), which define the fundamental principles of cell mechanics. Such aspects are the basis for understanding the complex cell rheology from a physical point of view. These principles were defined as the universal aspects of cell mechanics and establish a relationship between the important parameters of stiffness, contractility and force transmission, as it will be discussed.

When talking about CSK dynamics or rheology, most of the *in vitro* studies refer to measuring the dependence of the cell deformation over time or frequency. When subjected to external physical forces, cells deform showing both solid-like elastic and fluid-like viscous properties. Therefore, cells are better described as viscoelastic materials and the specific mechanical properties measured will depend on the time scale (Hoffman & Crocker, 2009). Cells exhibit a slow-time and frequency dependent deformation. As long as the applied external stress or strain is small, the viscoelastic response of the cell is linear, which considerably simplifies the interpretation of cell mechanical measurements.

The dynamic responses of the cytoskeleton to mechanical perturbation was investigated from viscoelastic creep and stress relaxation tests, using oscillatory MTC (Fabry et al., 2001; Hoffman et al., 2006; Trepats et al., 2007) and AFM (Alcaraz et al., 2003; Mahaffy et al., 2004) on different cell types. Based on the experimental observations of these studies, the viscoelastic properties of adherent cells were believed to be governed by a power-law. As typically ductile engineering materials (such as steel) deform in response to applied forces following the Hooke's law, a living cells, an engineering material itself, deforms following a power-law. In 1969, Hildebrandt discovered the accuracy of power-law for describing tissue biomechanics, which was also applied to cells (reviewed in Kollmannsberger & Fabry 2011). The

time-dependence response of a cell  $J(t)$  follows a weak power-law:

$$J(t) = \frac{d(t)}{F} = j_0(t/\tau_0)^\beta \quad (2.3)$$

that is better defined from a creep experiment but also for stress-relaxation experiments, where a force  $F$  is applied to the cell and the deformation  $d$  is measured over time  $t$ . In this function,  $j_0$  characterises the softness (compliance) of the material and is the inverse of stiffness and it is normalised by a time factor  $\tau_0$ , which is arbitrarily set. These two parameters are not free-fit parameters but constants for a given system such as a cell line, and  $\beta$  is the power-law exponent. When cells are tested with a sinusoidal force instead of a constant force, the complex shear modulus is defined as a function of radial frequency  $\omega$ :

$$G^*(\omega) = \frac{d(\omega)}{F(\omega)} = G'(\omega) + iG''(\omega) \quad (2.4)$$

which is defined as the complex ratio in the frequency domain between the applied force and the resulting deformation. The real part  $G'$  is called the storage modulus and accounts for the elastic contribution whereas the imaginary part  $G''$  is called the loss modulus and represents the dissipative contribution. The power-law exponent  $\beta = G''/G'$  is an index of deformability (a ratio of viscous to elastic contribution), where  $0 \leq \beta \leq 1$ . After the external force is removed, if the material springs back to its original shape,  $\beta$  approaches 0 and the equation 2.3 simplifies to  $d/F = j_0$  and the material corresponds to an elastic solid. If  $\beta$  approaches 1, equation 2.3 simplifies to  $d/F = j_0 t$ , which is the Newton's law of viscous fluid deformation. The slope of the deformation-time relationship is indicative of the corresponding  $\beta$  (see Figure 2.5).

Power-law rheology was defined as a universal property of adherent cells (Trepap et al., 2008). Nonetheless, a biological explanation of the meaning

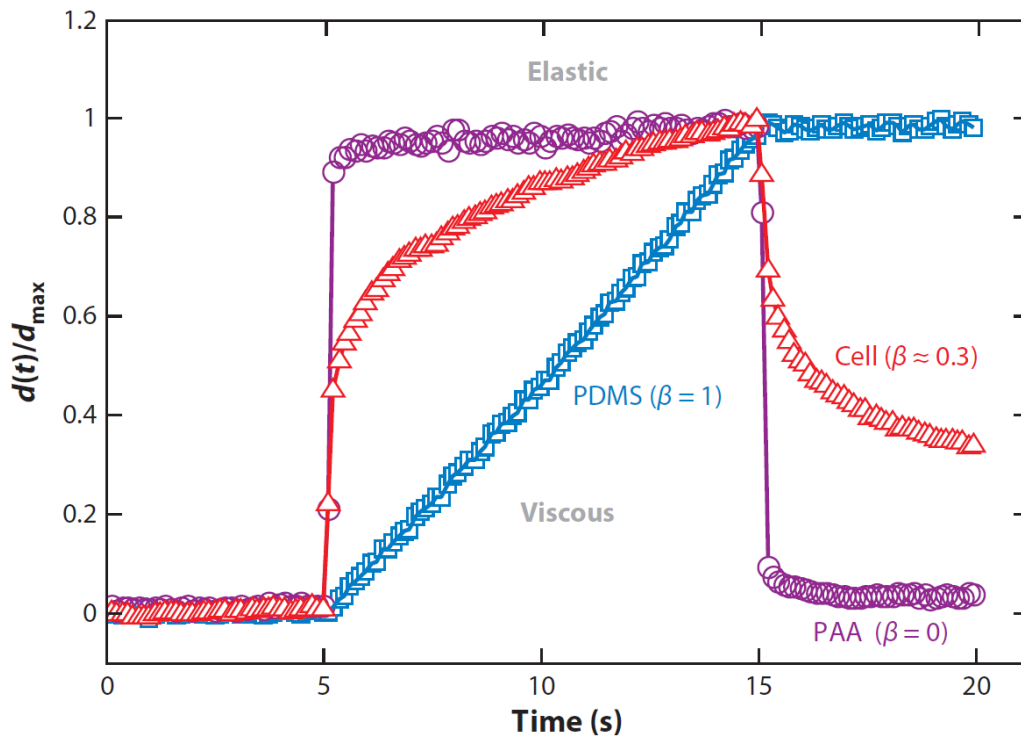


Figure 2.5: Power-law creep response of an elastic material [polyacrylamide-bis-acrylamide (PAA) hydrogel in the purple curve], a viscous material [polydimethylsiloxane (PDMS) silicone oil in the blue curve] and a cell [F9 embryonic carcinoma cell measured with magnetic twisting in the red curve], with  $\beta$  representing the power-law exponent (Kollmannsberger & Fabry, 2011).

of  $\beta$  in cells became possible with the introduction of the theory of soft glassy materials (SGMs) (Sollich, 1998; Sollich et al., 1997) to explain the weak power-law dependence of cell stiffness on loading frequency (Bursac et al., 2005; Fabry et al., 2001). The values of stiffness mentioned earlier for living cells are the same as pastes, foams, emulsions, slurries and colloid suspensions, materials that belong to a class of SGMs (Fabry et al., 2003). At first, it seems to be a diverse group but in fact their mechanical behaviour is surprisingly alike. The generic features that all of the materials of this group share are that each one is composed of elements that are discrete, numerous and aggregated with another via weak interactions. Also, these materials are not in thermodynamic equilibrium and are arrayed in a micro-structural geometry that is inherently disordered and metastable. The cell, and more precisely the cytoskeleton, share all of these features.

Sollich et al. (1997) developed the soft glassy rheology (SGR) model to explain the behaviour of soft glasses, which are characterised by structural disorder: under a load, they undergo structural rearrangements in a never-ending search for order. On the macroscale, this results in a system that slowly deforms over a wide range of timescales. Typically, these materials are characterised by a simple relationship described by the power-law.

The theory pictures a material that consists of a large number of elements that are trapped in cages formed by their neighbours. An individual element sees an energy landscape of traps of various depths and, when activated, hops into another trap. Sollich further claimed that activation is due to the interactions between elements and so, rearrangements somewhere in the material could cause rearrangements elsewhere. This coupling between elements is unspecified in the model and is solely represented by an effective abstract noise temperature  $x = \beta + 1$  (Sollich, 1998; Sollich et al., 1997) that

is related to the PL exponent, that reflects the system dynamics. This shows that a cell can change its properties, stiffness and fluidisation, only through changes in the exponent  $\beta$ .

The finding that a theory from soft matter physics can describe certain cell behaviours from mechanical experiments is extremely useful. SGR predicted that the behaviour of different types of cells follows a single power-law which is frequency and time insensitive when measured with different techniques over limited frequencies and timescales, respectively. Dynamic measurements of  $G^*$  have revealed that the viscoelastic behaviour of living cells are independent of the time and frequency scales, for small ranges, according to the hypothesis of SGR (Bursac et al., 2005; Fabry et al., 2001). However, a recent report showed that dynamic mechanics of living cells is timescale-dependent of mechanical loading (Stamenović, 2006; Stamenović et al., 2007), in contrast to the prevailing view.

These latter studies were performed for extended physiological mechanical loading frequencies and longer timescales (minutes) and revealed that two (maybe three) distinct regimes exist in living cells, which are characterised by different power-laws (Figure 2.6). The oscillatory response of the same cultured human airway smooth muscle (HASM) cells, that were used in the original studies describing the SGR theory phenomenon, was measured with the same oscillatory twisting technique but considering a wider range of frequencies (Stamenović et al., 2007). Importantly, the analysis of the data from  $10^0$  to  $10^3$  Hz is fully consistent with previous reports claiming that HASM cells exhibit a single power-law (Fabry et al., 2001). However, by including the data from  $10^{-3}$  to  $10^0$  Hz, it was observed that these same cells exhibit multiple regimes that cannot be described by a single power-law. Three regimes were defined to characterise the creep response of cells (Figure

2.6). The storage modulus of cells was found to depend on the frequency, according to a weak power-law with a constant exponent between 0.1 and 0.4, (Mandadapu et al., 2008).

### 2.3.4 Stiffness, prestress and power-law

The cytoskeleton is known to be a tensed network, meaning that these filaments bear a pre-existing tension even in the absence of external loading, which is called prestress. This prestress is carried out by the molecular motors that generate forces, transmitted by F-actin and intermediate filaments and counterbalanced by microtubules and the ECM (Wang et al., 2001b). Prestress is an intrinsic characteristic of adherent cells.

Stiffness, power-law and prestress were found to be related: an increase in prestress would cause a decrease in deformation and a decrease in  $\beta$ , indicating a more solid-like behaviour (Rosenblatt et al., 2006; Stamenovic et al., 2004; Trepac et al., 2004; Wang et al., 2001b). The fact that  $\beta$  changes with prestress suggests that this parameter also regulates the transition between liquid and solid behaviour in cells. When different values of cytoskeleton prestress were modulated, it was still observed the three regimes with cell-specific transition times over well-defined timescales (Overby et al., 2005). In this regard, contractile agonists such as histamine and thrombin have been used to increase prestress, whereas relaxing agonists such as latrunculin-A and cytochalasin can be used to decrease prestress (Stamenovic et al., 2004). Integrated mechanical events of the cell (spreading, crawling, contracting, re-orienting) are set within timescales that correspond to the intermediate-slow time regimes.

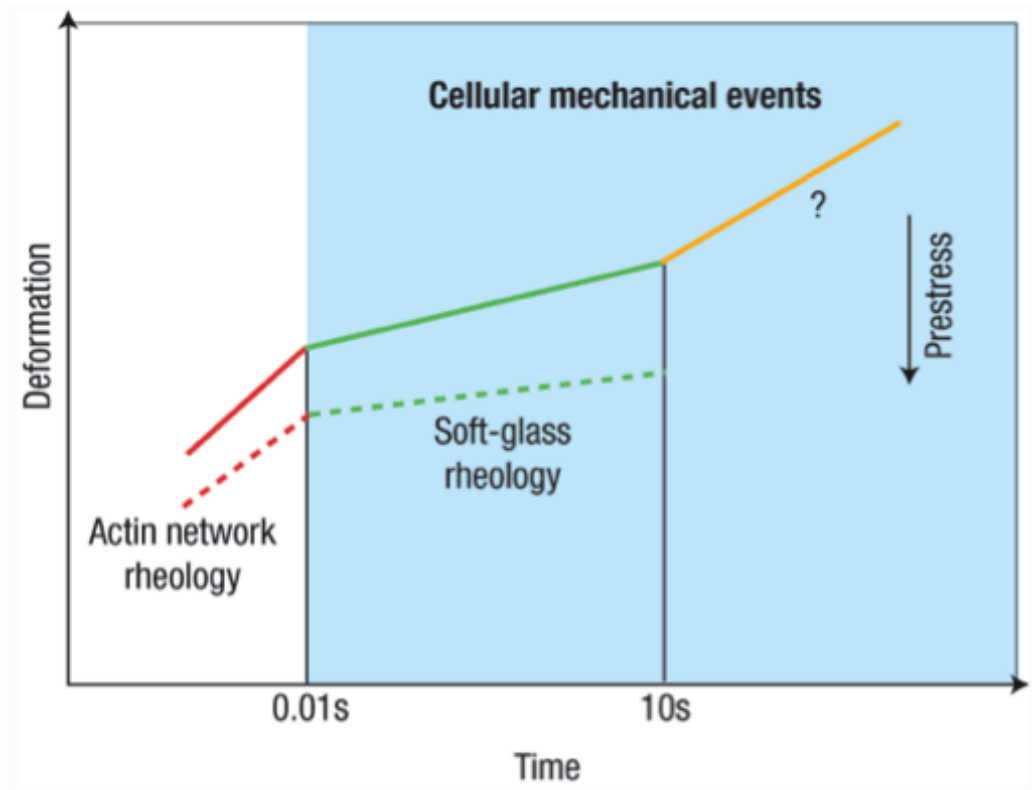


Figure 2.6: The creep response of a cell: a time course of cell deformation produced by a constant applied stress (Stamenović, 2006). Three regimes were defined to characterise the creep response of cells (Figure 2.6): an initial fast creep ( $\sim 0 - 0.01$  s) governed by the viscoelastic behaviour attributable to fluctuations in semi-flexible actin network driven by thermal forces (scales with the power-law exponent  $\beta = 0.75$ ); a very slow creep ( $\sim 0.01 - 10$  s) governed by the SGMs rheology dynamics ( $\beta \approx 0.05 - 0.35$ ); and an intermediate slow creep (above  $\sim 10$  s) governed by mechanisms that are still unknown ( $\beta \approx 0.5$ ).

### 2.3.5 Stiffening and fluidisation

Within the cell, the cytoskeleton is continually remodelling to maintain cell stability every time that cell is perturbed. [Trepap et al. \(2007\)](#) demonstrate results that support the idea that the cell interior is at once a crowded chemical space and a fragile soft material in which the effects of biochemistry, molecular crowding and physical forces are complex and inseparable. Other than the forces cells exert on the substrates, adherent cells within lungs, heart or blood vessels experience large periodic stretches. The viscoelasticity of cells becomes non-linear at high stresses ([Kollmannsberger et al., 2011](#)). The power-law behaviour of cells, defining the non-linear response to large stretches, has been extensively studied with intriguing results that represent a paradigm for viscoelasticity ([Wolff et al., 2012](#)).

Although, some literature uniformly emphasises that as an acute response to such stresses, the cell stiffens ([Matthews et al., 2006](#); [Pourati et al., 1998](#); [Wang et al., 2002](#)), new findings showed that living cells fluidise followed by slowly re-solidification prevails in most expected physiological conditions ([Trepap et al., 2007](#)). These experiments were performed for different types of cells with similar responses in quality but markedly disparate in magnitude and time course. This shows that cytoskeleton is thought to have structural rearrangements that are slow and localised ([Trepap et al., 2008](#)). Accordingly, the different behaviours were attributed to distinct network architecture ([Gardel et al., 2004](#)).

Therefore, two principles might be the basis in governing cell mechanics: one stating that stiffness is a function of the power-law exponent; and the other stating that stiffness is a function of contractile prestress (Figure 2.7). This equivalence of external and internal stress has important consequences for the nonlinear behaviour of cell in high-force regime. The relationship

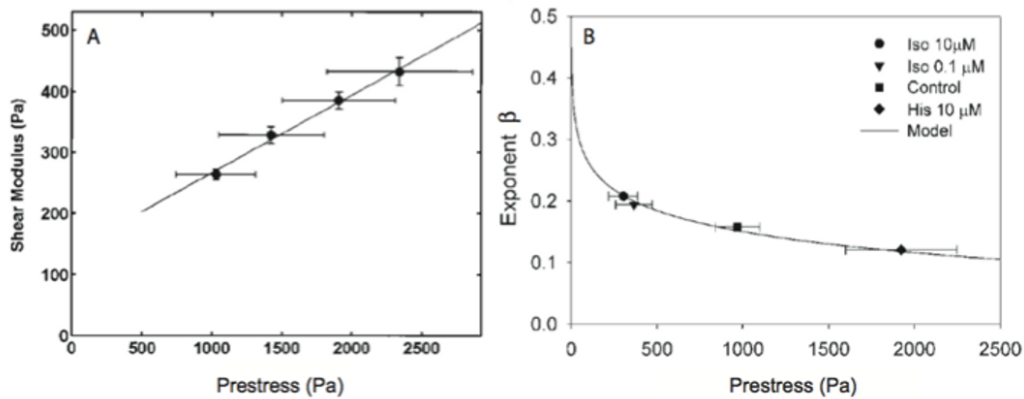


Figure 2.7: Cell rheology is related with prestress. (A) Plot of shear modulus as a function of prestress. Solid line is a linear fit. (B) The power-law exponent ( $\beta$ ) decreases with increasing prestress. Experimental data correspond to different cell treatments. Solid line represents an empirical master curve, (Stamenovic et al., 2004).

between prestress and stiffness was extended from the linear to the nonlinear regime showing that the stiffer, more contractile, solid-like cells fluidise during stretch more than the softer, less contractile, and fluid-like cells do (Bursac et al., 2005; Kollmannsberger et al., 2011). Interestingly, the fluidisation of most cells under stress-controlled loading conditions does not exceed a limit that corresponds to a PL exponent of 0.5 in normal conditions, which is only observed during creep experiments immediately prior to catastrophic cell rupture or detachment (Kollmannsberger et al., 2011). The results showed that by modulating the internal cell tension, cells can actively control their mechanical properties with simultaneous increase in stiffness and PL exponent, showing the nonlinear viscoelastic behaviour of adherent cells is controlled by cytoskeletal prestress.

There is now phenomenological evidences that dynamics in the cytoskeleton of the living cell revolve around the power-law rheology exponent param-

eter  $\beta$ , which sets the rate of nanoscale structural rearrangements and their relaxation, the extent of fluidisation in response to stretch and the rate of subsequent resolidification (Trepap et al., 2007). And in turn, the power-law rheology exponent is set by cytoskeletal prestress. These phenomena taken together, define the most fundamental features of the cytoskeletal phenotype, namely, its abilities to deform, to contract and to remodel.

### 2.3.6 Cytoskeleton disruption

The previous results led experimentalists to investigate the mechanisms responsible for the time-dependent changes in cell rheology and mechanical responses. Researchers also investigated if different results on the time-dependence rheological behaviour would be due to the experimental technique used. It was observed that even in the same cell type, the multiple techniques reported similar rheological values, confirming the universality of PL responses, but distinct mechanical responses. More specifically, techniques probing from the outside and with intracellular tracers were used in the same cell types, including epithelial cells (Dailey & Ghadiali, 2010), smooth muscle cells (Fabry et al., 2001; Lenormand et al., 2004; Smith et al., 2005) and endothelial cells (Dahl et al., 2005), showed two different exponents (Figure 2.8) but the two responses were not dependent on the method used. This suggested different mechanical roles of the internal cellular components. Furthermore, it confirmed the presence of mechanically different structures inside the cell that were also mechanically coupled and forces generated in one network can be transferred to another. However, the individual mechanical role of these structures is still poorly explained.

At low indentation (less than  $0.2 \mu\text{m}$ ) the cell showed an almost ideal elastic response that might be associated with the properties in the actin

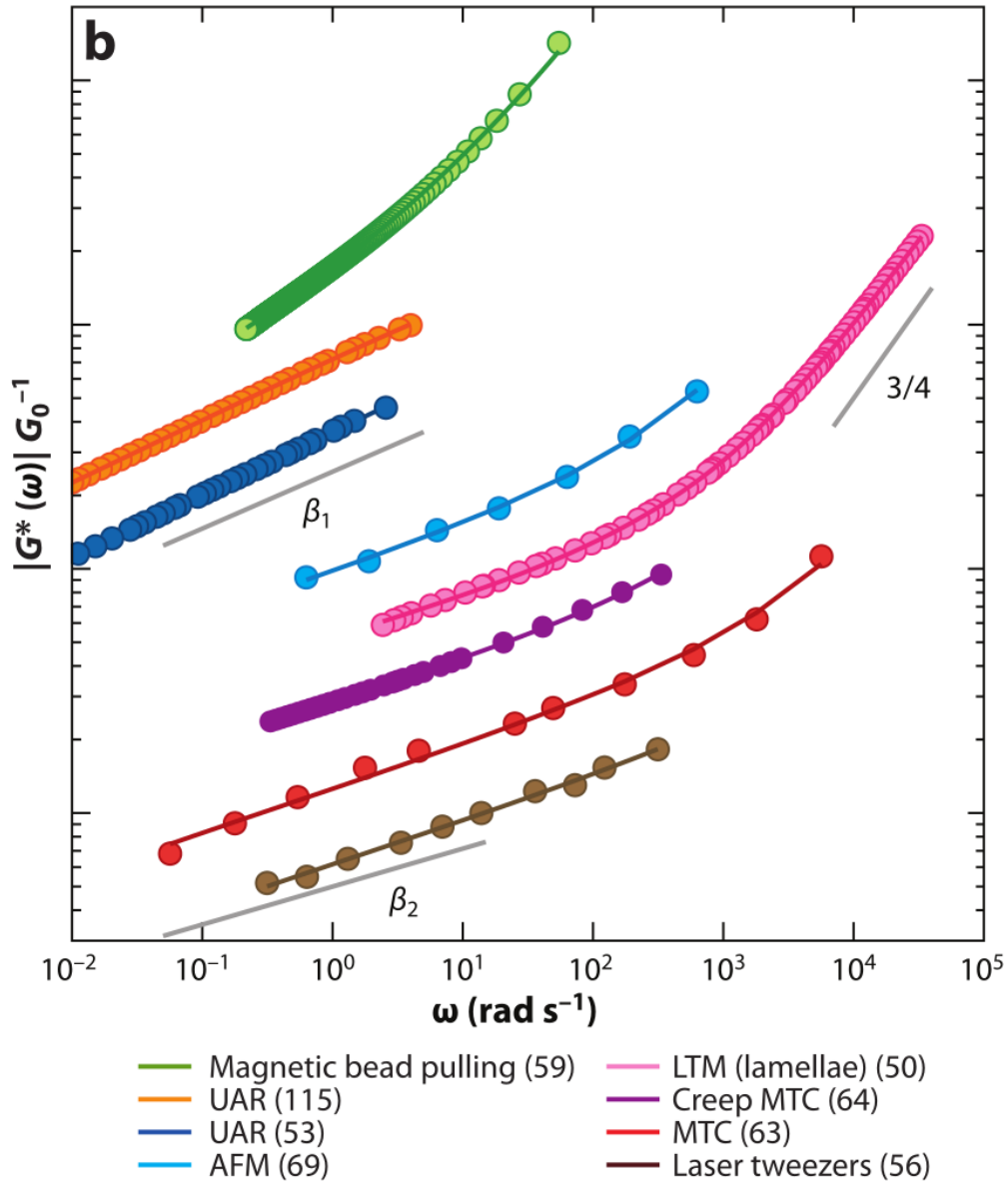


Figure 2.8: A comparison of the frequency dependence of several cell rheology experiments. The top three curves resemble the interior master curve, with exponent  $\beta_1$ , whereas the rest resemble the cortical master curve, with exponent  $\beta_2$ . UAR - uniaxial rheometry; AFM - atomic force microscopy, (Hoffman & Crocker, 2009).

cortex, whereas at larger indentation (around  $1\mu\text{m}$ ) the measured cell stiffness was dependent on the loading rate following a weak power-law (Nawaz et al., 2012). This was performed using both optical trap and AFM. Also, a recent study to explain cell rheology using microindentation tests in conjunction with mechanical, chemical and genetic treatments showed that for very small time scales, the cell behaves as a poroelastic material whereas for intermediate and long timescales, it behaves following a power-law (Moeendarbary et al., 2013). For very short timescales, the water redistribution through the solid phase of the cytoplasm plays a fundamental role in setting cell rheology. It could also be due to the fact that, changes in prestress conditions due to non-existent CSK remodelling processes are not occurring in these very short timescales.

Another way of testing the mechanical properties of the different structures of the cell is by combining the previous stimulating techniques (with probes that go more or less deeper in the cells) with CSK-disruptor chemical drugs. Some of the most common drugs used to selectively disrupt the individual cytoskeletal components include: cytochalasine-D (cyto-D) to destabilise actin networks; actin stabilising agent jasplakinolide; nocodazole (noc) to destabilise microtubules; colchicine to inhibit microtubules polymerisation; taxol that promotes microtubule stability due to tubulin polymerisation; blebbistatin, a key agent to inhibit nonmuscle myosin II, important to investigate contractility from the overall contribution of actin constituents in the mechanical response of cells; and acrylamide that disrupts intermediate filaments. Experimental results for different cell types have reported that disruption of all CSK components showed a decrease in force when measured with different single-cell stimulating techniques such as, traction force microscopy (Brown et al., 1996; Pelham & Wang, 1999), MTC (Wang, 1998),

and AFM (Charras & Horton, 2002a; Kasas et al., 2005).

However, the same general understanding regarding the effect of disruption of each CSK fibres on cellular force balance is not yet clear. For example, increase in traction force was observed in smooth muscle cells after microtubule disruption (Stamenović et al., 2002; Wang et al., 2001b, 2002), while the elastic modulus of skeletal muscle cells (Collinsworth et al., 2002) and osteoblasts (Takai et al., 2005) was not affected after microtubules disruption using AFM. On the other hand, Brown et al. (1996) measured changes in force in fibroblasts cultured in collagen lattices. The forces increased 33% when microtubules were disrupted by colchicine and decreased 50% when microtubules were stabilised with taxol. However, interpretation of such data is often complicated, because nocodazole treatment was found to be associated with increased myosin light-chain phosphorylation, which might account for at least part of the increased contraction in fibroblasts (Kolodney & Elson, 1995). Moreover, 20% decrease in cell stiffness was measured after microtubule disruption in endothelial cells using MTC (Wang, 1998), and 30% stiffness decrease in smooth muscle cells during *quasi-in situ* tensile testing (Nagayama & Matsumoto, 2008). In the previous mentioned studies, a decrease in force was always observed for disruption of actin structures. Nonetheless, it was not possible to isolate the role of the actin cortex from other actin networks to study its contribution for cell integrity.

## 2.4 Models to describe cell behaviour

The attempts to find a relationship between the parameters that define force, power-law and prestress are purely phenomenological but do not provide a mechanistic understanding. The different experimental techniques mentioned

above have led to the development of a variety of different mechanical models. These models aim to explain the outcome of a particular series of cell mechanics experiments and understand the physical origin of cell stiffness and rheological properties.

The passive cellular response, as well as active characteristics defined by CSK remodelling, need to be considered. Likely, there is not a single correct model to describe cells behaviour. Rather, one model may prove to capture some phenomenological aspects of cell mechanics under certain circumstances, while another model may be better suited in others. The ability of a model to describe an experimental observation is highly dependent on the type of cell, the experimental conditions and the time scale (Zhu et al., 2000). A complete model should account for the stress-dependent stiffening, the heterogeneity of the cell, the power-law behaviour, and the non-equilibrium features of the cytoskeleton (Sunyer, 2008).

### 2.4.1 Models for suspended cells

Early studies of cell mechanics considered the cell as a homogenous continuum structure and looked at the distribution of whole-cell stress and strain. Most of the continuum models were developed taking into account the rheology of cells under the micropipette aspiration technique. The Newtonian liquid drop model was developed by Yeung & Evans (1989) simulating liquid-like cells, such as leucocytes. The model was defined as a viscous fluid surrounded by a cortical shell. Later, more complex models, which take into consideration two different tensions of both cortex and nuclear membrane, together with two separate viscosities for the cytoplasm and the nucleus were developed (Dong et al., 1991). Dong et al. (1988) succeeded in explaining the initial jump in deformation during micropipette aspiration and the initial

rapid elastic rebound during recovery of cells held in the pipette for a very short time. This was done by adding an elastic component to the model and defining the Maxwell liquid drop model.

However, these models were still inconsistent in predicting certain experimental observations of micropipette aspiration: the speed of aspiration predicted was almost constant along all the analysis but in the real experiment there is an acceleration at the end of the aspiration immediately before the whole cell was sucked in. In order to better fit this course of aspiration, the power-law constitutive relation was incorporated into the cortical shell-liquid core model (Tsai et al., 1993). In this model, the cortex of the cell is still modelled as a layer with constant tension, while the cytoplasm is modelled as a shear thinning liquid governed by a power-law.

A continuum would suit when describing whole-cell deformations, but would not be adequate to fit results obtained for smaller scales (Zhu et al., 2000). Therefore, it became clear that many other observations could not be accounted for by using the continuum approach alone, specially for tissue cells.

## 2.4.2 Models of cytoskeletal networks

The previous models are better used to describe the mechanics of cells in suspension, but there is a growing recognition that the shape, function and mechanical properties of tissue and therefore, adherent cells, depend much more on the mechanical properties of the CSK than of the properties of non-adherent cells (Heidemann & Wirtz, 2004; Ingber, 1993; Janmey, 1998). One example includes the non-uniformity of the distribution of strain throughout the cell (Bausch et al., 1998), and the propagation of forces over long distances across the cytoskeleton (Maniotis et al., 1997). For adherent cells, it is more

reasonable to model the cytoskeleton as the key structure to define their mechanical properties.

Simple spring-dashpot models, including different Hookean elastic springs and Newtonian dashpots ascribed to different cell components, were sufficient to fit early experimental results on viscoelastic creep and stress relaxation tests, due to limited time and frequency resolution of the first experimental techniques used (Wang & Ingber, 1994). The number of elements needed to fit the data depends on the time or frequency scales. A Maxwell model, with springs in series with a dashpot and the Kelvin-Voigt model, where the elements are in parallel, appeared to fit the single cell response to a step stretch reasonably well. Also, with the development of more sophisticated experimental techniques, the accessible ranges of time and frequency, and the resolution of the experimental data were increased, which made it necessary to introduce more complex models of cell mechanics. Different mechanical equivalent of the continuum spring-dashpot models were used to represent different elastic and viscous elements of the membrane, actin cortex and nucleus, and were later thought to reflect the deep cytoskeleton (Bausch et al., 1998).

Other than the viscoelastic models and the SGR theory, models considering that cell mechanics is likely dependent on the structure of actin networks were developed, since it may be suspected actin is the main component in the definition of cell rheological properties (Pullarkat et al., 2007). This includes the open-cell foams, a model to describe the mechanical behaviour of the actin cytoskeleton of cultured endothelial cells (Satcher & Dewey, 1996). In this approach, it was assumed that bending and twisting of actin filaments is the basic mode by which the actin network develops mechanical stress. When the material is mechanically loaded, the fibres transmit forces and undergo

deformation. This assumption was based on the apparent similarity between the actin network in endothelial cells and microstructural networks of various natural and synthetic materials, which also have a complex topology as the connections of the filaments of the cytoskeleton. The drawback of this structural model is that stiffness is over-predicted (Ethier & Simmons, 2007) and does not include other components of the cytoskeleton that can carry stresses, such as stress fibres and microtubules. Despite the proposed models based on actin filaments, force measurements in fibroblasts and endothelial cells treated with nocodazole and with taxol decreased the isomeric force transmitted to the ECM, suggesting that microtubules also have a mechanical role for cells behaviour (Kolodney & Elson, 1995; Kolodney & Wysolmerski, 1992).

The worm-like chain (WLC) model is another physical model that defines the elasticity of individual semiflexible polymers such as the CSK elements as entropic, at high applied stresses (Rosenblatt et al., 2006). In the WLC model, an enthalpic effect leads to nonlinear elasticity of bonds, causing a strain hardening behaviour where the stiffness of the chains rises and the frequency dependence of the rheology flattens as stress is applied. Therefore, it explains the observed stiffening in cells that the SGR model could not explain. This model is thermodynamically driven and represents a potential link between the concept of applied prestress from tensegrity (discussed below) and polymer dynamics (Hoffman & Crocker, 2009). However, WLC model does not readily predict weak power-law rheology in its current formulation.

This limitation has been overcome by combining SGR and WLC models into the glassy worm-like chain (GWLC) model to explain stiffening, fluidisation and power-law rheology in a single model (Kroy & Glaser, 2007). It explains the stiffening/fluidisation observations in terms of two antagonistic

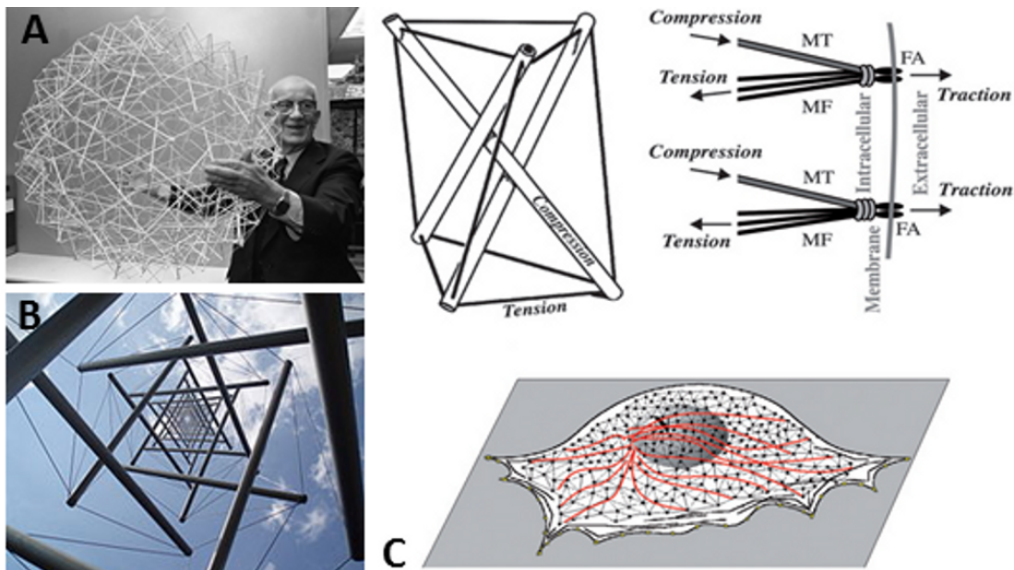


Figure 2.9: Tensegrity structures in: (A) architecture by the modern and futurist architect R. Buckminster Fuller ([www.forbes.com](http://www.forbes.com)); (B) sculpture of the Needle Tower II by Kenneth Snelson (1969) at the Kröller-Müller Museum in Netherlands ([commons.wikimedia.org](https://commons.wikimedia.org)); and (C) cells (Stamenović & Ingber, 2009).

physical mechanisms, the nonlinear viscoelastic resistance of biopolymers to stretch, and the breaking of weak transient bonds between them.

These previous models explain some of the cell behaviour but do not explain how the observed cell behaviour can be related to the composition and structure of the CSK. There was a gap to explain cells from both physical and mechanical point of views. This was overcome by defining a structural model for adherent cells by drawing analogy to the tensegrity structures (Ingber, 1993), introduced by the modern architect Buckminster Fuller, and widely used by the contemporary sculptor and photographer Kenneth Snelson (Figure 2.9). Tensegrity was defined as "The Architecture of Life" by Donald E. Ingber.

Tensegrity is a discrete structural cell model that has gained a certain traction in the literature due to the close resemblance of its predictions to certain experimental observations (Ingber, 1997, 2003b). Tensegrity is a building technique in which the mechanical integrity of a structure is maintained by some members that are under tension (cables) and others that are under compression (struts). Furthermore, the structural stability is maintained by a pre-existing stress (prestress) created in the mechanical elements. In the absence of prestress the cell would lose its stability and collapse. At the level of adherent cells, it was proposed that the actin and intermediate filaments play the role of the tension elements, while microtubules are the compressive elements (Ingber, 2003b).

The tensegrity model had been extensively used to investigate cellular deformability as a mean to represent the various structural elements of the cytoskeleton and its adhesion to the ECM. Researchers have shown that the tensegrity model can reproduce a number of features observed in living adherent cells during mechanical tests, that support the applicability of this concept to cell mechanics. It was found that cell stiffness increases directly proportional with increasing contractile stress (Hu et al., 2003; Stamenović & Coughlin, 1999). Pulling and pushing with an integrin coated micropipette showed the coordinated deformation of the cytoskeleton and the nucleus, indicating connectivity of cytoskeletal filaments from the cell surface to the nucleus (Maniotis et al., 1997). Microtubules can carry large compressive loads (Brangwynne et al., 2006) that in turn balance a substantial portion of the cytoskeleton prestress, as well as the intermediate filaments, which appear to be important contributors to cell contractility under application of large forces and facilitate the transfer of loads between the cell surface and the nucleus (Wang et al., 2001b).

However, tensegrity does not take into account other main components of cell such as cortical membrane, cytoplasm and nucleus. Tensegrity fails to predict the active dynamic properties of the cytoskeleton, such as remodelling, and the frequency dependence following a power-law response. Consequently, the tensegrity model in its current state only accounts for the static properties of the cytoskeleton.

### 2.4.3 Finite element models

Another set of models used to explain the behaviour of living cells are based on finite-elements simulations. Finite element modeling is particularly useful in the study of cell mechanics for the cases where loading conditions or mechanical responses cannot be easily quantified experimentally. Most of the developed FE models seek to explore the transmission of forces within the cytoskeleton when probed by different tools such as magnetic tweezers or micropipette aspiration (Karcher et al., 2003; Mijailovich et al., 2002; Ohayon & Tracqui, 2005) or simply to predict the overall behaviour of a cell under a stimulus (McGarry & Prendergast, 2004). Although the information given by finite-elements simulations is useful to interpret experimental measurements, the predictions of these approaches are limited by the exact parameters used to describe the cytoskeleton. Nonetheless, the biggest advantage in the biological context is that integrated models that combine aspects of discrete and continuous approaches, including all the cellular components of mechanical interest, are better achieved using FE theory. FE simulations in cell mechanics are also useful in predicting the response of living cells at physiologically relevant temporal and spatial scales. This is done by solving together the continuum and discrete scale constitutive equations arising in multi-scale biomechanics problems.

Therefore, the effects of frequency or time-dependence, prestress and stiffness can be naturally incorporate into a FE model as main parameters to describe cell behaviour. Because of the high complexity FE models can achieve at low computational time to solve difficult mechanical equations, they are normally used to predict large cellular processes including, migration, adhesion, division and remodelling. Both material and geometrical nonlinearities can easily be incorporated for the wide range of cellular processes and a better output control on the specific parameters affecting these cellular processes is obtained. With sufficient information for the organisation and properties, the FE structural models are also able to describe deformations at the whole-cell scale (Wang & Ingber, 1994).

Examples of some 3D models developed based on FE analysis consider the simulation of bead embedded in a cell to predict localised cell deformation during MTC (Mijailovich et al., 2002). The authors quantified the cell stiffness-dependence on the degree of bead embedding after stimulus by modelling a cell as homogeneous, without any intracellular component. Another FE study simulating similar experimental conditions of the latter, modelled the cell with viscoelastic material properties and specified the membrane/cortex but not the nucleus (Karcher et al., 2003). Therefore, it can not be used for predicting mechanotransduction since it was found that the nucleus and CSK are connected and establish the pathways for certain gene transcription that would be turned on or off in the nucleus by direct mechanical stimulus (Ingber, 1997).

Biomechanical 3D FE models have been developed to predict cell-cell interactions (Viens & Brodland, 2007). The internal structure of cells is simplified to a system of orthogonal dashpots with a single viscoelastic parameter and space-filling cytoplasmic elements, defined to overcome the modelling

challenges associated with cell rearrangements. This simulation predicts mechanical interactions between pairs of similar and dissimilar cells that are consistent with experiments, and can be further developed to model aggregates of several hundreds of cells without difficulty. This model is a promising tool for measuring surface and interfacial tension in cells.

Cell-specific FE models based on confocal images were developed to study cell mechanics involving large deformations, considering the effects of cell shape of myoblasts (Slomka & Gefen, 2010; Slomka et al., 2011) and fibroblasts and adipocytes (Or-Tzadikario & Gefen, 2011). It was demonstrated that cell-specific FE models are versatile enough to deal with cells of substantially different geometrical shapes. It was found that in order to induce large tensile strains (more than 5%) in the plasma membrane and nucleus surface, one needs to apply more than 15% of global cell deformation in cell compression tests, or more than 3% of tensile strains in the elastic plate substrate in cell stretching experiments (Slomka & Gefen, 2010). Utilisation of such models can substantially enrich experimental cell mechanics studies in classic cell loading designs that typically involve large cell deformations, such as static and cyclic stretching, cell compression, micropipette aspiration and shear flow. This type of simulation could provide magnitudes and distributions of the localised cellular strains specific from each setup and cell type, which could then be associated with the applied stimuli. Once again, the authors did not include the cytoskeletal fibres extending from the nucleus to the plasma membrane. This was based on the idea that modelling cell-specific shape is sufficient to predict accurate strains under large deformation (Slomka et al., 2011), which does not agree with the later findings supporting the discrete theory for inclusion of specific CSK mechanics for modelling the behaviour of adherent cells.

For this purpose, another FE model of cell-specific geometries was developed from confocal images and including discrete structures to represent the actin stress fibres randomly distributed in the cell. However, microtubules were considered as an homogeneous simplification distributed throughout the cell due to the high complexity observed in living cells (Wood et al., 2012). In this model, indentation of  $0.5\mu\text{m}$  from AFM force measurements was simulated and force appeared to be insensitive to both number and diameter of the fibres representing the actin in the interior of the cell. This model might not include the most relevant mechanical components for this type of static load. Furthermore, the actin system is not prestressed, which is not in agreement with the experimental findings presented in previous sections. Common misrepresentation of the cytoskeleton structures in the cells to simulate specific loading conditions is still happening and the author believes that a study showing the mechanical contribution of the different cellular components is still missing in literature.

Later, FE models incorporating the tensegrity structure were also developed (Figure 2.10). McGarry & Prendergast (2004) developed a finite element cell model based on tensegrity to describe the microtubules and the actin filaments of the prestressed CSK. This model also incorporates, in an idealised geometry, the other cellular components considered structurally significant: the cytoplasm, nucleus and membrane components (Figure 2.10 A). The results obtained by applying external forces suggest a key role for the cytoskeleton in determining cellular stiffness. The model is proposed as one that is sufficiently complex to capture the non-linear structural behaviours, such as stiffening and prestress effects, and variable compliance along the cell surface. Parametrical studies reveal that material properties of the cytoplasm (elasticity and compressibility) also have a large influence on cellular

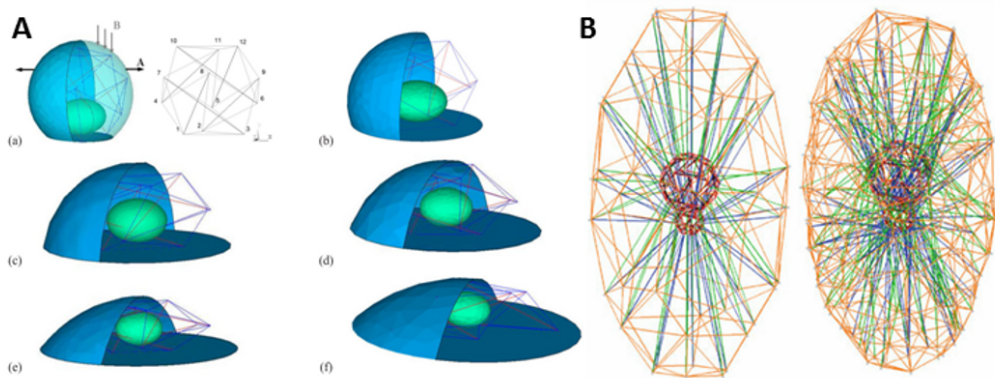


Figure 2.10: FE models based on tensegrity. (A) FE of *McGarry & Prendergast (2004)*, including discrete elements for microtubules (red) and actin filaments (light blue), and solid elements for the nucleus (green) and cytoplasm and cell membrane. (B) FE model of *Kardas et al. (2012)*, illustrating the cytoskeleton components of FE models with different complexities. The model includes microtubules (blue), intermediate filaments (green), actin filaments (yellow), centrosome and nucleus (red), and integrins in the outside.

stiffness (McGarry & Prendergast, 2004). This model was further developed to make qualitative and quantitative predictions of the differences in cellular deformation caused by fluid shear stress and substrate strain at magnitudes commonly applied *in vitro* (McGarry et al., 2005a), and for cell-substrate contact during cyclic substrate deformation (McGarry et al., 2005b).

A more recent FE tensegrity-based model was developed to study the mechanosensory process of osteocytes due to the direct connection of the cytoskeleton to the nucleus (Kardas et al., 2012). This has an impact on the remodelling and mineralisation of bone tissue. The computational cell model includes the major components with respect to mechanical aspects: the integrins that connect the cell with the extracellular bone matrix; prestressed tensegrity elements representing microtubules and intermediate filaments; the membrane-cytoskeleton; the nucleus and the centrosome (Figure 2.10 B). This is a more complete model where the cell is simulated on its physiological environment, representing *in vivo* conditions. The results showed that the deformation of the membrane-CSK, with actin properties, is directly mapped to the nucleus, with this latter being more affected if the elements that carry the forces are randomly distributed.

#### 2.4.4 Models for CSK dynamics

In this thesis, the author focuses on the development of a multistructural single cell model to investigate the passive response of its components during compression and stretching, by modelling contractility of actin bundles through the incorporation of a prestrain at the beginning of the FE analysis. However, it is important to acknowledge that the process of tension generation is complex and it is associated with CSK remodelling.

Predictive computational models have been developed to predict stress

fibre formation and contractility (Deshpande et al., 2007; Kaunas & Hsu, 2009; Veroney & Farsad, 2011). Deshpande et al. (2007) has proposed a novel computational model of contractile stress fibre behaviour based on the biochemistry of stress fibre formation, where stress fibre distributions of cells and contractility are dynamically governed by cellular signalling and tension dependent dissociation via a muscle-like constitutive law. McGarry et al. (2009) used Deshpande et al. (2006) theory to predict the relation between cell tractions and contractility of cells adhered to arrays of microposts, as well as to predict the effects of the stiffness and geometry of the microposts on the response of smooth muscle cells, mesenchymal stem cells and fibroblasts using FE analysis. This study showed that, consistent with measurements, the model predicted that the forces exerted by the cells would increase with both increasing post stiffness and area of cell spreading.

Kaunas & Hsu (2009) used a kinetic model based on constrained mixture theory to model stress fibre dynamics with a formulation assuming that stress fibres dissociation occurs when a fibre has been stretched past a critical length. In response to a step change in matrix stretch, this model predicted that stress fibers are initially stretched in registry with the matrix, but that these overly stretched fibers are gradually replaced by new fibers assembled with the homeostatic level of stretch in the new configuration of the matrix. The model was able to describe experimentally measured time courses of stress fiber reorientation perpendicular to the direction of cyclic uniaxial stretch, as well as the lack of alignment in response to equibiaxial stretch, in accordance with the *in vitro* experiments with endothelial cells (Kaunas et al., 2006). Furthermore, the model of Kaunas & Hsu (2009) predicted that the rate of stretch-induced stress fiber disassembly determines the rate of alignment, and that stress fibers tend to orient toward the direction of min-

imum matrix stretch where the rate of stress fiber turnover is a minimum. Later, [Kaunas et al. \(2011\)](#) developed a simple quantitative sarcomeric model of stress fibres to predict the role of actomyosin crossbridge cycling in stress fibre tension regulation and reorientation in response to cyclic stretching, showing that: under static conditions, the steady-state levels of stress fibre tension were determined by the fiber passive stiffness and the stall force of the myosin filaments; and that myosin sliding contributed to stress fibre turnover, resulting in stress fibre reorientation away from the direction of stretching at high, but not low, stretch frequencies.

The model of [Vereney & Farsad \(2011\)](#) is based on a description of cells that incorporate four key components of contractility: a passive solid cytoskeleton, an interstitial fluid representing the cytosol, an anisotropic network of stress fibres and a pool of globular actin monomers that freely diffuse in the cytosol, using a formulation assuming that the rate of stress fibres formation is increased by fibre tension. Numerical investigations showed that this multiphasic model was able to capture the dependency of cell contraction on the stiffness of the mechanical environment and accurately described the development of an oriented stress fibre network observed in contracting fibroblasts.

However, these models are confined to a single plane, restricting the ability to accurately represent *in vitro* conditions. For this reason, [Ronan et al. \(2012\)](#) expanded the formulation presented in the study of [McGarry et al. \(2009\)](#) into a fully 3D framework to account for the simulation of realistic cell geometries, including round and spread cell configurations, with the inclusion of a separately modeled nucleus. This study was used to investigate differences in stress fibre evolution in a range of cell types with varying contractility. The authors predicted that highly contractile cells form more

dominant circumferential stress fibres to provide greater resistance to compression, whereas fewer stress fibres were predicted for round cells with lower resistance to compression. Furthermore, the work of [Weafer et al. \(2013\)](#) simulated irregular geometries while including a complex active constitutive law for stress fibre formation and distribution. The passive mechanical properties of the cytoplasm and nucleus are simulated with a passive hyperelastic material model, combined with active actin contractility parameters, to simulate the experimental data of AFM compression for osteoblasts. The study showed that cells treated with cyto-D had about a 50 % decrease in the mean cell compression force compared to untreated control cells, demonstrating that the actin cytoskeleton plays a significant role in the resistance of osteoblasts to compression. The model also simulated the experimental observations of increased resistance to cell compression due to the presence of actin cytoskeleton contractility.

The study of [Weafer et al. \(2013\)](#) demonstrated that osteoblasts are highly contractile and that significant changes to the cell and nucleus geometries occur when stress fiber contractility is removed. The results of [Weafer et al. \(2013\)](#) and [Ronan et al. \(2012\)](#) are in accordance with the experimental results of [Ofek et al. \(2009\)](#), in which it was demonstrated that the actin cytoskeleton contributes more significantly to the resistance of cells to compression than intermediate filaments or microtubules. Other experimental studies also suggest the existence of a link between cell contractility and resistance to compression: long stress fibres were found to extend during compression, leading to a high compression force in myoblasts ([Peeters et al., 2004](#)); peak forces of 2500 nN were reported for highly contractile myoblasts ([Peeters et al., 2005](#)); less contractile chondrocytes exhibit a much lower compression force ([Ofek et al., 2009](#)); and endothelial cells, which are somewhere in be-

tween contractile myoblasts and chondrocytes were found to exhibit forces of about 500 nN (Caille et al., 2002). This suggests that highly contractile cells provide greater resistance to applied external compression.

Also, Dowling et al. (2012) separates the passive and active response of chondrocytes to applied shear mechanical deformation, considering both physiological and abnormal strain fields. Even for chondrocytes, which are not very contractile cells, the active contractility of the actin cytoskeleton was shown to dominate cell response to shear, demonstrating the importance of considering cell contractility to model cell response to external applied forces. Another study of Dowling et al. (2013) used the calibrated active chondrocyte model to predict the *in vivo* response of chondrocytes in cartilage to pathological and dynamic loading. The study demonstrated that the presence of a focal defect significantly affects cellular deformation, increases the stress experienced by the nucleus and cytoplasm, and alters the distribution of the actin cytoskeleton, and it was observed that cyclic tension caused a continuous dissociation of the actin cytoskeleton, which did not happen during static loading.

## 2.5 Conclusions

Given the general lack of agreement between the different experimental methods presented, a single model focusing on a single experiment is not expected to explain all findings. Two general frameworks, tensegrity and soft glass rheology have been proposed to explain passive cell mechanics from two different perspectives. Although elegant, both fail to fully comply with all of the present experimental data. The broad frequency spectrum of relaxation times of the cytoskeleton still remains to be explained, and details to relate

this idea with CSK mechanics still need to be worked out (Pullarkat et al., 2007). There is still lot of work ahead for modelling just the passive aspects of cell rheology. Although recent models of active remodelling of the stress fibres and cell contractility have been developed and incorporated with formulations to explain the passive response of cells, they lack on explaining the contributions of other cytoskeletal components and in differentiating the mechanical role of different actin networks focusing mainly on the behaviour of stress fibres.

There are several, mostly active aspects of live cell dynamics, which cannot be easily reproduced in *in vitro* experiments to date, such as the CSK remodelling and mechano-chemical signalling mechanisms. For example, how a cell quickly change its mechanical properties from a short term response to remodelling of its entire cytoskeleton, while exhibiting fluid-like behaviour is still not clear. Such processes include complex signal transduction pathways, which need to be explored in the context of cell rheological properties. Combining the powerful experimental techniques with theoretical and *in silico* studies may enlighten researchers for the understanding of the relationship between cytoskeleton mechanics and cell functions.

Therefore, new models should aim at describing a larger consensus picture of cell mechanical structure-function to make proper predictions about the absolute value of cell stiffness, the nonlinear effects of cell mechanics, the role of forces, and dynamic heterogeneity. But all of these predictions are only possible after an accurate description of the passive responses of cells. New structural cell models should further aim to be compatible with known cell signaling pathways to be useful for understanding processes such as cell migration and mechanotransduction.

The goal of this thesis is to develop a sufficiently generic cell FE model to

predict, reproduce consistently, and compared cell mechanical properties between various probing techniques, across different cell types, but that is at the same time detailed enough to be mechanistically useful at describing relevant cell substructures and their passive response. These mechanical properties of individual cells are the basis for understanding the complex universal aspects of cell mechanics, such as the role that forces play in regulating the structure and function of cells and how it has been implicated at the tissues and organ levels.

---

# FINITE ELEMENT MODEL FOR A SINGLE ADHERENT CELL <sup>1</sup>

---

## 3.1 Introduction

All cells in the organism are exposed to mechanical stresses, and these physical factors regulate biological processes including growth, differentiation, migration, gene expression and in particular signal transduction. It is well accepted that such signalling pathways start with mechanosensitive receptors at the cell surface including primary cilia (Hoey et al., 2012; Malone et al., 2007), stress-sensitive ions channels (Kearney et al., 2008), integrins and the focal adhesion complexes (Balaban et al., 2001; Schwarz et al., 2002). Changes in these mechanoreceptors then activate intracellular components such as the nucleus and the CSK, which are key in this process (Shafrir & Forgacs, 2002). Intracellular force transmission and changes in the cellular behaviour were associated with changes of the nucleus structure (Caille et al., 2002; Guilak & Mow, 2000; Maniotis et al., 1997; Tapley & Starr, 2013; Wang

---

<sup>1</sup>This chapter includes results from the paper published as: S. Barreto, C. H. Clausen, C. M. Perrault, D. A. Fletcher, D. Lacroix, *A multi-structural single cell model of force-induced interactions of cytoskeletal components*, DOI: 10.1016/J. Biomaterials, 2013, 04.022

et al., 2009) and nucleus function of transport and gene expression (Ingber et al., 2000). Also, contact with the ECM via integrins have also been shown to modulate cell stiffness and thus, strains transmission. Structural coupling between ECM molecules, integrins and actin filaments through the formation of focal adhesions complexes was suggested to induce cell shape changes mediated by alterations in the CSK organisation (Janmey 1998; Sims et al. 1992). This coupling was seen as a possible integrated mechanism for altering cell structure in response to changes of the extracellular environment (Hamill & Martinac 2001). Cellular contractility, known as prestress, was another possible factor proposed to be involved in mechanotransduction (Chen et al. 2001; Stamenović & Coughlin 1999). This concept of prestress was clarified as the internal stresses generated by the cell in the absence of external mechanical forces. This initiated the controversial idea that cellular forces have a bi-directional cell-signalling and therefore can adapt to, but also modify, the external surroundings.

Studies of single adherent cells are important for the analysis of the role of forces generated by cells, to determine changes in their shape and rigidity and identify the role of the different components that are believed to be involved in signal transduction. Although some experimental studies highlight a key role for the CSK in determining cellular stiffness (Kasas et al. 2005; Ofek et al. 2009) it is still not clear the specific relationship between the cytoskeletal interconnected structure, cell mechanics and intracellular signaling. It is of special interest to know how the components of this interconnected filamentous cytoskeletal structure react to different forces to permit or impair the transmission of the mechanical stimuli.

In this context, the use of theoretical models for cellular mechanics can provide a better control over the structure and modulation of individual

CSK components thus, providing unique information for whole cell mechanics (Karcher et al., 2003; Maurin et al., 2008; McGarry et al., 2005a; McGarry & Prendergast, 2004; Mijailovich et al., 2002; Ujihara et al., 2010; Vaziri & Gopinath, 2008; Viens & Brodland, 2007). Experimental work with force measurements has shown discrete propagation of force in cells, although these results were highly specific on the stimulation technique used (Bischofs et al., 2009; Hu et al., 2003). The overall evidence on the generation and transmission of force in the CSK of adherent cells is in favour of the discrete theory to describe the structural mechanics of cells (Jonas & Duschl, 2010). The most prominent discrete model developed so far is tensegrity. The main characteristics are that force transmission is locally discrete in the actin cables and microtubules struts (Ingber, 1993, 2003b), yet globally integrated in a continuous cytoplasm and in contact with the extracellular matrix. The idea of combining both continuum models and discrete models to study cell deformation over a larger scale has been proposed (Hochmuth, 2000; Milner et al., 2012) and this concept has been put together with FE analysis to investigate the mechanisms for force generation and propagation considering a wide range of cellular processes at various time-scales (McGarry et al., 2005a; Prendergast, 2007; Vaziri & Gopinath, 2008).

However, these tensegrity-based models, in which the structural organisation for cell integrity relies on prestress and interdependence of the CSK components, do not elucidate the role of individual CSK components in generating and propagating forces. This critical aspect for the understanding of cellular mechanics thus calls for a modification of the FE models based on tensegrity. Therefore, a new theoretical multi-structural model is needed for delineation of the contribution of each intracellular component to whole-cellular mechanical properties and force balance. A multi-structural 3D FE

cell model as a fusion of continuum and discrete formulations, including cytoplasm, nucleus, microtubules, actin cortex and actin bundles is proposed. The key features of this mechanical model keep fundamental principles governing cell behaviour, including prestress and interplay of the discrete components, with a more accurate morphological representation of the CSK, where they are free to move independently of each other, as opposite to the tensegrity theory.

The hypothesis in this chapter is that the multi-structural model can describe the cellular structural behaviour and determine stress and strain response of cells to various mechanical stimuli by applying compressive and shear loads. The aim is to predict the distributions of intracellular forces and deformation, and the influence of cell contractility in the CSK network for the whole cell mechanics. It is not only important to know how cells respond to local deformation of the external environment but also if they respond differently depending on the stimulus. For that, the author simulates adherent cells probed by two of the most common techniques to measure forces on the range of living cells, the atomic force microscopy and magnetic twisting cytometry. These experimental techniques helped to build the link between biochemical and structural mechanical environment of cells. The purpose of this model is to extend the knowledge of how forces and strains propagate within cells. More specifically, to know which are the cellular components of interest and the magnitude of mechanical signals that appears as crucial factors for further understanding of how processes such as mechanotransduction and gene expression are mechanically controlled.

## 3.2 Material and methods

### 3.2.1 Finite element single-cell model

A computational 3D finite element model of a single cell was developed including the intracellular components likely to be mechanically significant for cell behaviour: the cytoplasm, the nucleus and certain cytoskeleton networks, namely actin and microtubules, see Figure 3.1.

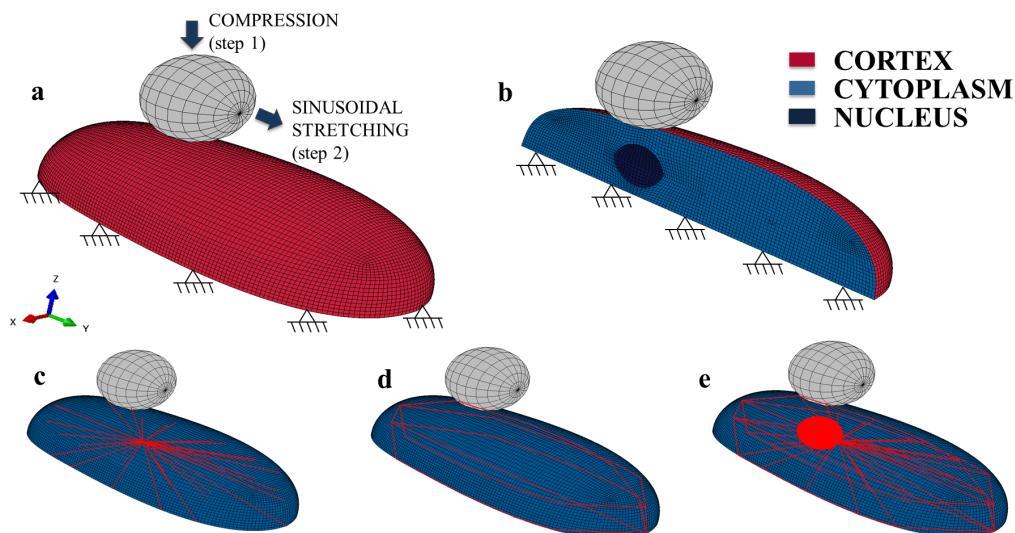


Figure 3.1: FE model of a single cell. (A) Cell model with boundary conditions and representation of the movement of the bead for the cycle of compression followed by the cycle of stretching; (B) section of the cell with the continuum elements: cytoplasm, nucleus and cortex; (C) microtubules distribution; (D) actin bundles distribution; (E) interaction of actin bundles and microtubules and position with respect to the nucleus.

In the model, continuum and discrete elements were used to represent the continuum media and the fibres of the cytoskeleton, respectively. *In situ* microscope observations of cells shape adhered to a substrate, as well as images

of actin and microtubules distribution, were used to create the 3D model of the cell and the architectural structure of the intracellular components. The geometry of the cell was developed and meshed using the finite element software Abaqus standard (Simulia, USA). The shape of the cell was defined based on a semi-ellipsoidal profile with  $19 \mu\text{m}$  diameter on the long-axis ( $y$ -direction),  $8 \mu\text{m}$  on the smaller-axis ( $x$ -direction) and about  $4 \mu\text{m}$  height ( $z$ -direction) on the highest part of the cell that corresponds to the centre of the  $y$  axis. However, the centre of the cell is located  $3.5 \mu\text{m}$  from the centre of the  $y$  axis. The nucleus was modelled with an ellipsoidal shape, which is consistent with measures reported by [Caille et al. \(2002\)](#) and it is positioned at the centre of the  $y$  axis (that corresponds to the highest portion in the cell) and  $2.5 \mu\text{m}$  from the bottom of the cell. The remaining space is filled with cytoplasm. Both cytoplasm and nucleus were modelled with 8-nodes continuum hexahedral solid elements (Table 3.1).

*Table 3.1: Cell mesh properties in Abaqus*

Cell component	Element type	Element definition	N <sup>o</sup> of elements
Cytoplasm	Solid continuum	C3D8R	95151
Nucleus	Solid continuum	C3D8R	5484
Microtubules	Beam	B31	277
Actin cortex	Shell	S4R	11748
Actin bundles	Truss	T3D2	33

The cytoplasm was covered with a surface representing the actin cortex. The cortex is a thin layer of cytoskeleton actin-gel, that exists in all types of animal cells, and is represented in the current cell model with shell elements (Table 3.1), originated from the outer surface of the quadrilateral elements

of the cytoplasm, with a thickness of  $0.2 \mu\text{m}$  (Unnikrishnan et al., 2007). Discrete elements were included within the cytoplasm to represent other CSK components, microtubules and actin bundles. Beam elements were used to model the microtubules structure (Table 3.1), originated from one common node near the nucleus, representing the centrosome. The beams were defined with a pipe section with external radius of  $12.5 \text{ nm}$  and wall thickness of  $5 \text{ nm}$ . Microtubules are long and arranged in a star-shape that grow from the centrosome to the cortex, see Figure 3.1 C. This spatial distribution of the microtubules in the current model has been used by other authors (Kaverina et al., 1998; Maurin et al., 2008) and is corroborated with microscopic images of human mesenchymal stem cells, see Figure 3.2.

In many cells, actin is present in large groups of actin fibres, parallel to each other, joined by actin binding proteins, known as actin bundles, normally localised around the cell periphery, that are referred to as dense peripheral band (Deguchi et al., 2006). In this model, they are arranged in the whole cell above the cortex and both ends are anchored to it, (Figure 3.1 D). The actin bundles were modelled as discrete truss elements (Table 3.1) with a radius of  $12.5 \text{ nm}$  (Deguchi et al., 2006).

Truss elements are one-dimensional line elements that have 2 nodes, and can be oriented anywhere in 3D space. Truss elements are long, slender structural members that have only axial stiffness and are 3 degrees-of-freedom elements, which allow translation only and not rotation. Therefore, truss elements do not transmit moments. For this reasons, they were selected to better represent the mechanical behaviour of actin bundles that behave in a similar way as ropes. Beam elements are a one-dimensional line element in 3D space or in the XY plane that has stiffness associated with deformation of the line (the beam's axis). Two nodes define element geometry, and the third

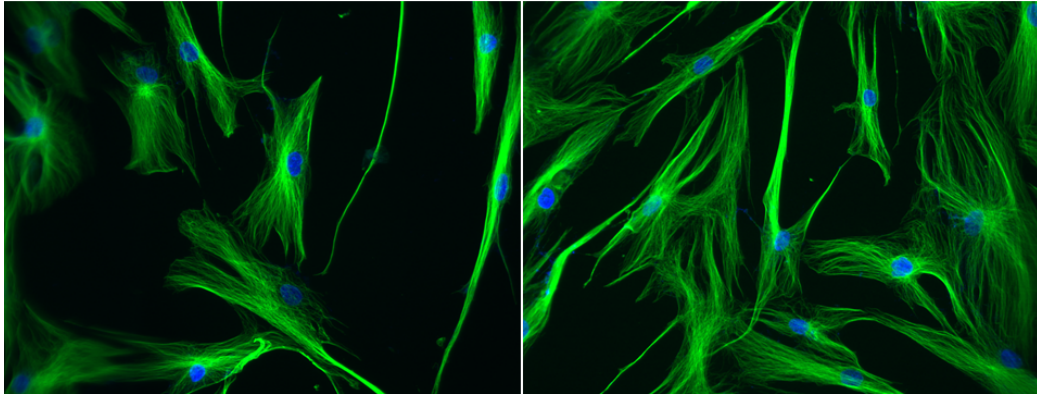


*Figure 3.2: Confocal images of microtubules staining of human mesenchymal stem cells. Immunocytochemistry was the technique used to label the  $\alpha$ -tubulin of the microtubules using primary mouse antibody anti- $\alpha$ -tubulin and secondary anti-IgG-FITC (green), and the nuclei was stained with DAPI.*

node defines the cross sectional orientation. Beam elements are 6 degrees-of-freedom elements allowing both translation and rotation at each end node. Beam elements offer additional flexibility associated with transverse shear deformation between the beam's axis and its cross-section directions. That is the primary difference between beam and truss elements.

Interaction between all the components of the CSK is ensured at the cortex, where the elements of microtubules and actin bundles are connected by sharing the same end nodes (Figure 3.3).

### 3.2.2 Material properties

Homogeneous, isotropic and elastic material properties were assumed for all the components and were taken from literature (summarised in Table 3.2). Cytoplasm and nucleus were assigned Young's modulus ( $E$ ) of 250 Pa and 1 kPa, and Poisson's ratio ( $\nu$ ) of 0.49 and 0.3, respectively. Actin cortex was simulated considering  $E$  of 2 kPa and  $\nu$  of 0.3. Cell membrane was

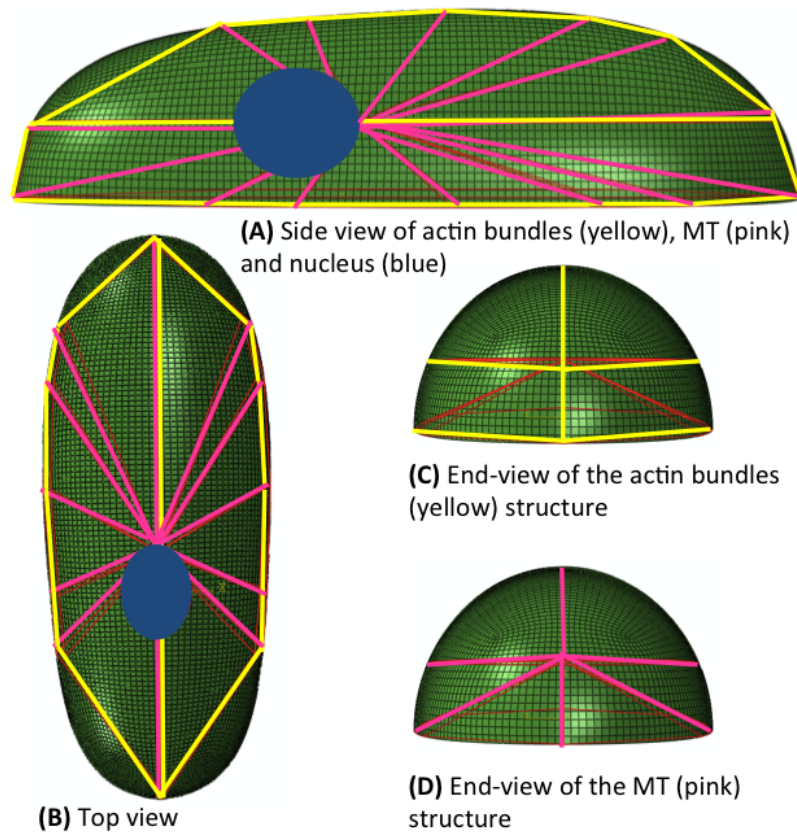


*Figure 3.3: Projections of actin bundles and microtubules distribution in the cell model with respect to the nucleus. (A) side-view of actin bundles (yellow) and MT (pink) with respect to the nucleus; (B) Top-view of actin bundles (yellow) and MT (pink), with a similar distribution of the discrete CSK components as it is found in the bottom-view (not shown); (C) End-view distribution of actin bundles; and (D) End-view distribution of MT.*

not considered in this model since it is softer and thinner than the adjacent actin cortex and thus, its material properties were not considered to have a significant impact to resist mechanical deformation.

*Table 3.2: Material properties*

Cell component	$E$	$\nu$	Reference
Cytoplasm	0.25 kPa	0.49	(Mathur et al., 2001)
Nucleus	1 kPa	0.3	(Guilak & Mow, 2000)
Microtubules	2 GPa	0.3	(Stricker et al., 2010)
Actin cortex	2 kPa	0.3	(Pampaloni & Florin, 2008)
Actin bundles	341 kPa	0.3	(Deguchi et al., 2006)

The mechanical behaviour of living cells is mainly defined by the polymer fibres of the CSK that contribute to the mechanical stiffness of the cell (Karcher et al., 2003; Maurin et al., 2008; Mijailovich et al., 2002). The different element types for actin bundles and microtubules were chosen to better represent their idealised structural role.

Microtubules are a very stiff structure with  $E$  of 2 GPa and  $\nu$  of 0.3. Although microtubules were thought to have compression-only behaviour, there is now evidence that they can buckle and appear highly curved in living cell, when compression reaches critical values (Schaap et al., 2006; Stamenović & Coughlin, 1999; Stamenović et al., 2002). Thus, microtubules were simulated to resist both compressive and tensional forces.

Stiffness of actin bundles varies depending on both the number of fibres aligned together and on the mechanics of the type of actin binding proteins that holds them together. In the current model, actin bundles were considered to have  $E$  of 341 kPa and  $\nu$  of 0.3. Actin bundles are reported as

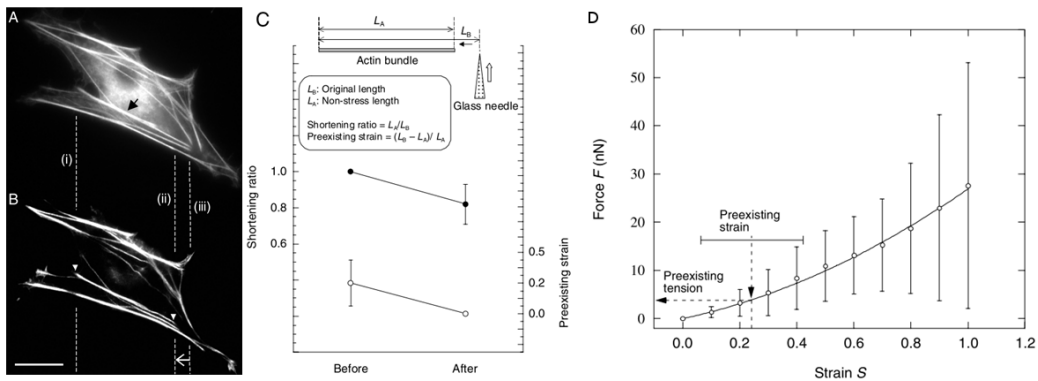


Figure 3.4: Methods to calculate tension in actin bundles of endothelial cells from their level of pre-existing strain, using glass needle manipulation (Deguchi et al., 2005). GFP-actin microscopic images of a cultured endothelial cell (A) before and (B) after the glass manipulation needle, where the right end of the actin bundle was displaced from (iii) to (ii) due to a release of pre-existing tension. (C) Shortening ratio and pre-existing strain before and after cutting the fibres. (D) Relationship between tensile force and stretching strain, where error bars indicate standard deviation ( $N = 6$ ).

rope-like behaviour, and were modelled to resist only to tensional forces. These fibres have an inherent tensile stress and are internally prestressed even without application of an external load. Thus, these are the components in the model responsible for generating contractile forces. Previous experimental studies reported pre-existing strain values of  $0.24 \pm 0.18$  and pre-existing force level of 4.08 nN (Deguchi et al., 2005) in actin filaments. The force-strain relationship measured by the previous authors (Figure 3.4) was used to calculate the mechanical properties for the actin bundles of the current model: Young's modulus and prestress. The value of 82 kPa, calculated from experimental studies (Deguchi et al., 2005; Kumar et al., 2006) was introduced in the model using UMAT subroutine of Abaqus (Simulia,

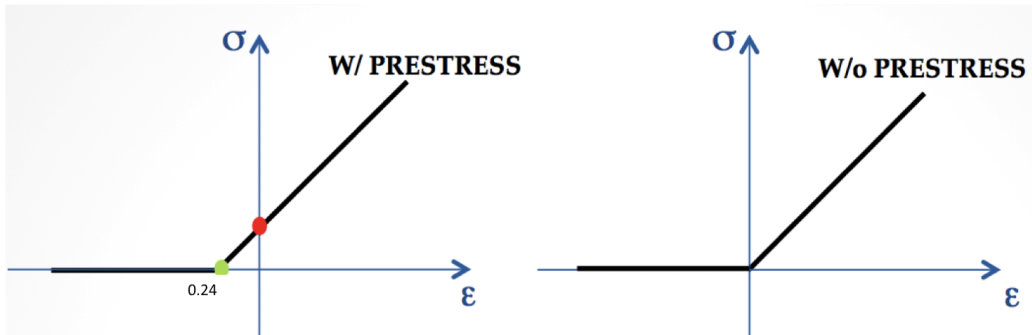


Figure 3.5: Stress-strain relationship defining the mechanical behaviour of actin bundles with and without prestained conditions. The green dot defines the amount of prestrain defined for the actin bundles in the subroutine UMAT, whereas the red dot defines the resultant prestress (i.e., the stress for zero deformation), which is imposed at the beginning of the FE simulation.

USA), which was modified to define the stress-strain relationship for actin bundles taking into account the initial state of stress caused by the 24% of initial strain of the bundles (see Appendix A). The actin cortex, the other actin network in the model, was modelled as merely linear elastic and does not have a prestrain.

UMAT is the Abaqus subroutine used to define the mechanical constitutive behaviour of a material, which is called at all material calculation points of elements at the end of each increment for which the material definition includes a user-defined material behaviour. In this case the material Jacobian matrix is calculated for the actin bundles, where the UMAT subroutine is customised for the application of a prestrain of 24%. Briefly, at the beginning of the simulation, for zero deformation of the actin bundles, a prestress of 82 kPa is defined. During the following increments, if the deformation of the bundles is higher than 24%, then the stress-strain relationship is linear; and if the deformation of the actin bundles is smaller than 24%, then

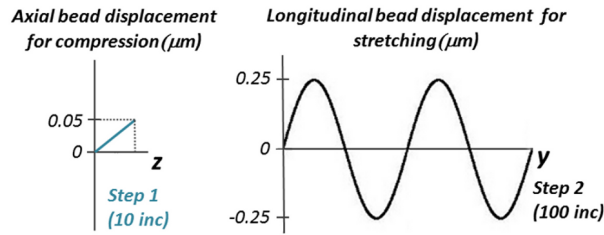


Figure 3.6: Loading conditions applied to the model cell for the simulations of compression followed by stretching.

the resultant stress in these elements is zero, as it can be seen in Figure 3.5. All the actin bundles in the model are prestrained to the same level, for simplification.

### 3.2.3 Loads and boundary conditions

Indentation and stretching was simulated with the inclusion of a microbead on the top of the single adherent cell model. A  $4.5 \mu\text{m}$  diameter bead was modelled above the nucleus to exert different external mechanical stimuli and measure the reaction force and deformation of the cell for the different loading conditions (Figure 3.1 A). The bead was moved toward the cell in the axial direction to establish the contact and further compression, followed by stretching, see Figure 3.6. The axial displacement of the bead was set at  $0.5 \mu\text{m}$  for compression, simulating experiments with AFM. The bead was then moved horizontally with a sinusoidal movement with amplitude of  $0.25 \mu\text{m}$  to stretch the cell and simulate the movement of the bead in MTC experiments (Mijailovich et al., 2002). From the stretching, longitudinal forces are computed.

A mathematical model for the *quasi-static*, non-linear contact problem between two independent elastic bodies, the bead and the cell, was consid-

ered. The contact problem between the two bodies was solved using the Lagrangian algorithm following the pure Lagrange method. To establish the contact between two curve surfaces, the Lagrangian algorithm is constantly switching between the states of contact and non-contact. On one hand, this fact makes the algorithm computationally heavy but on the other hand it provides excellent accuracy on non-interpenetration of the two contact surfaces. Lagrange Multipliers are identified as the contact force applied into the cell. This value must be large enough to stabilise the contact but at the same time small enough to prevent the interpenetration of one contact surface against the other. Therefore, this algorithm requires numerically zero interpenetration values, which give the essential stability to the process. The validation domain of this formulation is the domain of the geometric and material linearity. Together with friction coefficient of 0.001, the functions *approach* and *stabilise*, control rigid body motion by providing enough damping to eliminate the rigid body modes without having a major effect on the accuracy of the solution. These functions introduce the controls for the non-linear contact problem that may cause large stresses and strains. Therefore, they correct and account for these large deformations.

Contact fully bonded properties were established between the cell surface and the microbead to guarantee that the bead never detach from the cell. This is similar to experiments of AFM or MTC, where beads are coated with suitable molecules that bind to integrins on the cell surface, providing a direct and firm link between them.

The nodes at the bottom part of the cell were constrained in all degrees of freedom to simulate a cell fully attached to a rigid substrate. At the beginning of the simulation, the nodes for CSK interaction (i.e., the end nodes of actin bundles that are connected with the end nodes of the microtubules) were

constrained in all degrees of freedom for the initial convergence of the analysis due to the imposed prestress. In this way, the initial length of the actin bundles is maintained for the first increment when prestress is calculated in the analysis.

### 3.2.4 Finite element simulations

The FE method was used to evaluate force and deformation of the cell when external forces were applied, and how those forces were transmitted inside the cell. The deformation of the different cell components was analysed in terms of major principal strains, which was calculated in Abaqus using the UVARM subroutine (see Appendix B). The subroutine UVARM calculates the major principal strains by selecting the maximum absolute value of the computed maximum and minimum principal strains for each element, which is now the major that it is shown for that element with the correct signal, indication if the element is more in compression or in tension.

Sensitivity analysis for force and cellular deformation were performed to evaluate the effect of considering discrete elements on the resultant cell force. Mesh-independence of the results was assessed by increasing the number of continuum elements in the mesh.

Cell contractility was also evaluated with the FE method by comparing reaction force of the cell with and without prestress in the actin bundles. The effect of including physiological values of prestress was investigated with a parametric analysis. Different values of prestrain in the actin bundles were varied from 0, 1, 10 % and compared to the physiological value of 24%.

Lastly, the position of the bead was changed on the top of the cell to evaluate the effect of local indentation on the force obtained. The local indentation was changed from a position above the nucleus to the right to a

maximum of  $8\ \mu\text{m}$  from the initial position, as represented in Figure 3.7. This is particularly important to investigate in this study due to the heterogeneity of the cellular components that might be responsible for variation of forces in different parts of the cell.

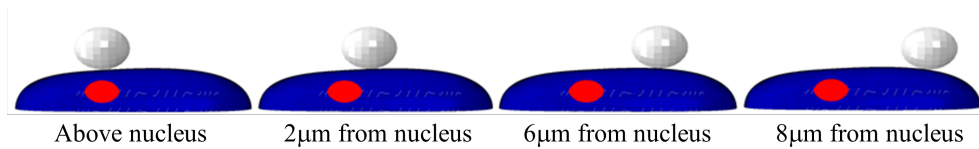


Figure 3.7: Different bead positions for indentation on the top of the cell.

### 3.3 Results

Cell forces and deformation to resist compression and stretching were evaluated by looking at the importance of incorporating different components of the cell (such as the cortical and deep CSK components), but also other factors (such as prestress, and different external stimuli). Perspectives, assumptions and limitations of computational modelling of single-cell under physiological load will be discussed based on these numerical results for an accurate representation of the mechanical behaviour of adherent cells.

#### 3.3.1 Mesh-independence of the results

One of the first principles of the FE analysis is to ensure mesh-independence of the results for a good approximation of the solution and therefore, valid results. Mesh size was increased from a coarse mesh (with 4546 elements) to a finer mesh (with 168188 elements), while the total time of simulation, including compression and stretching, was analysed concurrently (Figure 3.8). Three other mesh sizes were tested considering 21916, 75516 and 112382

elements in the mesh. Convergence of the results was analysed in terms of maximum *von Mises* stresses obtained for both compression (first step of the analysis) and stretching (second step of the analysis).

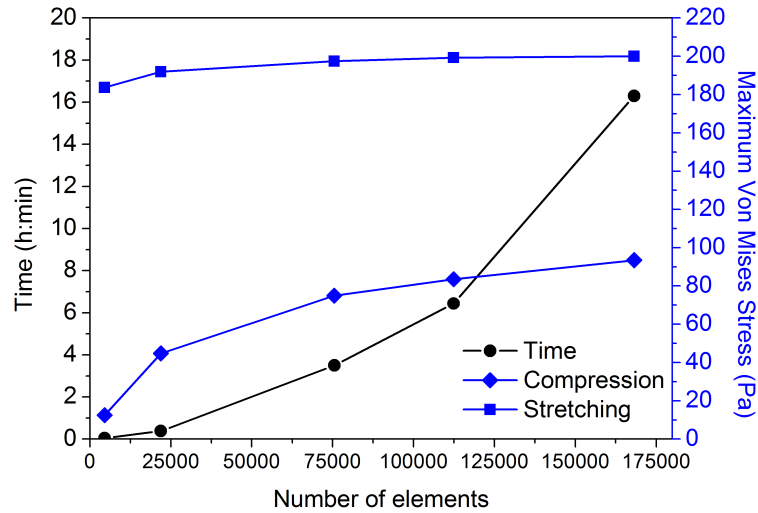


Figure 3.8: Mesh-independence of the results using continuum hexahedral elements.

When the cell was compressed, stress increased with mesh refinement and therefore, it was highly affected by the mesh size. The results in terms of stress obtained during stretching tend to converge very quickly and can be considered independent of the mesh size. Therefore, to decide on the mesh to use for further studies the author looked at the best relation between convergence of the results during compression and total running time of the analysis, for the different meshes tested. Although, the plateau of convergence was not achieved for the stress results in compression, the results obtained with the three finer meshes tended to become closer to each other. On the other hand, the time of the simulation increased exponentially for the two last finer meshes tested, and the gain in terms of convergence for the

results did not compensate the running time of the process from the model with 112382 elements upwards. The best optimisation between convergence of the results and time of simulation was achieved using the cell model with 112382 solid elements. Therefore, this was the mesh used for further studies.

### 3.3.2 Prediction of cell deformation

Measuring deformation of cells as a response to external stimuli is a common way to evaluate and characterise cell mechanical properties. With this model the author can analyse if cell deformation is associated with either specific components of the CSK or the remaining cytoplasm, by looking at the strains in the individual elements of the model (Figure 3.9). Strains observed in the cortex, nucleus and cytoplasm reached a maximum of about 40% when the cell was compressed. During stretching, maximum strain was about 74%. These high strains are due to localised deformation of the nodes caused by the attached discrete elements of the cytoskeleton. Low strains in microtubules are predicted by the model, which can be explained by microtubules' high rigidity. Depending on the stimulus (compression or stretching), microtubules would be more under compression (blue) or under stretching (red). Although maximum and minimum principal strains in the microtubules have the same limits in compression and stretching, microtubules, that were sustaining compressive loads during compression, become more under tension after stretching. Higher strains were observed for the actin bundles comparing to strains observed in microtubules highlighting the effect of this component on cell deformation. Actin bundles have the same effect on cell deformation during compression and stretching since their compressive and tensile strains are in the same range of magnitude.

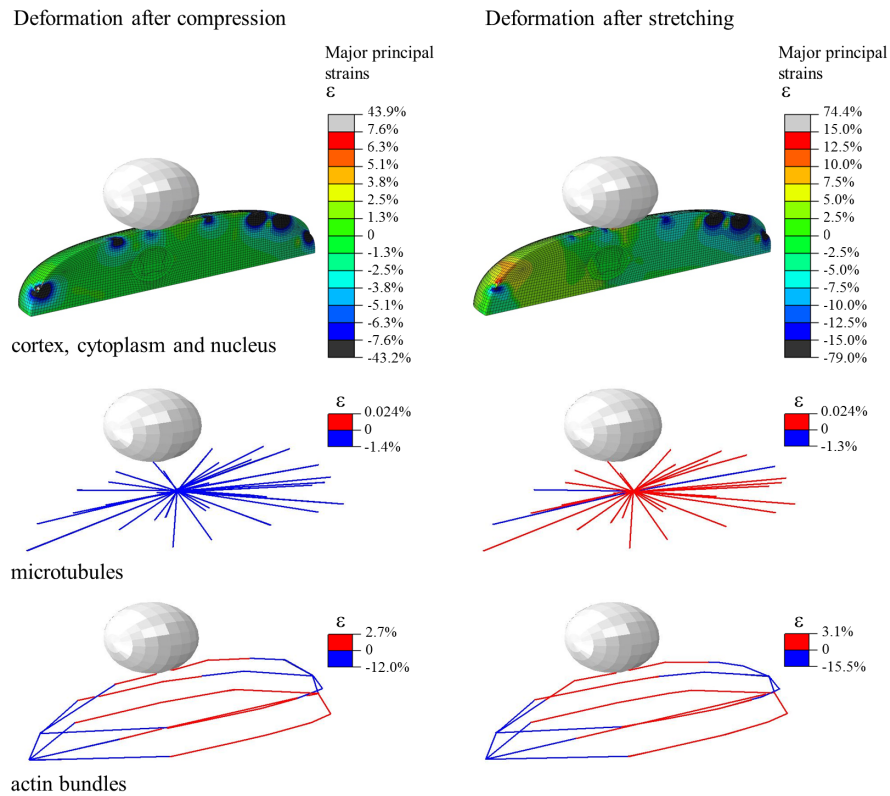


Figure 3.9: Deformation of the different cellular components. Top represents strain distribution in the cortex, cytoplasm and nucleus after compression and stretching; middle shows deformation of microtubules after compression and stretching; and bottom shows deformation of actin bundles upon compression and stretching.

### 3.3.3 Distribution of forces in the cell

Analysis of the distribution of forces in the bottom area of the cell is important for the understanding of how forces are transferred to the ECM. The components of the CSK play an important role in force transduction and following that thought, the distributions of forces were evaluated with and without the inclusion of the discrete elements of the CSK in the model (Figure 3.10). Cell forces were higher when the CSK components were present in the model, for both compression and stretching. On one hand, this observation emphasises the importance of incorporating discrete elements of the CSK for an accurate representation of cellular behaviour. On the other hand, higher forces developed by the cell are a consequence of overall smaller deformation that the cell undergoes when the CSK components are present. In the presence of discrete CSK components, higher forces were concentrated in the nodes of interaction between microtubules and actin bundles. Also, during stretching, higher forces were localised and spread all over the cell periphery. The maximum force value registered in the cell was about 11 nN for both stimuli of compression and stretching in the presence of the CSK components, while it was  $9 \times 10^{-3}$  nN for compression, and  $5 \times 10^{-1}$  nN after stretching, without the CSK components in the model.

### 3.3.4 Cell contractility

For the understanding of cell contractility, the maximum force of cell (sum of the force obtained in all the nodes) with and without prestress was compared for both compression and stretching. Application of physiological prestress in the model yielded important changes in force (see Figure 3.11 A).

During compression, the resultant maximum axial force obtained was

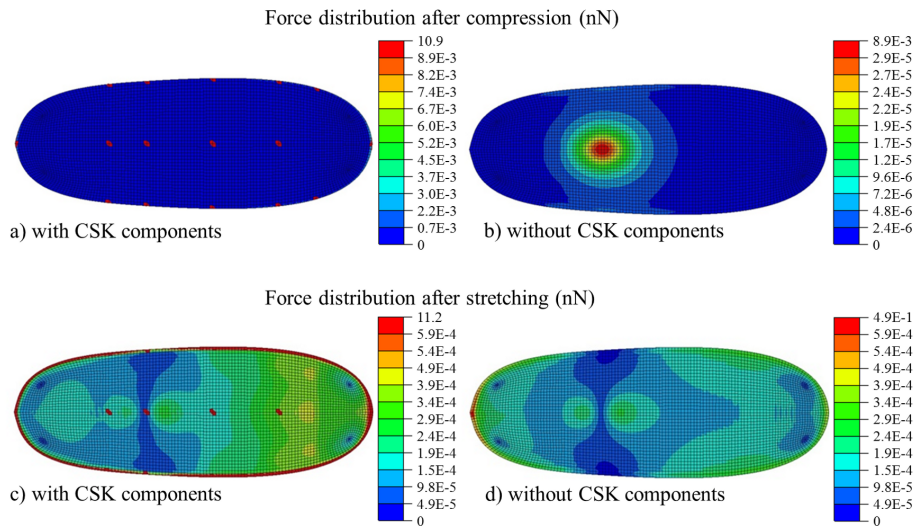


Figure 3.10: Distribution of forces in the bottom part of the cell after (A, B) maximum compression, and (C, D) maximum stretching, considering whether CSK components are present. Values of force for maximum stretching were measured when bead is displaced to the right in the y axis.

similar for the models with and without prestress. Prestress is associated with prestrain of actin bundles in the model. Further explanation of this result will be investigated in the following chapter when the role of actin bundles to resist compression is analysed. During stretching, the maximum longitudinal reaction force in a cell without prestress was 3.0-times lower than a cell with prestress. The rigidity of the cell was higher when prestress was included. The inclusion of prestress, through strain increase of 24%, showed an increase of 67% in reaction force of the cell in stretching, associated with an increase in stiffness to the same amount of stimulus. Modelling prestress is therefore very important for an accurate description of the mechanical behaviour of actin bundles, and consequently of the entire cell.

The maximum axial and longitudinal forces were computed for each in-

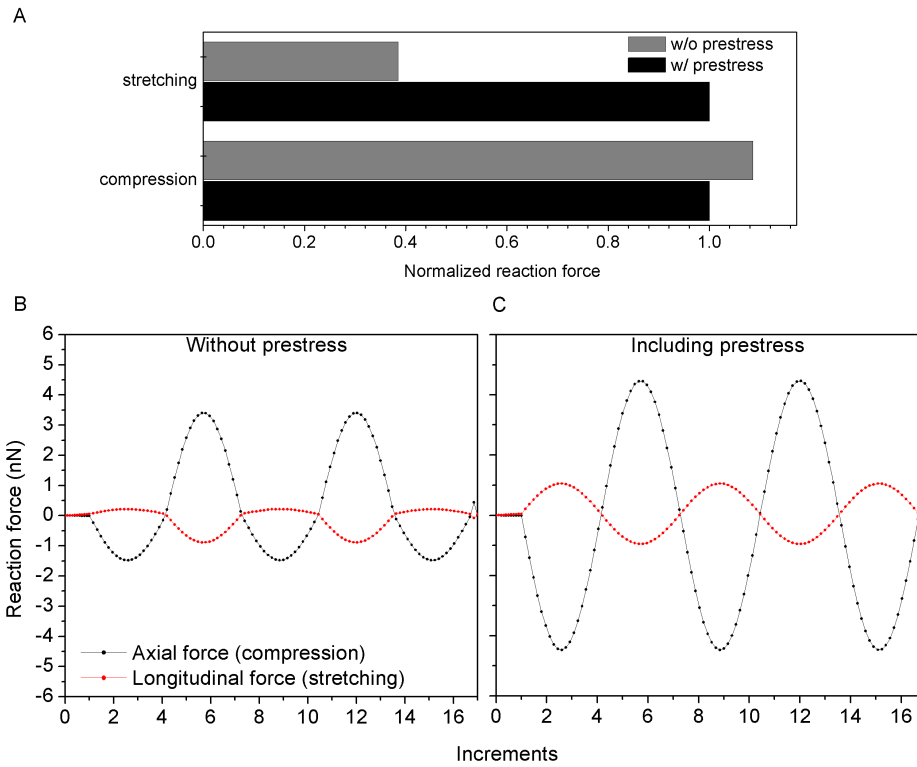


Figure 3.11: Effect of prestress on cell response. (A) Comparison of cell response with and without the initially state of stress, under compression and stretching. Reaction force of the cell for the different models is normalised to the base model including prestress. (B, C) The effect of prestress on reaction force during the cycle of load, under compression and stretching.

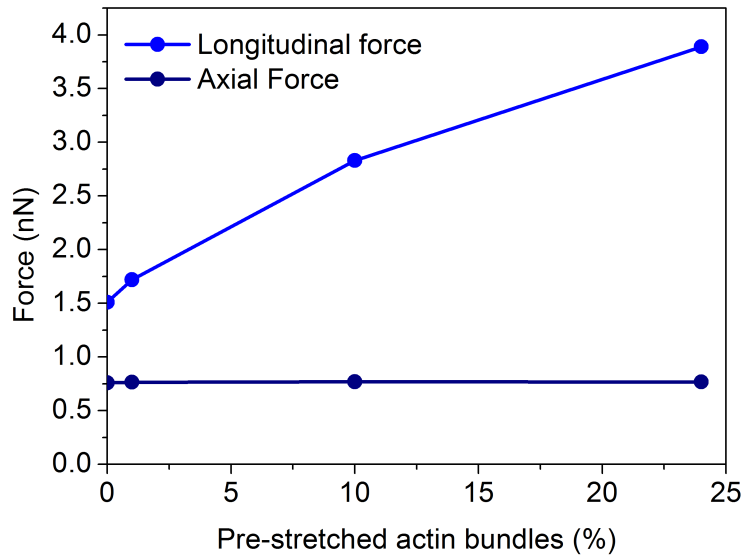


Figure 3.12: Variation of prestrain in the actin bundles and the effect on cell contractility for compression and stretching.

stance of the stretching cycle with and without prestress, see Figure 3.11 B and C. During the cyclic stretching, the cell underwent compressive and tensional forces as the bead was moved from right to left and *vice-versa*, and the amplitude of the axial and longitudinal forces was not symmetric without considering prestress. This asymmetry was expected due to the behaviour of actin bundles, which only resist tensile forces. Since they do not resist compression, their reaction was zero when compressed. When prestress was included, both axial and longitudinal reaction forces became symmetric. This symmetry remains when prestress is included, as confirmed with the current model, as long as the value of the prestrain is high enough to overcome the external stimulus applied by the bead that compresses the actin bundles. When prestress is included, actin bundles are prestrained and thus, the fibres take less time to reach the point where they start to sense tensile forces.

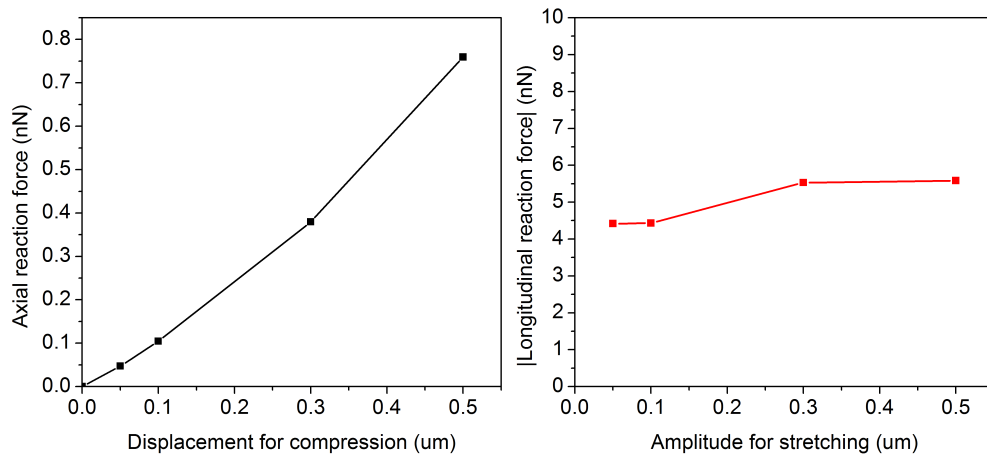


Figure 3.13: Effect of variation of indentation depth on (A) axial forces after compression and (B) longitudinal forces after the cycle of stretching.

The number of actin bundles sustaining compressive loads is thus lower when prestress is modelled, resulting also in higher reaction force. Such changes occurred not only at the initial step but during the entire cycle. Then, if the longitudinal displacement applied is too high compared to the prestrain, actin bundles should be all undergoing tensile forces and asymmetry should become visible again (this is observed in the following section in Figure 3.14, when the displacement in stretching is increased).

Variation of the level of prestrain in the actin bundles changed cell contractility during stretching but had no effect during compression when the cell was fully constrained, keeping constant the amount of compression and stretching (Figure 3.12 A). Since actin bundles do not resist compressive loads, the reaction force of the cell was kept constant for variation of prestress during compression. During stretching, increasing of prestress levels until the physiological values of 24% increased the reaction force of the cell progressively in a non-linear way.

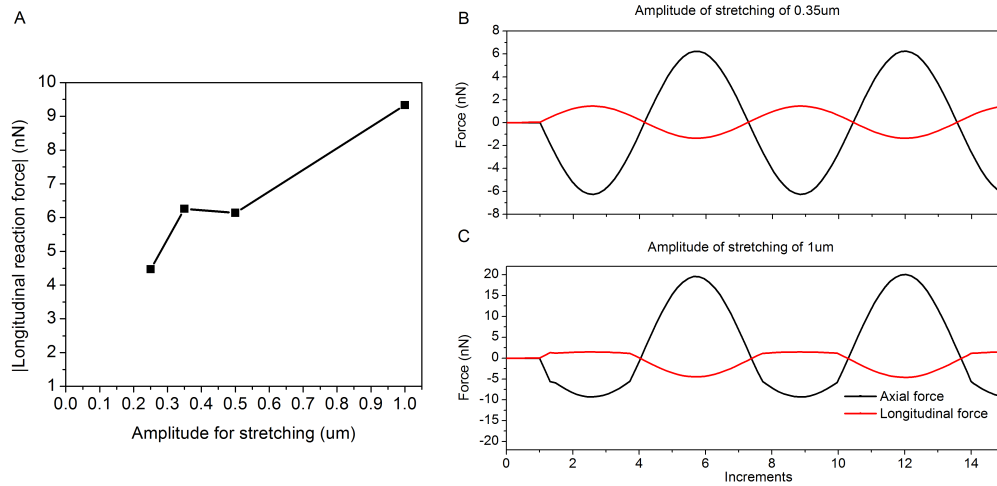


Figure 3.14: Effect of the variation of the amplitude of stretching on cell forces. (A) Variation of longitudinal forces. Cycle of forces obtained (B) using  $0.35 \mu\text{m}$  and (C)  $1 \mu\text{m}$  amplitude during stretching.

### 3.3.5 Sensitivity study

Previous results on the relationship between prestress and external applied stimuli showed the importance for conducting a sensitivity analysis on the effect of varying the amount of stimuli of compression and stretching. This was performed also to understand if the step of stretching that follows the step of compression are independent from each other. For different values of compression, the resultant axial response of the cell increased in a non-linear way, as shown in Figure 3.13. This non-linearity was more pronounced for small values of compression, which might be related to the degree of embedding to establish contact accurately. The results showed that the degree of bead embedding affects the results during compression but not during stretching.

In this study, analysis for compression is followed by a step of stretching. Variation of compressive forces showed no major influence on the results during the stretching cycle, see Figure 3.13 B, and was almost constant for

stimuli in the physiological range tested. This emphasised the fact that application of loads in the current study is step-independent, as required in a FE analysis. This shows that it is possible to study the response of a cell in stretching despite cell-bead degree of contact. On the other hand, varying the amplitude of stretching from  $0.25\ \mu\text{m}$  to  $1\ \mu\text{m}$  also changed the reaction force of the cell in a non-linear way (Figure 3.14). This fact is again related to the non-linear behaviour of actin bundles and prestress (whether the amount of actin bundles compressed and stretched varies in relation to the amount of stretching), and a "prestress plateau" was identified for the relationship between load and prestress, (Figure 3.14 A).

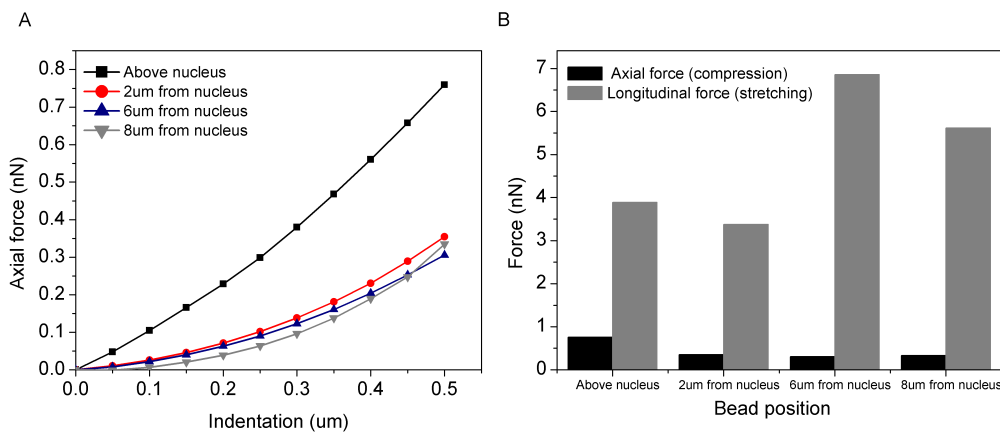


Figure 3.15: Cell force considering different indentation positions. (A) Force-indentation relationship for different bead positions. (B) Maximum axial and longitudinal forces for different bead positions, for indentation of  $0.5\ \mu\text{m}$  and shear amplitude of  $0.25\ \mu\text{m}$ , respectively.

Lastly, the indentation position-dependence on the results was evaluated by changing the bead position on the top of the cell with respect to the nucleus and the resultant axial force was measured. Higher forces were registered when the bead was located above the nucleus, while forces decreased

when the location of indentation was further away from the top of nucleus, as shown in Figure 3.15 A. However, forces did not change considerably when the bead was in other positions away from the nucleus, showing that the rigidity of the nucleus has an important effect on the amount of forces developed by the cell to resist external loads. The cell response in stretching varied in a non-uniform way for different bead positions (Figure 3.15 B), which might be related to the position of the individual elements of the CSK structure other than the nucleus, to resist stretching.

## 3.4 Discussion

### 3.4.1 The cell model concept

A FE model of an adherent cell was developed, including all the structurally relevant components to simulate the response of cells to different mechanical stimuli. The developed model is a fusion of the contrasting theories to describe cells, the continuum and discrete approaches, and includes the nucleus and a continuum cytoplasm with actin cortex, discrete actin bundles and microtubules. A key feature of this model is the structural stability defined for the CSK, that accounts for the interconnectivity between the elements, as well as allowing changes of form and organisation of the individual components, without collapsing the cell shape if they are removed. This type of fusion of models was previously done by McGarry & Prendergast (2004) by integrating continuum models with the tensegrity theory of Ingber (1997), where the CSK is represented to behave as a prestressed interconnected network.

However, in order to have a stable structure, the concept of tensegrity defines that all the elements of the model must bear either pure compression,

such as the microtubules, or pure tension, such as the actin filaments, in order to have mechanical stability, with tensional prestress, which allows cables representing actin to be rigid in tension (Ingber, 1997). Thus, no bending or torsion is allowed in these elements, as they all have to be straight. The loads can exclusively be applied to the joints of the interconnection between the elements. Although the tensegrity structure provided understanding of the relation between cell mechanics and biological functions (Ingber et al., 2000), the molecular structure of the individual components of the CSK, that is essential for several cellular processes, is not taken into account in these type of structural models.

The current model improves this structural concept, as there is no restriction on the spatial distribution of the fibres. A more accurate behaviour for the microtubules is accounted for, where they can bend and resist to both compression and tension, as shown experimentally (Schaap et al., 2006; Stamenović & Coughlin, 1999; Stamenović et al., 2002). The application of forces is not restricted to the nodes of interconnection between discrete elements and a more realistic representation of the application of loads as in the experimental methods is achieved. The concept implemented to define the CSK structure in this FE model describes prestress as an essential parameter to generate initial force and maintain cell shape, although not essential to define the interplay between discrete components. Therefore, the simplified spatial morphology for the CSK structure resembles that of a living cell.

The current model accounts for physiological distribution of the CSK components, and incorporates at the same time, the role of other components such as the nucleus and cytoplasm, which are represented as the continuum, and were shown to have a mechanical role when modelling cellular behaviour. Microtubules act as a transportation system and as stabilising

elements for other cytoskeletal systems (Maniotis et al., 1997; Pourati et al., 1998). Therefore microtubules are distributed along the whole cell in a star-shape connecting the exterior of the cell at the cortex level with the nucleus in the interior of the cell. The structure of actin cortex and bundles are interconnected with the structure of microtubules for force transmission and therefore, forces sensed in the entire CSK structure are transmitted to the continuum elements of the cytoplasm and nucleus.

However, the effect of the nucleus for signalling transmission is not considered in this model since it requires a multi-scale model including the nucleoskeleton discrete structure to accurately represent the biological effect of the forces sensed at the nucleus level. Intermediate filaments, the third type of CSK fibres, were not considered in the current model. Intermediate filaments are thought to be involved in transferring the information sensed by mechanical receptors to the nucleus to process that information (Fletcher & Mullins, 2010). Though they impart mechanical integrity to cells (Fletcher & Mullins, 2010; Wang, 1998) for higher deformations (Janmey et al., 1991; Wang & Stamenović, 2000), their mechanics are still controversial and poorly understood (Fudge et al., 2003). Therefore, intermediate filaments are not accounted for in this model.

Material properties used to represent the cell in this model were taken from the literature and were previously used in other cell models and experimental studies. However, the mechanical properties for each cell component of the model are not necessarily from the same cell type. Therefore, a parametrical study of the effect of considering different mechanical properties is of utmost importance, and chapter 5 will be dedicated to this study in combination with experimental data to either support or refute the numerical findings.

### 3.4.2 Prestress in actin bundles

Physiological value of prestress in the actin bundles is included and the structural behaviour of the different actin networks, such as actin cortex and actin bundles, are considered and modelled separately. Prestress defines cell contractility, an initial state of equilibrium in the absence of external forces (Deguchi et al., 2005; Ingber, 2003b; Kumar et al., 2006; Stamenović, 2006; Trepap et al., 2007). Prestress is associated with the different length of the actin with and without the two ends attached to the ECM, that is seen as actin inside and outside the cells: experiments where filaments of actin were isolated from the cell showed that once outside, the filaments decrease in length compared to when inside the cell (Deguchi et al., 2005; Stamenović, 2006). The filaments inside the cell are prestrained and this induces an initial state of stress in the cell.

The inclusion of prestress has shown an increase in reaction force of the cell in stretching, which might mean an increase in stiffness in response to the same amount of stimulus. Additionally, the increase in reaction force registered due to an increase of prestrain of 24% was about 67% when the cell was stretched. Application of physiological prestress in the model yielded changes in force and strain magnitude for the entire cell. Previous experimental studies have also shown the importance of prestress in giving the cell the structural stability to resist cellular deformation (Deguchi et al., 2005; Kumar et al., 2006; Wang et al., 2002).

However, during compression, no changes in cell force were predicted with this model in opposition to what has been observed experimentally in literature for different cell types showing different levels of contractility: more contractile cells exhibit higher compression forces (Caille et al., 2002; Ofek et al., 2009; Peeters et al., 2004; Weafer et al., 2013), as discussed in

detail in the literature review of this thesis. The author believes this lack of correlation between cell contractility and compression forces is due to the configuration/orientation of the actin bundles used in the simulations of this study, which will be further discussed in chapter 5.

The prestress used in the actin bundles of the current model was calculated from the 24% of prestrain measured experimentally (Deguchi et al., 2005). Other authors using different methods, obtained prestrain values in the range of 15-25% (Kumar et al., 2006). Previous numerical simulations of cellular mechanics also accounted for prestress although considering only 1% of actin fibres prestrain and therefore, do not account for the values measured in living cells (De Santis et al., 2011; McGarry & Prendergast, 2004). The reason for this choice might be related to the computational time required to run simulations with such complexity, where prestress was included simulating changes in the length of the actin fibres at the beginning of the simulations. However, in the current model physiological prestrain and prestress values were implemented using a UMAT subroutine of Abaqus, where the entire mechanical behaviour of the actin fibres (stress-strain relationship) was manually redefined. This methodology is less likely to introduce discontinuities at the beginning of the simulations and thus, it is the first model accounting for higher values of prestress that are required for an accurate description of the mechanical behaviour of actin bundles.

### **3.4.3 Relationship between deformation, force and focal adhesions**

Force distribution and deformation of an adherent cell were predicted with this 3D model, whose CSK geometry was based on observations from the distribution of living cell components. The idealised geometry and elastic

properties were shown to be sufficient to explore the static response to the imposed loads. Discrete elements, representing CSK fibres, were merged with the continuum and therefore, localised high strains were obtained in the continuum elements of the cytoplasm and cortex, caused by the attached discrete elements of the CSK. The location of these high strains was on the nodes of interaction between CSK components at the cortex level. Therefore, it is important to see if these large strains that are equivalent to large stresses do not introduce discontinuities for the model accuracy: if the tension in the shell cortex in the current model is below the surface tension measured in cell membranes then, the shell would withstand those deformations without breaking or collapsing. The value of maximum von Mises stresses measured in the cortex of the model cell was 433.3 Pa, which is far below the documented values of 2400 Pa for membrane surface tension (discussed in the review of [Lim et al. 2006](#)). Strains in the remaining cytoplasm and nucleus were low, and below 5%. Moreover, low strains were also registered at the components of the CSK. The very low strains registered in microtubules was due to their high rigidity and higher strains on actin bundles suggested the role of this component on cell deformation.

Heterogeneous distribution of force on the bottom of the cell was obtained when the discrete elements of the CSK were introduced in a homogeneous elastic continuum model. The bottom part of the cell was fully constrained, simulating the contact with a rigid substrate. Higher localised forces were obtained on the end nodes of interconnection between actin bundles and microtubules, forming punctuated concentrations of force in the periphery of the cell. The maximum value of force obtained was 11 nN for both stimuli of compression and stretching. This high concentration of forces is very likely associated with the formation of focal adhesions, which connects integrins

from the substrate with the CSK in the interior of the cell. Previous experimental studies have shown that the stress and strain manifested within an adherent cell may be regionally concentrated, resulting in peak values that significantly exceed the magnitude of the applied stimuli (Han et al., 2004; Stops et al., 2008). A study to understand the influence of cell's spreading area and substrate stiffness presented evidence that traction forces and FAs have a close relationship in their response to mechanical cues. Also, average forces at FAs were measured in the range of 5-20 nN depending on the substrate stiffness (Han et al., 2012). Force measurements using elastic micropatterned substrates have shown that the force transmitted by a single adhesion lies within the magnitude of 10 nN (Balaban et al., 2001). Other experimental measurements of mechanical coupling between cell and substrate using traction force microscopy indicated values in the same order of magnitude (Chen et al., 2003; Chicurel et al., 1998), which corroborates the values obtained with the current model.

The preferential location for the formation of the focal adhesion complexes can be predicted by the numerical results, including the edge of the cell and the nodes of the CSK for force transmission to the substrate. The computed distribution of the force that the cell develops to resist the external stimulus in the presence of the CSK, directs the formation of focal points, corresponding to the end-nodes of the CSK and the edge of the cell. The fact that higher forces were registered when the discrete elements of the CSK were included in the cell model indicates the importance of these elements in the cell to resist mechanical perturbations from the exterior. Thus, the CSK in addition to FAs, are essential origins of local stresses in the cell. In accordance with the numerical results of the distribution of forces in the current study, Trichet et al. (2012) observed the highest traction forces as well

as the largest focal adhesions in the proximity of the cell edge and their results provided evidence for a cytoskeleton-based rigidity-sensing mechanism to respond external forces.

Furthermore, for the cell shape considered in the model, forces developed in the bottom of the cell in response to stretching tend to be more concentrated at the periphery, with higher concentration in the two cell extremities defining an axis of orientation in the direction of the applied stretching. This distribution of forces indicating a potential preferential cell orientation is supported by the cell polarisation theory (Besser & Safran, 2006; Rehfeldt & Discher, 2007; Zemel & Safran, 2007). This theory defines that cell orientation is governed by a contractile force dipole along the axis of orientation defined with respect to the applied force. The dipoles defining cell polarisation are generated either by forces applied externally or generated internally due to prestress (Zemel & Safran, 2007). Experiments in favor of this theory showed that for static or *quasi-static* strain, cells generally align parallel to the direction of principal strain (Collinsworth et al., 2000), while cyclic strain drives a near-perpendicular orientation of cells (Kurpinski et al., 2006; Wang et al., 2001a). The local tensile forces that were originated in the extremities of the discrete CSK elements can be seen when the CSK was modelled and these forces were higher when prestress was modelled in response to shearing, as discussed before. Even though the actin bundles in the model cell were not all aligned in the same direction, it is still possible to see a preferential direction of higher local forces in the cell model that relates prestress, CSK and FAs obtained in this FE analysis.

### 3.4.4 How cells sense and respond to different mechanical stimuli

The model was used to compute cell forces and deformation due to various *in vitro* mechanical stimuli, such as compression and stretching, as sensed by cells due to cell-cell interactions and under fluid flow conditions. When indentation of  $0.5\ \mu\text{m}$  was applied, the force of the cell in response to compression was  $0.76\ \text{nN}$ , 5-times smaller than the response when  $0.25\ \mu\text{m}$  stretching was applied ( $3.95\ \text{nN}$ ), considering the same order of magnitude of the stimuli applied to compress and to stretch the cell. This allows comparison of the effect of two single-cell stimulation methods, AFM and MTC, by application of the appropriate loading conditions in order to understand the biomechanical origins of differences in observed cell response. Other mechanical loading conditions could be applied in this model to study different mechanical environments or to compare different single-cell stimulation techniques, such as optical tweezers or microplate manipulation.

As an attempt to investigate as many cellular responses possible, different indentation positions and amplitudes of stimuli were considered to probe cells. Also, small and large application of forces were investigated for a more complete picture of cellular mechanical responses. In this case, a *quasi-static* cellular response was analysed. Variation of the compressive stimulus in the present study, showed that the results in terms of reaction force were dependent of the degree of bead embedding in the cell, which is in agreement with results reported by other authors using single-cell FE simulations (Karcher et al., 2003; Mijailovich et al., 2002). Nonetheless, the degree of embedding did not show to affect the response of the cell in stretching. A non-linear increase of the reaction force of the cell when the compressive stimulus is increased was verified. The deformation of the cytoplasm, nucleus and cortex

to  $0.05 \mu\text{m}$  compression was 2-times than when the cell was compressed at  $0.5 \mu\text{m}$  (a 10-times increase in the applied stimulus). By observing separately the deformation of each component of the CSK, changes in the compressive strains of the elements for different values of compression were not noticed. The explanation for this non-linearity of the results in the model is due to high concentration of tensile strains in the cortex below the bead due to changes in the contact surface as the bead approaches the cell, originated from the non-linear problem of contact between the two surfaces. Nonetheless, compressive strains in the cortex do not depend on the applied force. Therefore, the non-linearity caused by tensile strains does not affect the deformation in compression. Single-cell techniques apply localised forces and the response of cells to those local stimuli is dependent on the distribution of the cellular components inside the cell and the application of the external stimuli (Nawaz et al., 2012; Xu et al., 2012). The rigidity of the nucleus has been reported in literature as 4 to 10-times higher than the rigidity of the surrounding cytoplasm (Guilak & Mow, 2000). For this reason, the effect of the position of the bead was shifted on the top of the cell with respect to the position of the nucleus showing that the indentation position in relation to nucleus position can be critical for reproducible results. These differences in the force depending on the bead position depend on the spatial distribution of the CSK components.

### 3.4.5 Main conclusions

The developed computational model specifies the elementary nature of the mechanical components to resist external stimuli and provides quantitative predictions of the structural behaviour that is mainly attributed to the cytoskeleton, and verifies the initial hypothesis.

This new methodology predicts the capacity of the cytoskeleton to establish an elastic network to sense and transmit mechanical stimuli and explains the different published results obtained with different experimental stimulation techniques, which are important for understanding the biomechanical origin of differences in the observed cell responses. The multi-structural model predicts changes of force and strains in whole cell for specific external loads, compression and stretching, applied to simulate different experimental conditions. This new concept explains cell mechano-physics by establishing a relationship between cell rigidity and prestress for the specific loading conditions that were simulated in the study.

The structural stability defined for the actin bundles and microtubules in this model concept takes into account the interconnectivity between the elements, as well as allows for different organisation of the individual components independent from each other to be considered, without cell collapse. This is a unique feature of the model that was not considered in previous structural models. For this reason, the multi-structural cell model opens new perspectives in studying the correlation of cellular mechanical properties and stress distribution within particular CSK components.

---

## EFFECT OF CYTOSKELETAL DISRUPTION ON FORCE TRANSMISSION <sup>1</sup>

---

### 4.1 Introduction

In living tissues, adherent cells are constantly exposed to a variety of mechanical forces. Cells interact with their extracellular environment, from which they gather information that influences their behaviour. These mechanical interactions are involved in changes in cell physiology, shape, gene expression and thus cell fate (Janmey, 1998). The CSK provides a bridge between the extracellular matrix and the intracellular environment, and enables cell morphological changes through cytoskeletal remodelling. However, the central mechanism of intracellular components as either passive contributors or enhancers for force transmission remains unclear. It has been suggested that the CSK components may have distinct mechanical roles in the cell and that they might form the structure that provides stiffness in the cell (Ingber, 2003b). The specific role of the CSK components depends both on their

---

<sup>1</sup>This chapter includes results from the paper published as: S. Barreto, C. H. Clausen, C. M. Perrault, D. A. Fletcher, D. Lacroix, *A multi-structural single cell model of force-induced interactions of cytoskeletal components*, DOI: 10.1016/J. Biomaterials, 2013, 04.022

distinctive functions and cellular physiology. For example, the actin component of the CSK can be organised within the cell into a variety of linear bundles, two-dimensional networks and/or three-dimensional gels, according to cell function and needs (Deguchi et al., 2006; Fletcher & Mullins, 2010). The actin bundles of migrating cells, cross-linked by actin-binding proteins (ABPs), form filopodia; while adherent cells develop strong stress fibres in between focal adhesion complex for contact with the extracellular matrix. In order to investigate the role of specific CSK components as mechanoreceptors and in maintaining whole cell-integrity, it is important to know the real mechanical properties of the individual fibres of the CSK in different cell types. However, CSK components are not isolated, and there is a force balance between CSK networks, focal adhesions, ECM and other cellular components (Huang et al., 2004). Due to this integrated system in cells, isolating individual components of the cell and identifying their role for force transmission is challenging.

CSK-disrupting drugs have been used in combination with different cell stimulation techniques to study the mechanical role of each CSK component by selectively disrupting actin, intermediate filaments and/or microtubules. Though many studies have been performed *in vitro* to investigate the adaptation of the individual CSK components to mechanical stimuli (Charras & Horton, 2002a; Collinsworth et al., 2002; Kasas et al., 2005; Pelham & Wang, 1999; Stamenović et al., 2002; Takai et al., 2005; Wang, 1998; Wang et al., 2001b, 2002), results from different stimulation techniques cannot be compared and the contribution of the individual fibres for the cellular response remains unknown, as it was presented in chapter 2.

In order to characterise and compare the biophysical and biomechanical differences in the observed cellular responses from diverse single-cell stimula-

tion techniques, the cell model presented in the previous chapter would give the opportunity to investigate the discrepancies from the different single-cell stimulating techniques studies combined with CSK disruptors. The model assumes that individual CSK components can change form and organisation without collapsing the cell shape when they are removed and therefore, can investigate how the particular CSK components contribute to the mechanics of adherent cells.

The goal is to interpret the mechanical role of the different cytoskeletal structures by simulating different static loads that are applied experimentally using the broad range of stimulation techniques. The hypothesis is that each component of the CSK has a different mechanical role to resist different types of stimuli. To corroborate this hypothesis, force-indentation curves and Young's modulus ( $E$ ) of two cell lines, NIH-3T3 fibroblasts and U2OS osteosarcoma cells were measured with AFM. CSK-disrupting drugs, such as cytochalasin-D used to disrupt actin fibres and nocodazole to disrupt microtubules, were added to the cell media during AFM measurements. In this way, the different networks of the CSK are isolated to analyse their contribution to cellular mechanics under controlled conditions that are verified with microscopic imaging. When creating this model, while it is understood that the CSK has a spectrum of elastic and viscous properties, in addition to a capacity to contract and remodel, it has been hypothesised that in the static regimen, there is a dominant elastic component to the mechanical properties and as such, these elastic properties dictate the response of the cell to a greater extent than the viscous properties.

## 4.2 Material and methods

### 4.2.1 Numerical approach

The single cell model and material properties described in the previous chapter were used as a base model for the current study of the role of the individual CSK components.

Accordingly, to evaluate the mechanical contribution of the individual cytoskeleton elements, the different components of the CSK were removed one by one from the base model. Force-indentation curves and material properties from three different cell models ("without actin bundles", "without actin cortex" and "without microtubules") were analysed. In order to evaluate the importance of interactions between CSK components on cell response, three other models were built where CSK components were removed from the base model in combination of two ("cell only with microtubules", "cell only with actin bundles" and "cell only with actin cortex"). The results from the different models were compared with both the base model (used as the control model) and with a model without any of the CSK networks ("cell without CSK").

Results were evaluated in terms of reaction force of the cell and for direct comparison with experimental results, Young's modulus was calculated from the computed force-indentation curves, using a modified Hertz model ([Rosenbluth et al., 2006](#)), described below in Equation 4.1. Displacement of  $0.5 \mu\text{m}$  for indentation with the bead was applied for compression followed by  $0.25 \mu\text{m}$  in amplitude for the sinusoidal movement during stretching.

## 4.2.2 Cell culture and drug treatment

Fibroblasts are cells of the connective tissue involved in the synthesis of collagen, glycosaminoglycans and other components of the ECM that also play a critical role in wound healing. The 3T3 is a standard cell line of fibroblasts. The U2OS cell line was originally cultivated from human bone with osteosarcoma that exhibit epithelial adherent morphology, widely used in various areas of biomedical research.

Both fibroblasts (NIH-3T3) isolated from mice, and human osteosarcoma cells (U2OS-GFP actin) were cultured at 37°C in an atmosphere of 5% CO<sub>2</sub> in DMEM supplemented with 10% FBS and 1% PS. Cells were harvested after a brief exposure to trypsin and plated on acrylic-reinforced glass coverslips coated with human fibronectin (BD Biosciences, Franklin Lakes, NJ). After this, fibroblasts were incubated for 30 minutes and osteosarcoma cells were incubated for 1 hour for cell adhesion.

The cytoskeletal disrupting drugs cytochalasin-D and nocodazole are frequently used in cell biology. Cytochalasin-D is a member of the fungal metabolites cytochalasins. By binding to the barbed end of actin filaments, Cyto-D prevents both association and dissociation of actin monomers at the end of the filament (Cooper, 1987). Treatments with Cyto-D have previously shown to reduce cell stiffness in 3T3 fibroblasts by up to a factor of 3, depending on concentration and incubation times (Rotsch & Radmacher, 2000). Nocodazole interferes with microtubule dynamics by inhibiting tubulin polymerisation (Vasquez et al., 1997). Treatments with nocodazole have shown to reduce cell stiffness in 3T3 fibroblasts (Pelling et al., 2007).

Therefore, in order to analyse distinct effect of drugs interfering with CSK integrity, cells were treated with CSK-destabilising agents, cytochalasin-D at a concentration of 0.5  $\mu$ M to disrupt actin, and nocodazole at a concentration

of 30  $\mu\text{M}$  to disrupt microtubules, both prepared in  $\text{CO}_2$ -independent media (BD Biosciences, Franklin Lakes, NJ). This media was used in order maintain ideal conditions for cells during the time of experiments, since it is ideal for handling different types of adherent cells under atmospheric conditions. The two cell lines were also treated with a combination of both drugs to disrupt the entire CSK.

### 4.2.3 Indentation experiments with atomic force microscopy

Imaging and force measurements were performed with BioScope<sup>TM</sup> Catalyst<sup>TM</sup> Atomic force microscope systems and Nanoscope V controller (Bruker, Santa Barbara, CA), fully integrated with Zeiss microscope Observer Z1, equipped with an Andor Ixon camera for imaging. The stiffness of single living cells was measured using a cantilever with a 5  $\mu\text{m}$ -diametrical bead attached to it, and with nominal spring constant  $k = 0.01 \text{ N/m}$  (model MLCT from Veeco Instruments, Santa Barbara, CA) measured with the thermal method (Butt & Jaschke, 1995). Deflection sensitivities were found to be between 33 and 46  $\text{nm/V}$ .

The bead is mounted on the cantilever using UV glue (Norland optical adhesive) and exposed to UV-light for 30 minutes before experiments. The 5  $\mu\text{m}$  bead spherical tip was the indenter shape chosen for the AFM measurements since it allows sufficient resolution for single-cell measurements, while avoiding artefacts due to cell inhomogeneity that would appear if sharper tips were used (which are normally used for higher resolution at the level of specific components inside cells). Both cell lines, cultured on the acrylic-reinforced glass coverslips, were transferred to the AFM sample holder and cell's sample media was replaced with  $\text{CO}_2$ -independent media (Gibco, Carls-

bad, CA). In these conditions, cells viability for about 2 hours per experiment was maintained.

Single-cell force-indentation curves were measured with indentations applied for 1 minute at a frequency of 0.1 Hz (6 measurements, one every 10 seconds), with a speed varying from 200 and 400 nm/s and an indentation threshold of 200 nm in liquid mode. After one minute recovery, another set of indentations was applied to the same cell. The force-indentation curves were measured, by plotting the deflection of the cantilever ( $d$ ) and the position of the sample (i.e., the piezo position,  $z$ ). The mechanical properties of living cells absorbed on coverslips with CO<sub>2</sub>-independent DMEM were measured for control. The media was then replaced by a buffer containing the CSK-destabilising drugs and the same measurements were performed for the same cells in the presence of drugs. Each set of indentations was repeated three to four times.

In order to record all the force-indentation curves onto the same spot near the centre of the cells,  $x$  and  $y$  positions of the piezo were registered and phase images with the cantilever on the top of the cell were used to align the cantilever before and after adding the drug (Figure 4.1). Force-indentation curves were collected with the bead of the cantilever positioned above the nucleus of the different cells to match the position of the bead in the FE simulation and therefore, allow direct comparison of experimental and numerical results.

#### 4.2.4 Data analysis for Young's modulus measurement

For quantification of cell elasticity, Young's modulus was derived from force-indentation curves using a custom Matlab (Mathworks, Natick, MA) code to fit the Hertz model to experimental data (Rosenbluth et al., 2006). As-

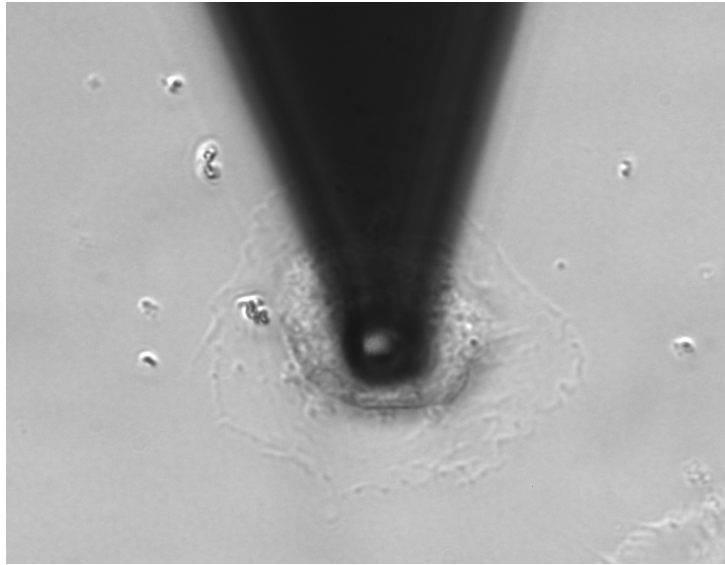


*Figure 4.1: Phase-contrast image of the cantilever used in the AFM to indent the cells, using a bead on the top of the nucleus of each living single-cell.*

assumptions from the Hertz theory were used for the indenter and cells tested. Briefly, contact model for a spherical tip indenting a homogeneous, isotropic, linear elastic half-space sample can be described by a classical elastic solution with the Hertz model:

$$F = \frac{4R^{\frac{1}{2}}E}{3(1-\nu^2)}\delta^{\frac{3}{2}} \quad (4.1)$$

where  $E$  and  $\nu$  are the elastic modulus and Poisson's ratio of the sample, respectively,  $\delta$  is the depth of indentation, and  $R$  is the radius of the spherical indenter.

From the cantilever deflection and displacement data obtained from AFM, the applied force  $F$  was determined by multiplying the cantilever stiffness  $k$  by its deflection via Hooke's law:

$$F = k(d - d_0) \quad (4.2)$$

and indentation  $\delta$  is calculated using:

$$\delta = z - z_0 - (d - d_0) \quad (4.3)$$

where  $d_0$  is the deflection and  $z_0$  is the displacement at the moment of contact. Therefore the Young's modulus can be described by the equation:

$$d = d_0 + \frac{4R^{\frac{1}{2}}E}{3(1-\nu^2)k} [z - z_0 - (d - d_0)]^{\frac{3}{2}} \quad (4.4)$$

For Young's modulus calculation using Equation 4.4, contact points ( $z_0$ ,  $d_0$ ) and  $E$  were fitted to the data using the nonlinear least squares optimisation method and considering  $\nu = 0.5$ . Both Young's modulus and force-indentation curves were averaged for each cell tested and compared with numerical results. Statistically significant differences among the Young's moduli calculated for treated and untreated cells at each time point were evaluated using a paired sample  $t$ -Test. An analysis report sheet was generated with the software OriginLab, used for the statistical analysis, showing the degrees of freedom,  $t$  statistics, the associated  $p$ -value, and the test conclusion.  $p \leq 0.05$  was considered statistically significant.

### 4.2.5 Immunofluorescence staining and imaging

Qualitative changes in the CSK structure of U2OS cells were possible to monitor with the AFM camera since this cell type has GFP-actin that allows fluorescent observation of actin structure before and after actin disruption with cytochalasin-D on the same cell. A x63 objective was used on Zeiss microscope observer Z1 equipped with an Andor Ixon camera for imaging of the U2OS cells. The combined AFM-fluorescence microscopy methods used here allow the application of well-defined perturbations, together with real-time fluorescence of the intracellular structural responses of U2OS GFP-actin cells.

Images of untreated U2OS cells were also acquired before and after AFM indentation to visualise how forces affect the structure of the actin of this cell type. For this purpose, short-time adhesion of 20 minutes was considered. To verify whether the changes in actin structure are due to force application, control images were acquired for the same time of the experiments without application of any force. Images were collected 6 minutes time apart from each other.

The same real-time approach was not possible for visualisation of structural changes of NIH-3T3 cells since these cells were not previously tagged with GFP cytoskeletal proteins. Actin-GFP transfections were not performed in any cell type used in the current study.

To monitor cytoskeletal changes with fluorescence microscopy, immunostaining was performed in NIH-3T3 cells for both control and after actin disruption with cytochalasin-D, in different 3T3 cells. NIH-3T3 cells were fixed in a PBS and water solution containing 3% paraformaldehyde for 20 minutes and permeabilised with 0.1% Triton X-100 buffer. The actin structure was first stained with rhodamine-phalloidin for 25 minutes and then the cell nuclei were stained with Hoechst for 5 minutes, both with a 1:500 dilution in PBS and triton X-100 solution. All coverslips were imaged with a x100 oil-immersion objective on a Leica confocal microscope and Andor camera. Fluorescent images were sequentially collected with emission wavelengths of 488, 561 and 405 nm for the fluorescein FITC, tetramethyl rhodamine TRITC and DAPI fluorophores, respectively. The microscopic images for both cell types were post-processed using image-J.

### 4.2.6 Numerical predictions for small indentations

AFM is often the quantitative method to measure cellular mechanical properties in living cells by using a probe to indent the cells. The AFM is however limited if high indentation forces or displacements are applied, which may damage the cells. On the other hand, if low forces or displacements are applied the measurements are limited by the thermal noise of the AFM cantilever in liquid. Although the lowest force that can be applied with AFM without thermal noise is around 20 pN (Eghiaian & Schaap, 2011), most of the AFM experiments are performed from 0.1 nN up to a few nN at which the absolute cell indentation is measured with accuracy (Nawaz et al., 2012). Low indentations for experiments with AFM are considered to be below 0.2  $\mu\text{m}$  and large indentations from up to 1  $\mu\text{m}$ . For the purpose of this study, the AFM is used to quantify the mechanical responses of cells considering indentations of 0.5  $\mu\text{m}$ , and to compare with the *quasi-static* numerical predictions. The value of indentation used in this study for calculation of the Young's modulus is within the range considered relatively small indentations. To evaluate the capabilities of the model in simulating the application of low forces, 0.05  $\mu\text{m}$  vertical displacement of the bead was also analysed and compared with the results obtained with 0.5  $\mu\text{m}$  bead displacement, considering all the models simulating CSK disruption.

## 4.3 Results

### 4.3.1 Corroboration of the numerical results with AFM

Computational and experimental approaches to measure compressive forces of cells were combined in this study to corroborate the numerical results under

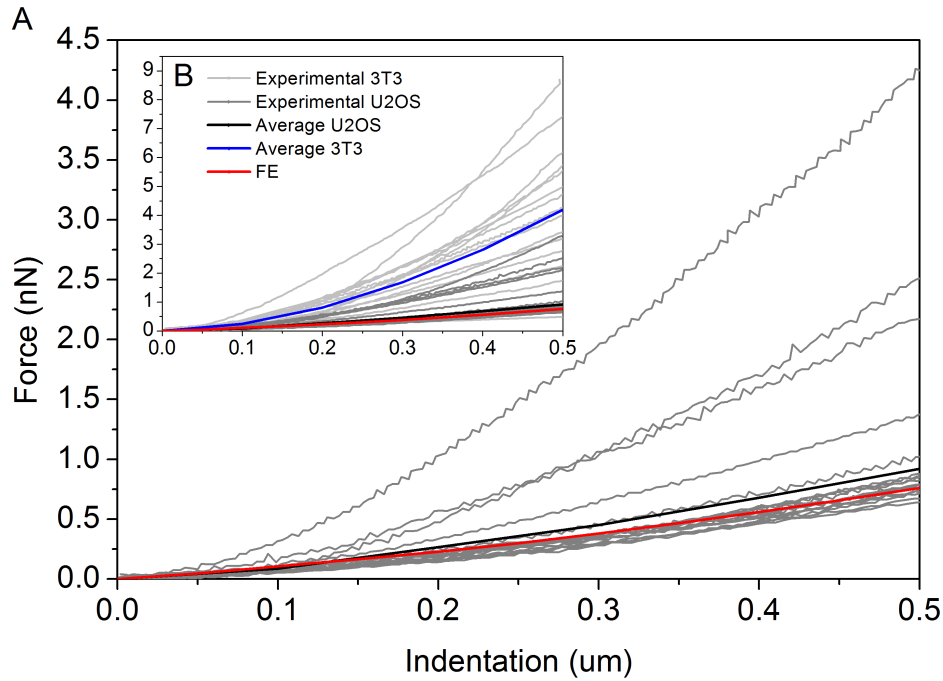


Figure 4.2: Corroboration of the model comparing numerical and AFM force-indentation curves. (A) 11 out of 34 cells used in this study had an apparent Young's modulus within the same range (0.6-0.8 kPa) of the overall Young's modulus of the numerical cell (0.7 kPa). The average of the Young's modulus of the cells with rigidity within the range of 0.6-0.8 kPa matches the numerical prediction. Force-indentation curves obtained experimentally for those cells are consistent with the computed force-indentation relationship of the model. (B) Force measurements with AFM of 34 cells including both NIH 3T3 and U2OS cells and comparison with the numerical force-indentation prediction.

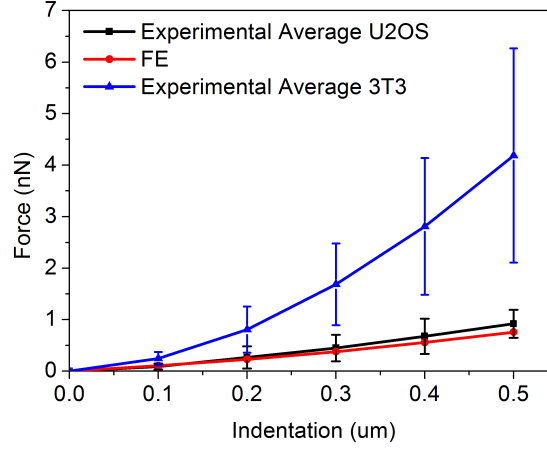


Figure 4.3: Statistical analysis of FE predictions and AFM force-indentation measurements for U2OS and 3T3 cells. Error bars are standard deviation ( $N = 16$  for 3T3 cells and  $N = 18$  for U2OS cells).

compressive loads. Different material properties were considered for each cellular component (Table 3.2) to predict force and deformation, from which the average numerical Young's modulus was calculated using a modified Hertz model. The average Young's modulus obtained from the FE analysis, for these initial given material properties and organisation of the cell components, was compared to the Young's modulus of two cell types with different morphologies, the U2OS osteosarcoma cells and 3T3 fibroblasts (Figure 4.2). From this composite numerical cell an average Young's modulus of 0.7 kPa was obtained for the whole cell. The average apparent Young's modulus calculated from AFM experiments was  $3.8 \pm 1.6$  kPa for 3T3 cells, and  $1.3 \pm 0.8$  kPa for U2OS cells (with 0.1 Hz indentation rate, 0.5  $\mu\text{m}$  indentation depth,  $N = 34$ ). The numerical predicted force-indentation curve matches the non-linear behaviour of experimental data obtained with AFM for 3T3 fibroblasts ( $R^2 = 0.98$ ) and for U2OS cells ( $R^2 = 0.99$ ) (Figure 4.2 B). The

average of the AFM force measurements for the two types of cells was calculated and compared to the numerical simulation. Statistical differences using unpaired *t*-Test were found for 3T3 fibroblasts ( $N = 16$ ). However, no statistical differences were found between computational force prediction and average of force for U2OS cells ( $N = 18$ ) and thus, it corroborates the proposed multi-structural model (Figure 4.2 A).

Further quantification of numerical CSK disruption was made with respect to this given model organisation and mechanical properties. After corroboration, the model can be used for the study of the relationship between whole cell mechanics and specific mechanical properties of the CSK components under compression and stretching. This was possible because the interplay between discrete components in this model can be disrupted for the study of the role of individual components of the CSK inside cells.

### 4.3.2 Role of the components of the CSK

The contribution of each component of the CSK, actin bundles, actin cortex and microtubules, to the cellular behaviour was evaluated using the FE model. In compression (Figure 4.4 A), the reaction force of a cell with complete CSK (considered as the control) was 5.3-times higher than a "cell without CSK". In stretching (Figure 4.4 B), the reaction force of a cell with CSK was 9.2-times higher than a "cell without CSK".

Under compression, the axial reaction force of a "cell without actin bundles" was slightly the same as the axial reaction force of the control, showing minimal effect of this component to cell rigidity during compression. When actin bundles were removed from the cell during stretching, the longitudinal reaction force was 3.7-times lower. When the cortex was removed the reaction force was 5-times lower in compression and 1.2-times lower in stretching.

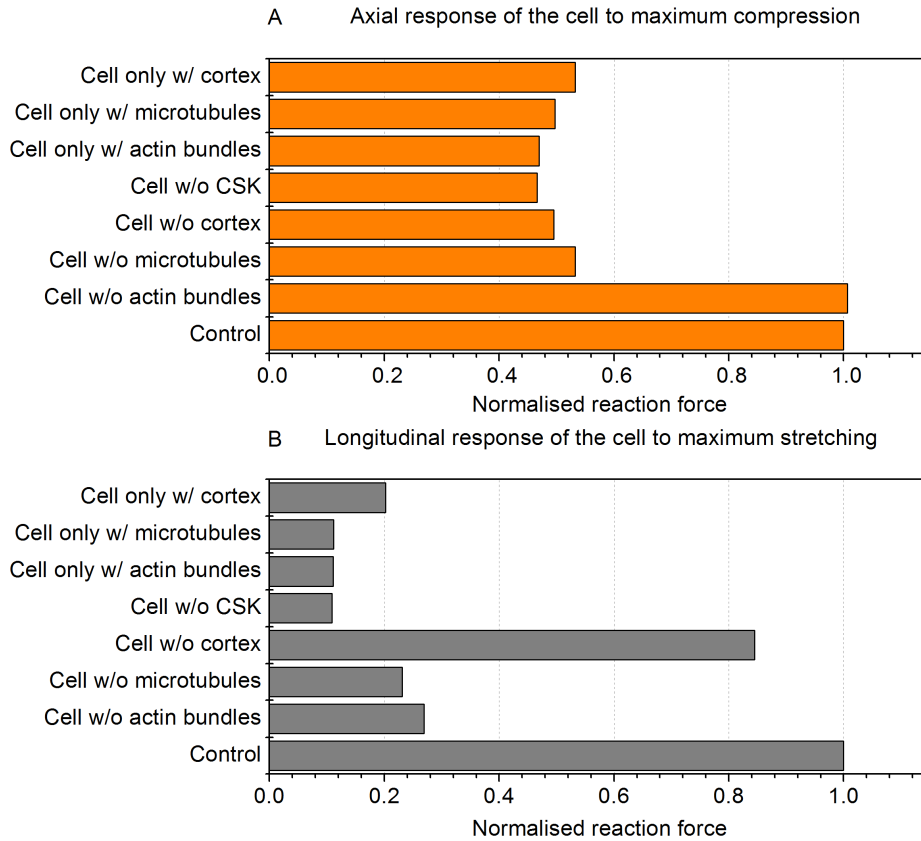


Figure 4.4: Contribution of each component of the cytoskeleton for the different stimuli, and effect of interaction between the elements of the cytoskeleton. (A) Axial force for maximum compression and (B) longitudinal force for maximum stretching. Reaction force of the cell for the different models is normalised to the control model.

Lastly, the reaction force of a "cell without microtubules" was 5.3-times lower in compression and 4.3-times lower in stretching. None of the three components was capable of maintaining cell rigidity by itself, demonstrating that their response must be dependent on the presence of the other CSK components. During compression, microtubules and actin cortex were essential to maintain cell force and rigidity. During stretching rigidity was maintained by an interplay between actin bundles and microtubules.

### 4.3.3 In the range of small forces

Cellular response to low forces were predicted for the different conditions of the CSK (Figure 4.5), which cannot be done experimentally using AFM due to the thermal noise limitation. With this numerical simulation, minimal indentations were applied to cells in the vertical direction. Therefore, Young's modulus and reaction forces can be predicted for the whole range of relatively small deformations, where the cellular response is known to be mainly elastic (Nawaz et al., 2012). When the indentation is increased 10-times from 0.05  $\mu\text{m}$  to 0.5  $\mu\text{m}$ , reaction forces and Young's modulus increased 16 and 2-times, respectively. For the two values of indentation applied in the model for the different cases of CSK disruption, the response of the cell follows the same trend independently of the amount of indentation, indicating that the response is largely elastic for the range of displacements applied in the simulations.

### 4.3.4 Force-induced changes in U2OS actin structure

To understand how forces affect actin CSK structure, AFM measurements were combined with real-time imaging of U2OS GFP-actin before and after AFM indentation. Force-induced movement of the actin structure that re-

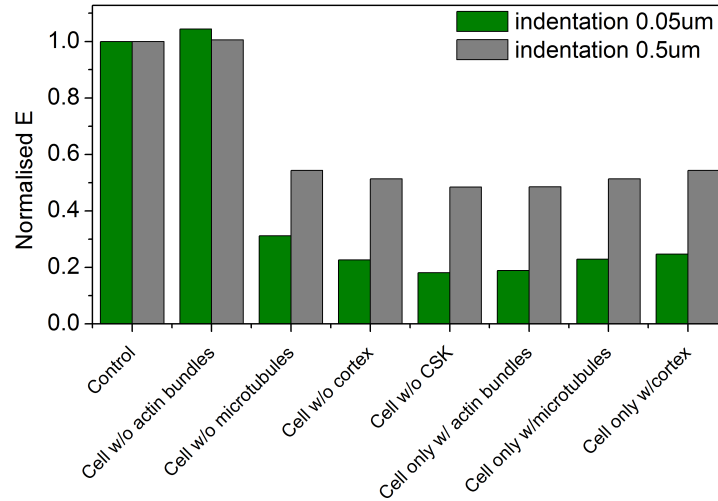


Figure 4.5: Cytoskeleton disruption for different small indentations. Young's modulus is normalised to the control model for the respective applied indentation.

sulted from the AFM indentation were observed in U2OS cells (Figure 4.6). Comparing the optical images before and after indentation states, changes in the actin fibres were visible mainly at locations far from the indentation point, but also under the bead location. To be sure these changes in the actin structure were due to application of force and not due to changes in the actin structure (in case the adhesion process was not totally completed), control images were taken within the same time interval without application of forces. In these cases, no major differences in the actin structure were found. Lastly, after AFM indentation the cells were exposed for 30 minutes to the different types of CSK-disrupting drugs used in this work to measure changes in the cell shape after CSK disruption. The optical images showed cell morphology to be affected by treatments with cytochalasin-D, nocodazole and combination of both drugs (Figure 4.6).

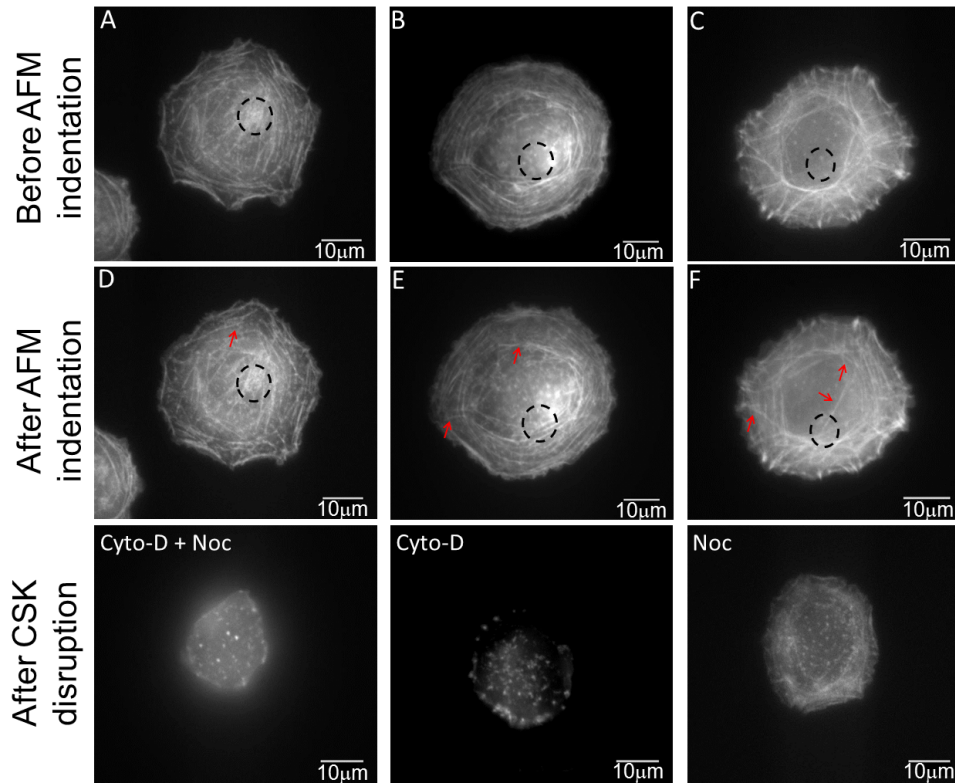


Figure 4.6: Fluorescence images of U2OS GFP-actin structure (A, B and C) before and (D, E and F) after AFM indentation, with 6 minutes interval between the two images of the same cell. Local changes in the actin structure can be seen in different points far from the indentation point, which is marked with dashed circles. Red arrows indicate the location of major changes of the actin structure after force. Cells shape changes due to CSK disruption were observed in each cell after exposed for 30 minutes to cytochalasin-D and nocodazole and indicated.

### 4.3.5 AFM measurements and imaging of living cells

Force measurements using AFM were performed for NIH-3T3 and U2OS cells before and after chemical disruption of the CSK components to isolate the different networks of the CSK and analyse their contribution to cellular mechanics. The average apparent Young's modulus calculated from AFM experiments was  $3.8 \pm 1.6$  kPa for NIH-3T3 cells and  $1.3 \pm 0.8$  kPa for U2OS cells (with 0.1 Hz indentation rate,  $0.5 \mu\text{m}$  indentation depth and  $N = 34$ ).

After treatment with cytochalasin-D for actin disruption, the apparent  $E$  of 3T3 cells was registered to be  $4.5 \pm 2.2$ -times lower than the control ( $N = 6$ ) and  $2.2 \pm 0.7$ -times lower for U2OS cells ( $N = 7$ ). After microtubules disruption with nocodazole the  $E$  of 3T3 cells was  $2.5 \pm 1.1$ -times smaller than the control ( $N = 5$ ) and  $1.2 \pm 0.2$ -times smaller for U2OS cells ( $N = 5$ ). After CSK disruption with both drugs, the apparent  $E$  of 3T3 cells was  $7.7 \pm 4.7$ -times smaller ( $N = 5$ ) and  $2.4 \pm 0.3$ -times smaller for U2OS cells ( $N = 6$ ) (Figure 4.7). A paired sample  $t$ -Test indicated that all last set of measurements with drugs for each cell were significantly different from control ( $p < 0.05$ , using a paired  $t$ -Test), except for the U2OS cells after disruption with nocodazole (Figure 4.7).

Some of the values of Young's modulus calculated in the two first sets of indentation after drug exposure showed to be higher than the Young's modulus of the untreated cell, and decreased in the last indentation sets after drug exposure. Real-time images during AFM indentation showed the nucleus moving away from the indenter for the cells where higher Young's moduli were registered after drug exposure. Although the  $x$  and  $y$  positions of the cells in the AFM chamber were recorded in between indentation sets, the position of the indenter on the top of the cell moved slightly as the drugs were

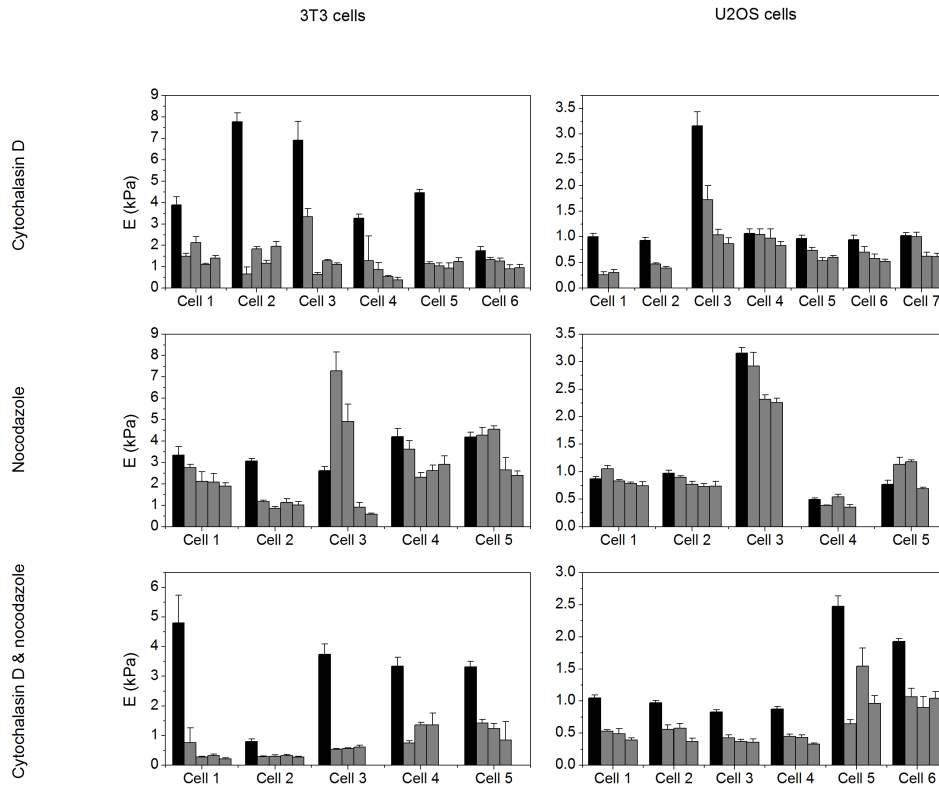
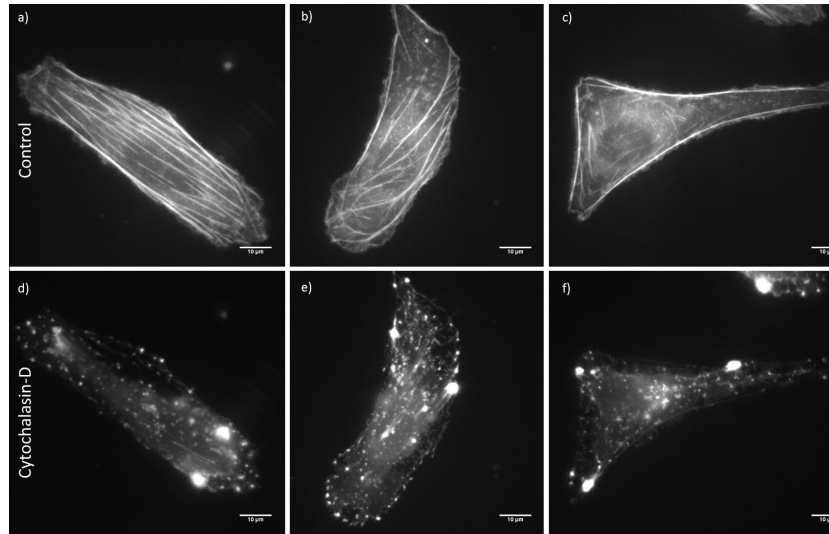


Figure 4.7: Young's modulus of 3T3 and U2OS cells before and after cytoskeleton disruption, calculated from AFM force measurements: the Young's modulus of 3T3 cells (left column) and of U2OS cells (right column) in control conditions (black bars) and when disrupted with cytochalasin-D, nocodazole and combination of both drugs (grey bars). The value of  $E$  presented is an average of the calculated  $E$  from all of the force-indentation curves obtained during AFM experiments for each cell. Error bars are standard deviation ( $n = 12$ ). A paired sample  $t$ -Test indicated that all last measurements with drug for each cell are significantly different from control, except for the U2OS cells after disruption with nocodazole ( $P < 0.05$ ).



*Figure 4.8: Microscopic images of the actin structure of U2OS GFP-actin cells before and after exposure to cytochalasin-D, during AFM experiments.*

introduced with a micropipette in the chamber containing the liquid buffer. For the last indentation sets, the AFM chamber is not subjected to any major external condition that would make the position of the indenter vary on the top of the cells with respect to the previous indentation set. Therefore, the effect of the drug in decreasing the rigidity of the cell is captured. This happened for both cell types, and more frequently to cells exposed to nocodazole, as seen in Figure 4.7. This variability of cell rigidity in time for microtubules disruption is related to variations of the position of the indenter with respect to the nucleus of cells. It can also be related to the dynamics of the different types of microtubules present in cells or with the effect of the nocodazole in the remaining CSK networks, which will be analysed in the discussion of the present chapter.

Fluorescence images of the cytoskeleton of both cells were taken before and after CSK disruption to confirm disruption and to evaluate differences in the CSK structure of the two cell lines. F-actin in the 3T3 cells was visualised

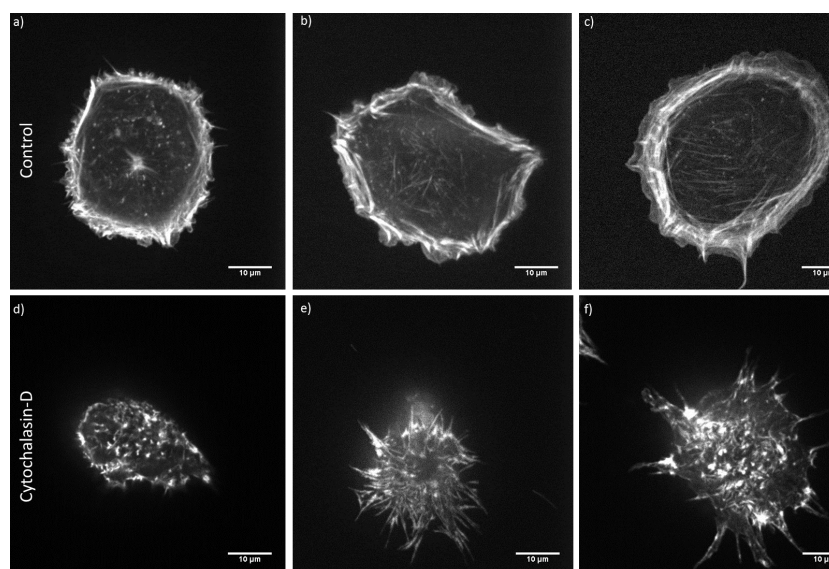


Figure 4.9: Fluorescence images of actin structures of NIH-3T3 fibroblasts (phalloidin staining) before and after 30 min exposure to cytochalasin-D.

with rhodamine-phalloidin (Figure 4.9), and F-actin in the U2OS cells was visualised with GFP-actin (Figure 4.8).

Visible differences in the distribution of actin in 3T3 and U2OS cells were observed. Less quantity of stress fibres in the interior of the cells and a thicker network of actin located at the edge of the cells was observed for the 3T3 cells (Figure 4.9) compared to the U2OS cells (Figure 4.8). In the U2OS, actin is arranged in stress fibres. Drug treatment caused both morphological changes and qualitatively differences in the CSK of both cell types. When subjected to the same concentration of cytochalasin-D, actin networks were affected differently for the two cell lines. Treatment of 3T3 cells with cytochalasin-D disrupted mainly the actin networks at the cell edge (Figure 4.9), while the same concentration of drug disrupted the entire structure of F-actin in the U2OS cells (Figure 4.8).

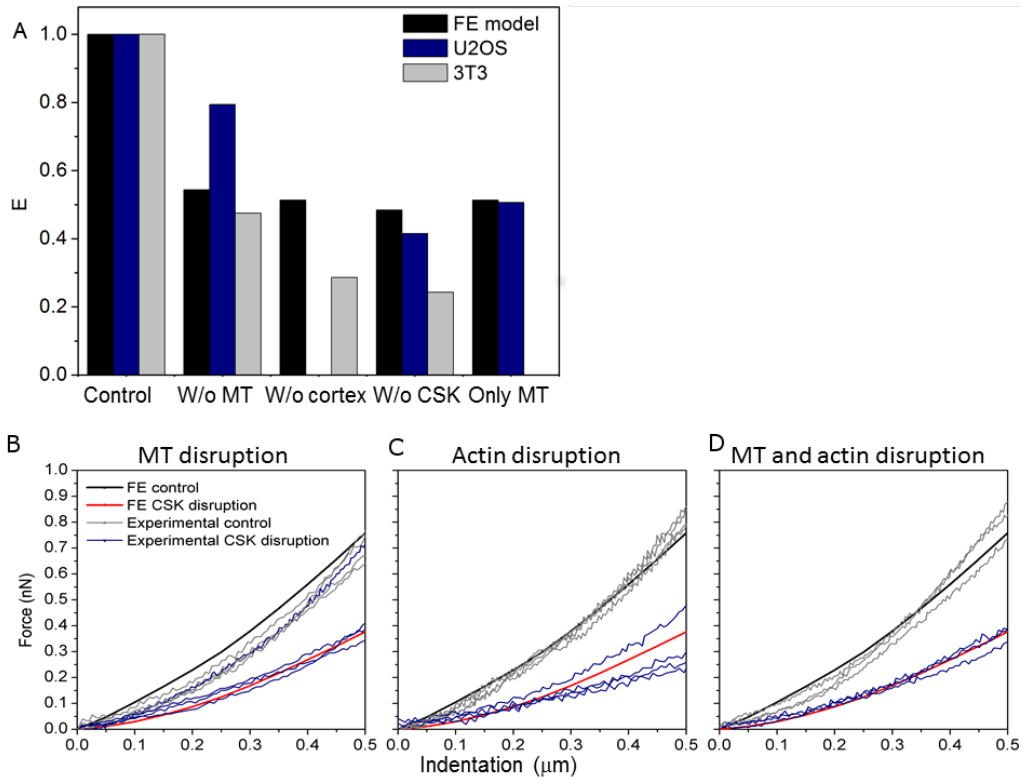


Figure 4.10: Overall Young's modulus and force obtained numerically and with AFM for cells with the same rigidity. Comparison of overall  $E$  obtained numerically and with AFM, (A) before and after CSK disruption for 3T3 and U2OS cells. The  $E$  calculated for the living cells is an average of the  $E$  of all cells measured. The different numerical models are compared with each specific case of CSK disruption based on the previous microscopic images of 3T3 and U2OS cells. The results for the control are normalised with respect to the average value obtained for each cell type in order to analyse the changes in cell rigidity when CSK components are disrupted. Comparison of numerical and experimental force-indentation curves of U2OS cells with the same rigidity before and after disruption with (B) nocodazole, (C) cytochalasin-D for both actin bundles and cortex disruption and (D) both drugs.

### 4.3.6 Comparison between numerical results and AFM measurements

Here, the author reports a comparison of force-indentation curves and Young's modulus between numerical finite element cell model and experimental determination of cellular mechanical properties of two cell lines by atomic force microscopy. The average apparent Young's modulus of cells with different rigidities was compared with the cell rigidity of the computational model (Figure 4.10 A). AFM measurements showed a decrease in cellular rigidity when the different CSK components were disrupted, as predicted by the current FE model (Figure 4.10 A). For accurate validation of the model after CSK disruption, computational predictions and experimental force-indentation relationship of U2OS cells were compared during control and then for each case of CSK component disruption (Figure 4.10 B - D). For statistical significance of the match between computational and experimental force-indentation curves, the  $p$ -value was calculated using an unpaired  $t$ -Test.

The force-indentation curve of untreated U2OS cells (control) matched the curve predicted computationally. After CSK disruption using the different drugs, the force-indentation curves obtained experimentally for these cells also matched the predicted computational results for all the different conditions of the CSK disruption. The experimental range of curves obtained after cytochalasin-D exposure showed the largest variability (Figure 4.10 C). Only one of the force-indentation curves after microtubules disruption did not match the decrease in force predicted computationally (Figure 4.10 B). Computational force-indentation curve using material properties from Table 3.2 matched average force-indentation curve of AFM measurements on U2OS. Higher forces and Young's modulus were measured for the 3T3 fibro-

lasts and for this cell type the force-indentation relationship did not fit the average of the experimental results during control (Figure 4.3).

## 4.4 Discussion

The methodology described here was used to evaluate the cytoskeleton's role in cellular force transmission. These findings have implications on the understanding of the connectivity of the different cytoskeletal networks in the cell and their relative impact on both stiffness and propagation of forces through the cell.

### 4.4.1 Force-induced changes in the actin structure of living cells

Microscopic images of U2OS GFP-actin showed changes in the entire F-actin structure in different regions of the cell when comparing static conditions (before indentation with the AFM cantilever) with images after a localised indentation with AFM. Without application of force, control images did not indicate changes in the actin structure after 6 minutes of experiment compared to the changes observed after an external force applied with the AFM cantilever. Thus, indicating that changes in the actin structure of U2OS cells are likely due to force application.

Following indentation with AFM, the changes were localised in different parts of the cell, which suggests that forces applied at the indentation point were transmitted through the cell, and raised the cytoskeleton as a key candidate responsible for this force propagation. This effect of force propagation over the cell, also termed "action at a distance", was also observed computationally (Blumenfeld, 2006) and experimentally (Ingber, 1993; Wang & Suo,

2005).

In order to test this hypothesis and establish the cytoskeleton as the medium that is responsible for the observed force transmission, known cytoskeletal active drugs were used, nocodazole and cytochalasin-D, to disrupt the integrity of microtubules and actin networks, respectively. Then the effect of disruption on cellular force was measured using AFM and compared to the force measured in the correspondent untreated cells. Finite element force prediction for the same CSK disrupted conditions was used to distinguish the specific role of each CSK components, especially for identifying the differences in the role of actin cortex and other deep actin bundles.

#### **4.4.2 Mechanical stimuli regulate CSK components' activation to resist external forces**

The current model showed how cells react to different mechanical stimuli and which components of the CSK affect cellular responses when external conditions are changed. Perception of the individual role of the main components of the cytoskeleton and their contribution to the overall biomechanics of different cells is a step forward to understand mechanotransduction. The author believes that this model is a useful tool that can be used to determine the magnitude and type of stimulus to apply to a cell to initiate different cellular processes, such as proliferation and differentiation.

The results indicate that during deformation, individual CSK components have different mechanical responses to specific external perturbation. This computational work explains the differences found in literature for force transmission predictions using different single-cell techniques. Although the model is a *quasi-static* analysis and does not include CSK remodelling essential for physiological cell functions, it suggests how the individual components

of the CSK interact with each other depending on the type of forces the cells sense. The results showed that the actin cortex together with microtubules, are the main components to resist compression, and that actin bundles and microtubules together are essential to resist stretching.

### 4.4.3 Mechanical role of actin cortex, and other actin and microtubules networks in compression

Simulation of CSK disruption quantified the changes in the overall reaction force of the cell. Computational results showed that when the bead is displaced  $0.5 \mu\text{m}$  in compression, about 53% of the cell force was inhibited when all three components of the CSK were removed. This emphasises the importance of incorporating discrete elements of the CSK to model cellular behaviour. The numerical results during compression were experimentally validated with the use of AFM for the same amount of indentation. The apparent Young's modulus, when CSK was disrupted with nocodazole and cytochalasin-D during the AFM experiments, decreased  $58 \pm 6\%$  for U2OS cells and  $76 \pm 13\%$  for 3T3 cells.

These differences might be related to the amount of CSK fibres and different structural organisation of the CSK components of the two cell types, as well as to the concentration of drugs used in this study. For the 3T3 fibroblasts, it was observed a higher concentration of actin at the cell periphery, which could be associated with a well-defined actin cortex for this cell type, and only a few stress fibres in the cell interior, as it is observed in the fluorescent images of untreated cells in Figure 4.9. For the untreated U2OS cells, in Figure 4.8, actin is more uniformly distributed all over the cell in the form of well-defined stress fibres. These factors affect the initial rigidity ( $E$ ) of the cells tested and therefore, the way their CSK is disrupted.

However, the quantitative differences found are also related to the fact that the computational  $E$  (simulating cell model rigidity) was compared with the average of the apparent  $E$  (from the experimental analysis).

For a more accurate analysis of the quantitative study during compression, both the disruption of the different actin networks in each cell type and the concentration of drug used, have to be taken into account. Fluorescence images of 3T3 cells with phalloidin-stained F-actin showed a large disruption of the actin cortex, while inner actin fibres remained partially intact. Computationally, 50% decrease in force is predicted for actin cortex disruption during compression, while  $71 \pm 14\%$  decrease in force is predicted for the apparent  $E$  of 3T3 cells with cytochalasin-D actin disruption. Fluorescence images of U2OS cells with GFP-actin showed disruption of the entire assembly of actin networks when exposed to  $0.5 \mu\text{M}$  of cytochalasin-D. In these conditions, a decrease in apparent  $E$  of  $49 \pm 17\%$  was obtained, which matched the 50% decrease in force obtained with the FE model when actin cortex and actin bundles were removed from the cell.

For both cell types, a decrease in cell rigidity was registered when microtubules were disrupted. The 53% decrease in force from the cell model matched the  $52 \pm 17\%$  decrease in the apparent  $E$  of 3T3 cells but did not match the  $21 \pm 7\%$  decrease found for U2OS cells. Further studies using fluorescence microscopy with microtubules labelled will be required to relate with the numerical results and understand which mechanical properties of the microtubules (density, diameter of fibres, rigidity or spatial distribution) affect the rigidity of different cell lines.

Previous works to test the mechanical role of microtubules reported very different results, depending on the cell type and technique used ([Kasas et al., 2005](#); [Rotsch & Radmacher, 2000](#); [Wang, 1998](#); [Wu et al., 1998](#)). Normally,

experiments to identify the role of microtubules are done in full serum condition, where the two sub-type of microtubules, the tyrosinated microtubules (Tyr-MTs) and detyrosinated microtubules (Glu-MTs), are present. To identify differences in the reaction of the two sub-types to the nocodazole, [Pelling et al. \(2007\)](#) tested the mechanical properties of these sub-types of microtubules of NIH-3T3 fibroblasts with AFM combined with immunofluorescence microscopy, in response to nocodazole. The authors identified tyr-MTs in both full serum and serum starvation conditions and Glu-MTs only in full serum conditions, and observed that the local Young's modulus of the cell decreases in response to the nocodazole for both conditions, but at different times. The response of the try-MTs, known as the "dynamically instable", happened within the first minutes of the experiment, while the Young's modulus of the cell in full serum conditions, in response to nocodazole decreased around 10 to 20% within the first 15 minutes, and decreased by 75% after that. The two different sub-types of microtubules react in different times to the nocodazole, which might be an explanation for the differences in the results of disruption of the microtubules. The duration of the experiments might also affect the results. Nonetheless, for both cases a decrease in the response of the cell after microtubules disruption was registered, which is in accordance with the results of this model.

Despite these limitations, the model predicts the overall role of the fibres during compression and is in good agreement with evidence from AFM experiments, showing the major role of the actin cortex followed by microtubules. Computational and AFM force-indentation curves obtained for cells with the same rigidity (Figure 4.10) showed a good match and are an effective validation of the computational results obtained during compression. Therefore, the predictions obtained with this FE model concur qualitatively

with the experimental findings that the internal cytoskeleton plays a key role in determining the structural properties of the model.

Chemical disruption of CSK fibres in combination with AFM has been used to indent cells and measure the force-indentation relationship during compression for different conditions of the CSK. There is a unanimous conclusion with respect to the use of cytochalasin-D to disrupt actin fibres in living cells during atomic force microscopy experiments. This drug was used to disrupt actin fibres of different types of fibroblasts (Rotsch & Radmacher, 2000) and endothelial (Callies et al., 2011) cells. The concentration of this drug was varied to disrupt different actin networks in an attempt to isolate the actin cortex of endothelial cells. Under these conditions, the stiffness was determined from the slope of the force-distance curves obtained with AFM (Callies et al., 2011; Kasas et al., 2005; Oberleithner et al., 2009). These curves presented different slopes and the authors identified the first slope of the curve to possibly correspond to disruption of cortex, registering the highest decrease in reaction force of the cells compared to other slopes of the same curve representing disruption of inner actin structures. These studies are in accordance with the results of this thesis obtained during compression, where disruption of actin cortex is the major responsible for decrease in cell stiffness.

Other attempts to quantify the contribution of the different actin networks to the mechanical properties of cells have been done experimentally (Ananthakrishnan et al., 2006; Lang et al., 2000; van Citters et al., 2006) but with difficulties in isolating the actin cortex at the cell periphery from deep actin cytoskeleton networks.

To overcome this issue, this multi-structural FE model is the first study that can accurately isolate and quantify the actin cortex role from other

actin networks within cells when subjected to different static loads. The results for compression, where disruption of the actin cortex is one of the main contributors to the decrease of cell stiffness, are also in accordance with previous experimental findings showing that variation of cytochalasin-D concentration is cell type-dependent. In these reported studies, variation of cyto-D can be used for targeting specific mechanical properties of the actin located at the cell edge that were believed to correspond to the actin cortex mechanical changes (Callies et al., 2011; Kasas et al., 2005; Oberleithner et al., 2009). Corroborating the current numerical results, other authors have suggested the cortex as the major contributor to the *quasi-static* cellular response and to define the elastic response of the cell (Nawaz et al., 2012), as mentioned above.

It has to be acknowledge that the 3T3 fibroblasts in cell culture have a heterogeneous morphology that can be either dendritic or stellate/bipolar appearance. However, the 3T3 morphology in this study was very round for all the cells observed with fluorescent microscopy, as seen in Figure 4.9. This could have been related to the time allowed for cell adhesion in culture in this study, which was 30 min, as normally used for this type of cells, and was increased to 1 hour before mechanical indentation with AFM on glass coated with fibronectin. Differences were not observed in the morphology of the 3T3 cells for the different times of cell adhesion. Furthermore, cells were viable during the times of experiments as observed with the cameras used together with the AFM system. Therefore, no clear explanation can be found for this unusual morphology of the 3T3.

#### 4.4.4 Mechanical role of actin cortex and deep actin and microtubules networks in stretching

The model allows a good characterisation of the mechanical properties of cells during control as well as for the contribution of the CSK components, which is corroborated with findings in literature. The 89% computationally predicted decrease in reaction force during stretching is in good agreement with the 75-80% decrease in stiffness found when drugs were combined to disrupt both actin and microtubules, and actin, microtubules and intermediate filaments (Wang, 1998), as shown in Figure 4.11. This author also verified the importance of the cross-talk between the components of the CSK to maintain cell stiffness during MTC. In this study, Wang (1998) measured cell stiffness of adherent endothelial cells showing 50% decrease in cell stiffness after actin disruption with cytochalasin-D and little variation in stiffness after both microtubules disruption with nocodazole and intermediate filaments disruption with acrylamide.

Quantitative analysis of individual components of the CSK of Wang (1998) does not corroborate the computational predictions of microtubules disruption in this study. Differences in the loading conditions between the two studies were observed: simulations of MTC include a lateral bead displacement applied along the cell, whereas in the experiments of Figure 4.11 were performed with the application of a torque to the cells through magnetic moment and angular rotation. This might contribute to the differences in the quantitative analysis of CSK disruption during stretching on MTC.

The current model showed the low ability of the cortex to resist stretching, which is also suggested experimentally by Wang et al. (2002). Another study by van Citters et al. (2006), compared the mechanical properties of the cortical region of the lamellipodal region with the F-actin in the interior

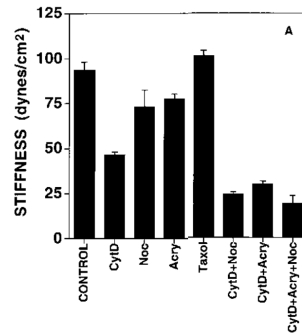


Figure 4.11: Mechanical role of microfilaments, microtubules and intermediate filaments on living adherent endothelial cells, (Wang, 1998). Stiffness was measured in normal conditions of the CSK and after cell treatment with: 0.1  $\mu\text{g}/\text{mL}$  cytochalasin-D to disrupt actin; 10  $\mu\text{g}/\text{mL}$  nocodazole to disrupt microtubules; 4 mmol/L acrylamide to disrupt intermediate filaments; and 15  $\mu\text{mol}/\text{L}$  taxol to induce polymerisation of microtubules.

of epithelial cells during stretching with MTC. The authors did not observe changes in cells stiffness of the cortical region upon actin disruption with Latrunculin-A after stretching, though that cell behaviour became closer to a pure elastic response when F-actin in the cell interior was disrupted. A purely elastic response is frequency-independent. Therefore, this experimental study corroborates the low ability of the cortex to resist shear forces for *quasi-static* conditions.

#### 4.4.5 Main conclusions

Reaction forces within the cell, that result from simulating both AFM indentation and stretching as in MTC, were determined using the developed multi-structural single-cell finite element model.

The combination of numerical and experimental approaches in this study gave two sets of data to learn more about the cytoskeleton's role for force

transmission through the cell. One is that this new cell model quantifies and explains the previously reported differences for the mechanical role of each CSK component for the diverse experimental single-cell stimulation techniques. Actin cortex and microtubules are the major CSK components to resist compressive loads, and actin bundles together with microtubules are essential to resist shearing loads. Finally, using this numerical cell model, the specific role of the actin cortex for cell integrity was isolated from the remaining CSK networks.

This second one, allows the characterisation of the biophysical and biochemical changes associated with cytoskeleton functions. Using this method of having both the AFM force-induced results before and after CSK-disruption recorded in the same cell ensures validity of the results, in spite of the natural diversity and variance between cells.

The model identifies which cytoskeleton components determine the physical properties of adherent cells and target cellular mechanosensitivity depending on the type of external force sensed by cells. This study illustrates that considering one elasticity to describe cellular mechanical properties on a whole cell basis is not sufficient, but it is also needs to consider variations of specific intracellular mechanical properties.

---

## SENSITIVITY ANALYSIS TO EXPLAIN CELL MECHANICS VARIABILITY

---

### 5.1 Introduction

Mechanical response of cells is dependent on the type, physiological conditions, and its mechanical environment. Distinct mechanical properties have been measured for different cell types, which can be related to their specific role in a tissue (Huang et al., 2005; Slomka et al., 2011; Wood et al., 2012). These mechanical differences happen either in different parts of the cell (Bausch et al., 1998) or during distinct cellular processes in the same cell type. Such differences are normally associated with the arrangement of the CSK components in certain locations (Huang et al., 2005; Wood et al., 2012). Typically, actin is enriched in the edges of cells and comprises the cell cortex, whereas the microtubules, intermediate filaments and deep actin fibres are predominantly located in the middle of the cell around the nucleus (Deguchi et al., 2006).

Concentration, organisation, and type of cytoskeletal polymers, that define the mechanical properties of a whole cell, are expected to vary widely among cell types and dictate not only phenotypic but also physiological conditions of cells. In terms of cell rigidity for different phenotypes, mechanical

characteristics of cells are dependent on the physical properties of the tissue of origin, and therefore associated with cell function. Examples include different ranges of Young's modulus found for different cell types: Young's modulus in the range of 0.2 - 1.4 kPa was measured for leukemia myeloid cells (HL60), a type of leukocytes (Rosenbluth et al., 2006); 1.3 to 7.2 kPa for human umbilical vein endothelial cells (HUVECs) (Mathur et al., 2004); 3 - 12 kPa for 3T3 fibroblasts with AFM mechanical testing (Rotsch et al., 1999); 14 - 21 kPa for chondrocytes (Nguyen et al., 2010); 0.4 - 20 kPa for osteoblasts (HBMSC) (Simon et al., 2003); and cardiocytes 90-110 (Mathur et al., 2001).

For example, in terms of the distribution of CSK components found in different cells, nervous cells have single actin filaments without stress fibres, whereas myocytes and osteoblasts have actin bundles organised into differently thick stress fibres (Gardel et al., 2004). Differences in the mechanical behaviour of alveolar cells could be due to phenotypic differences in biomechanical properties of their microstructure. The observed localised variation in alveolar deformation suggests that mechanical heterogeneity might play a central role in mechanotransduction and intercellular signalling (Azeloglu et al., 2008). Lymphocytes are known to change their rigidity from rigid spheres, that resist shear stress and protect from damage in circulation, into a highly deformable state for extravasation through the endothelial cells to the injury site (Brown et al., 2001). Other cellular processes, such as differentiation of stem cells, have been discovered to undergo massive structural changes upon changes in the cell state or function and involve nuclear changes needed for gene transcription and differentiation (Pajerowski et al., 2007). Also non-native processes, such as cancer progression have been associated with changes in the rigidity of cells and with changes in the biomechanical

environment of cells (Yu et al., 2011).

Mechanical changes in the cell interior enable cellular processes to occur and the CSK components are believed to contribute to define the mechanical response of a cell type. However, it is not always possible to identify the mechanical properties of the component responsible for such changes. This variability in cell mechanical properties adds a degree of complexity to biomechanical experimental and theoretical studies. Therefore, accurate *in vitro* phenotypic classification might be only possible in combination with numerical models.

To examine the intracellular distribution of mechanical properties in cells, and better understand the source of heterogeneity, a sensitivity study of the mechanical properties of the cellular components during finite element analysis is proposed in this study.

The results from fluorescent images of the actin distribution on the two cell types tested with AFM (chapter 4) showed different spatial arrangement of the actin networks as well as different rigidities for the two cell lines. Based on this observation, it was decided to investigate, with a sensitivity analysis, if there is a relationship between material properties of the CSK and cell rigidity in defining the properties of a cell line. If the results of the sensitivity study for the material properties of the cell model are presented within a wider variation covering biological changes for different cell types, then the results are more compelling than if for a single generic model.

In the study, this sensitivity analysis will be used to evaluate how alterations in material properties affect model predictions in terms of rigidity, to build up the structure-function relationship of living cells. The ultimate goal is to understand which are the important parameters that need to be measured experimentally for: an accurate classification of the cellular mechanical

behaviour of a cell line; and to identify which biological parameters in cells influence tissue mechanics the most. The ability to model the mechanical responses of different cells may present many opportunities to medical research to identify changes from physiological conditions to disease (Ingber, 2003a; Slomka & Gefen, 2010).

## 5.2 Methods

### 5.2.1 Parametrical analysis of the cellular components

Changes in the microstructural components of cells and in their mechanical properties can be indicative of the cell state or function. A parametrical analysis means that important input parameters of the condition settings are changed in order to analyse the results for multiple cases. In this case, the condition settings are the material properties of the single-cell model specified in Table 3.2, and the parameters are the mechanical properties of the different components of the cell. It is important to remember that sensitivity analysis is different from model calibration, where the same input parameters are changed in order to fit the experimental results.

This parametric study was performed to evaluate the effect of the material properties of the cellular components on cell response to understand mechanical features from different cell types. The material properties of the components in the cell model (the Young's modulus of all of the cell components, the thickness of the cortex and the Poisson's ratio of the cytoplasm) were 50% increased and decreased with respect to the initial value presented in Table 3.2. Depending on the range of values reported in literature, the material properties of some components were also varied in higher/lower orders of magnitude from the initial value reported in Table 3.2 to cover all the

possible range of values for the material properties measured experimentally.

One of the most difficult parameters to measure experimentally is the number of CSK fibres. However, the effect of the amount of fibres present in cells can be evaluated computationally. The number of the discrete components of the CSK in the model was varied and the effect was analysed in terms of reaction force. The changes in the number of fibres in the structure of the model were done with both actin bundles and microtubules generation algorithms. In order to replicate physical conditions and ensure that the model can be solved successfully, both ends of the new actin bundles were anchored at nodes along the cell cortex. Increased number of actin bundles was generated by the algorithm not only along the cell periphery but also in deeper locations at the cell interior. For the microtubules, the common node of origin, next to the nucleus, representing the centrosome was maintained and the end nodes were randomly chosen at the cell periphery in the cortex. For both generation algorithms the new created fibres were contained completely within the cytoplasmic volume of the model cell and were not allowed to exist inside of the nucleus. Lastly, the importance of interconnectivity between actin bundles, cortex and microtubules was tested by disintegrating this structure. The end nodes of the discrete components were changed from the cortex to different nodes in the cytoplasm, so none of the fibres was in contact with each other.

### **5.2.2 Measuring mechanical parameters in living cells**

Numerical quantification of cell rigidity and the parametric analysis of the mechanical properties of the cell components, which corresponds to modelling the CSK of different cell types, were combined with microscopic images of the two previously tested cell types, NIH-3T3 fibroblasts and U2OS osteosar-

coma cells. The two main parameters to be evaluated from the microscopic images were the thickness of the actin located at the cell periphery, and the area of adhesion of the two cell types in the acrylic chamber used for the AFM experiments. There is no experimental technique to date capable of accurately measure cortex thickness. Nevertheless, rough measurements of the amount of actin in the cell periphery were obtained from the fluorescent microscopic images of untreated NIH-3T3 and U2OS cells, using Image-J. This was done by zooming into the microscopic image of each cell and measuring the thickness of the actin intensity at the cell edge, after including the scale bar for calibration of each image according with the microscope and objective used. These measurements were compared with the numerical predictions of varying the thickness of the cortex in the sensitivity analysis.

Some researchers claim that the shape of the cell is one of the major factors affecting the mechanical response of cells. Therefore, numerical models should be cell-shape specific ([Diz-Muñoz et al., 2013](#); [Slomka et al., 2011](#)). To evaluate this cell-specific hypothesis, force measurements with AFM for the two cell types were combined with microscopic imaging to establish correlation between spreading area and Young's modulus. The spreading area of NIH-3T3 and U2OS cells was measured using Image-J after calibration for the respective microscope, camera and objectives used for imaging each cell type, as described in chapter 4. Correlation between variables was analysed using a Pearson's product moment correlation coefficient that measures the linear relationship between two normally distributed variables. Two-tailed test of significance was used. The value of the correlation coefficient varies from -1 to 1. A positive value means that the two variables under consideration have a positive linear relationship (i.e., an increase in one corresponds to an increase in the other) and are said to be positively correlated. A negative

value indicates that the variables considered have a negative linear relationship (i.e., an increase in one corresponds to a decrease in the other) and are said to be negatively correlated. The closer the value is to 1 or -1, the stronger the degree of linear dependence.

## 5.3 Results

### 5.3.1 Numerical analysis of the properties of the cellular components

Variation of both Young's modulus and thickness of the actin cortex (Figure 5.1 A and B) changed significantly the reaction force of the cell in compression. Increase in the Young's modulus of cortex from 2kPa to 20kPa (10-times increase) caused an increase of 4.2-times the reaction force of the cell during compression, and an increase of the thickness of the cortex from 0.2 to 1  $\mu\text{m}$  caused an increase of 3-times in cell response to compression.

During stretching, the variation in reaction force when both the Young's modulus and cortex thickness were changed was not as significant as in compression, which is suggested by the fact that the cortex does not play a major role in stretching.

Variation in the Young's modulus of microtubules to half or twice the normal value affects only slightly the reaction force in both compression and stretching (Figure 5.1 C). The rigidity of the microtubules is well documented in literature and the input values used in computational analysis are consistent. Therefore, other orders of magnitude were not analysed for the response of microtubules.

Variation of Young's modulus of actin bundles in compression did not

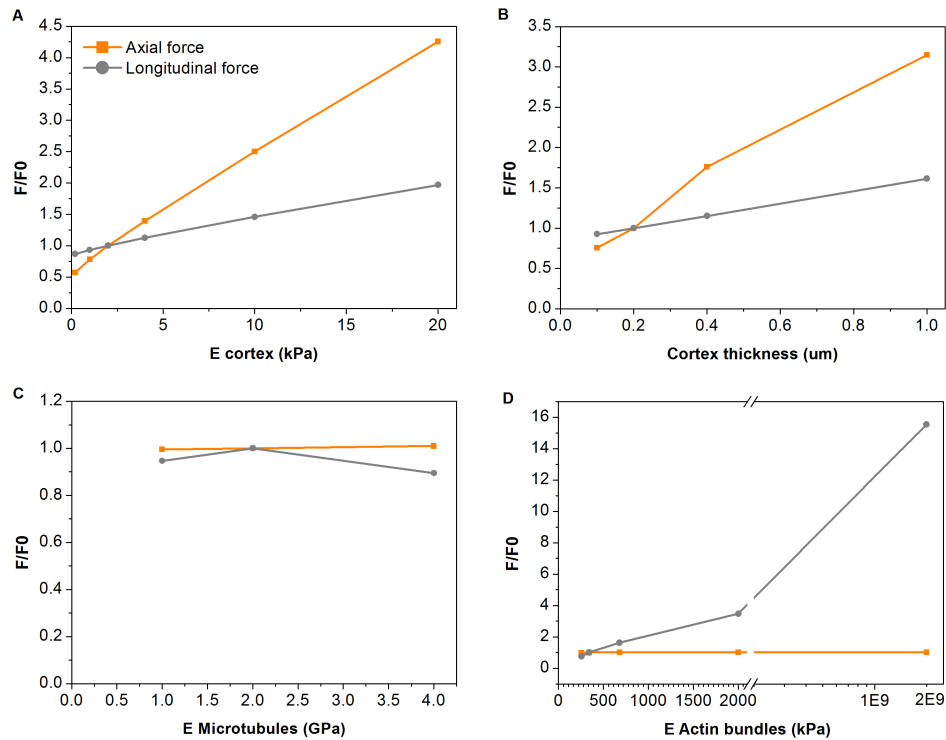


Figure 5.1: Parametrical study of the mechanical properties of the CSK components and the effect in the overall reaction force of the cell. The FE model parameter for the Young's modulus of cortex, actin bundles and microtubules, and cortex thickness were varied, showing the main effect of actin bundles rigidity, cortex rigidity and thickness in the shearing reaction forces, and the main effect of cortex rigidity and thickness in the compressive response of the cell. No effect of actin bundles rigidity in cell force during stretching was predicted for the current configuration of the fibres.

affect cell force (Figure 5.1 D). However, during stretching, when the Young's modulus of actin bundles is increased to twice the initial value, the reaction force is 1.6-times higher. Decrease of the Young's modulus of actin bundles by 25% during stretching had a similar effect, with a decrease of the reaction force by a factor of two. Due to inclusion of prestress in this component of the CSK and also due to the fact that they are interconnected with the rigid microtubules, decrease in 50% of the initial Young's modulus was not possible for convergence of the model. Furthermore, the actin fibres organise themselves in different networks with different mechanical properties and the Young's modulus was represented from values that vary from a few kPa to a few GPa (the same rigidity of microtubules), which corresponds to the rigidity of single stress fibres isolated from cells. In this latter case, the reaction force of the cell during stretching is 16-times higher, while it remains constant during compression.

Due to the complexity of the CSK, these structures are normally modelled as a simplification of reality. For this reason it is important to study the effect of the density of the fibres in the cell model, as well as the way they are interconnected to each other (Figure 5.2). The number of nodes shared between actin bundles and microtubules in the cortex, defining the interconnectivity between CSK components, affects the reaction force of the cell when responding to shear forces. The density of elements representing the microtubules in the model seems to be adequate since there was not much variation of the resulting cell force. Increase in the number of actin bundles had a significant effect when the cell was under compression but not when responding to shear forces. The actin bundles that were added to the original model were not only distributed along the periphery of the cell but also in the cell interior, which might be more under compression due to the

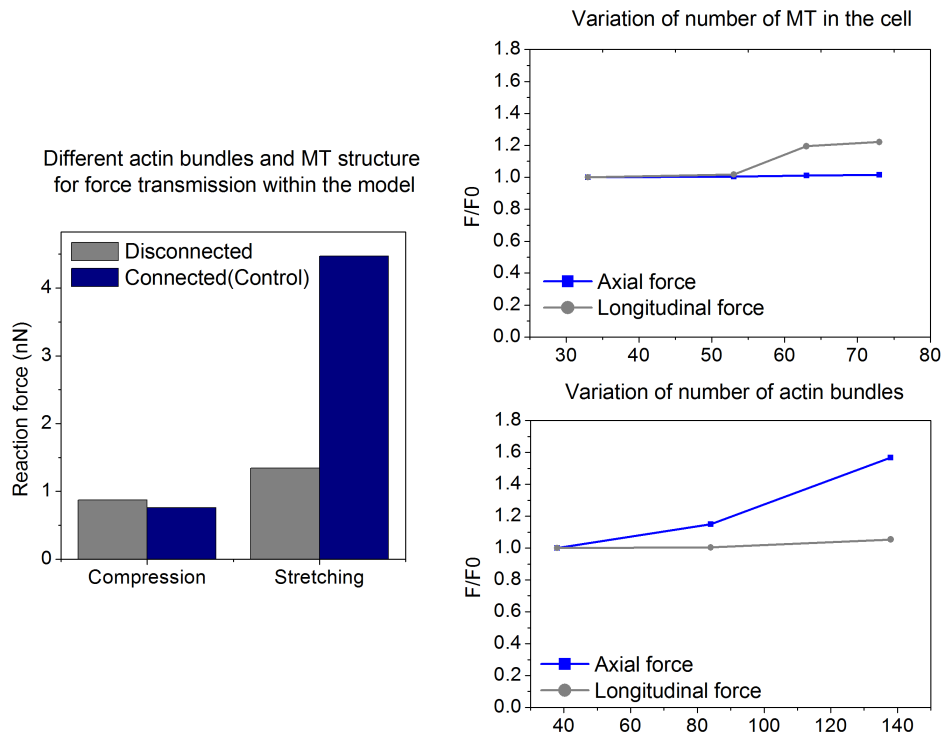


Figure 5.2: Structural and spatial variation of actin bundles and microtubules. Sensitive analysis of the discrete structure of the actin bundles and microtubules for force transmission (left). Effect of the density on cellular force was analysed for compression and stretching by varying the number of both microtubules and actin bundles (right).

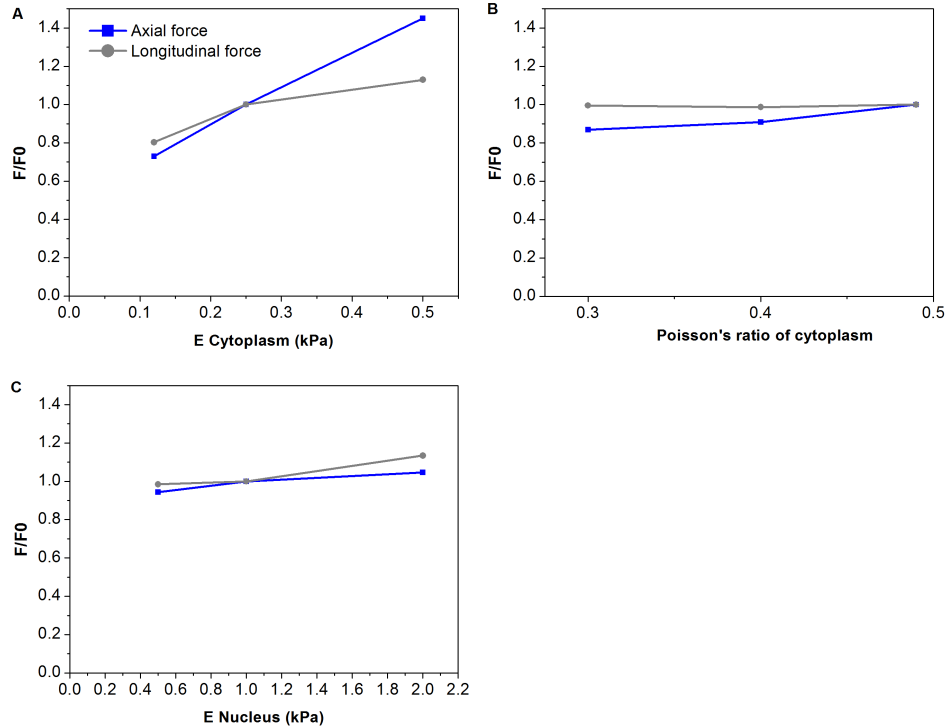


Figure 5.3: Parametrical study of the mechanical properties of the continuum elements of the cell (cytoplasm and nucleus) for the effect in the overall cell reaction force.

change of configuration. An increase in cell force during compression was always observed for increased number of actin bundles in the cell interior, even considering different random spatial distributions.

Parametrical analysis of the mechanical properties of cytoplasm and nucleus, the continuum elements of the cell model, were shown to have little effect on the mechanical response of the cell (Figure 5.3), when compared to variation of properties of the CSK components. Variation of cytoplasm rigidity, representing the cytosol, which is the largest structure of the cell,

was expected to have mechanical relevance, as seen in Figure 5.3 A.

A summary of the material properties affecting the model cell response is presented in Table 5.1.

*Table 5.1: Material properties affecting cell response*

Axial forces (Compression)	Longitudinal forces (Stretching)
	Cortex thickness
	Cortex rigidity
	Cytoplasm rigidity
	Rigidity of actin bundles
	Number of microtubules
Number of actin bundles	

### 5.3.2 Relationship between rigidity and spreading area of cells

In order to understand the effect of adhesion in cell stiffness, the surface of each cell in contact with the acrylic chamber (spreading area) was measured from the microscopic images. For the 3T3 fibroblasts, a very weak positive correlation value of 0.07 was found between cell rigidity and spreading area (Figure 5.4), indicating that the rigidity of the cell was not dependent the amount of spreading in the substrate. The average of the spreading area of 3T3 cells was  $1608.7 \mu\text{m}^2$ , the average  $E$  was 3.2 kPa, and the total number of cells for this study was  $N = 25$ .

The same analysis was made for U2OS cells with a negative correlation value of -0.4 between cell rigidity and spreading area (Figure 5.5 A and B),

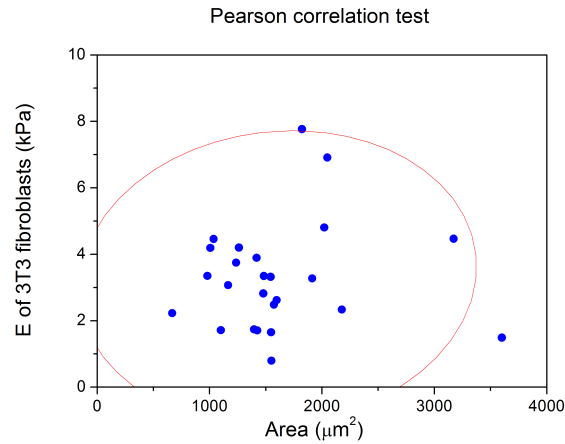


Figure 5.4: Confidence ellipse of the correlation between Young's modulus and spreading area of NIH 3T3 cells.

an average surface area of contact of  $1442.6 \mu\text{m}^2$  and average  $E$  of  $1.6 \text{ kPa}$  measured for a total of  $N = 27$  U2OS cells. For this cell type, the effect of adhesion time in the cell rigidity was also evaluated, as shown in Figure 5.5 C and D). For 30 minutes adhesion to the acrylic chamber before measurements, the correlation between  $E$  of U2OS cells and spreading area was  $0.5$  (Figure 5.5 C), considering  $N = 15$  cells, average area of  $1038.6 \mu\text{m}^2$  and average  $E$  of  $1.9 \text{ kPa}$ . For 1 hour of adhesion before measurements, the obtained correlation between the same variables was  $0.3$  (Figure 5.5 D), considering  $N = 12$  cells, average area of  $1947.5 \mu\text{m}^2$  and average  $E$  of  $1.3 \text{ kPa}$ . Correlation values were similar for 30 minutes and 1 hour adhesion time, showing that time did not affect the relation between surface area and rigidity. These correlation values were not sufficient to show a strong effect of spreading area in cells rigidity.

The parametrical study together with the AFM force-indentation curves and optical images were used to predict possible common characteristics for

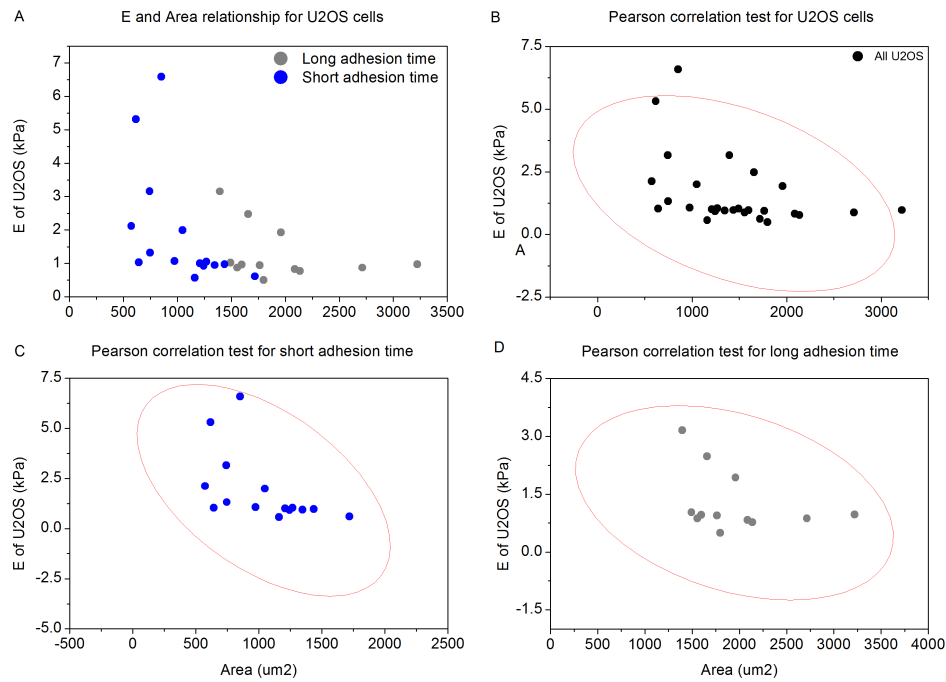


Figure 5.5: Confidence ellipse of the correlation between Young's modulus and spreading area of U2OS cells. U2OS cells were placed in the acrylic chamber for 30 min and 1 hour of adhesion before measurements and imaging with AFM, which corresponds to short and long adhesion time, respectively.

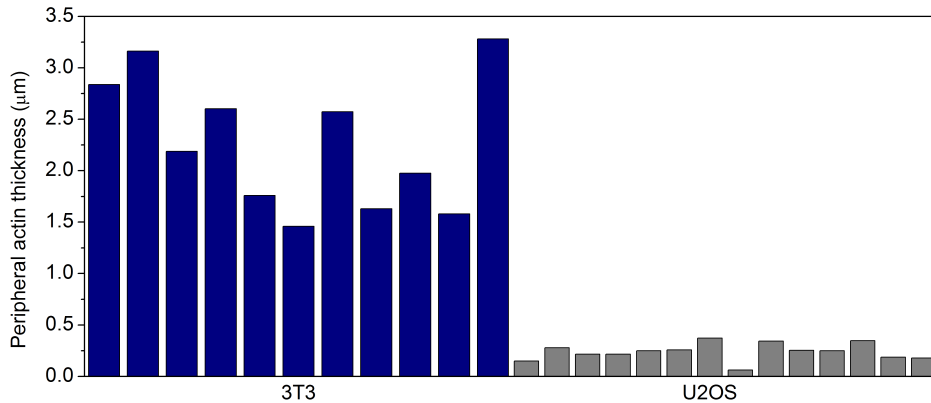


Figure 5.6: Measurements of peripheral actin thickness from microscopic images of living 3T3 and U2OS cells.

cells with different rigidities. Although the cortex thickness is difficult to measure experimentally (since it is difficult to identify this structure from microscopic images), it is possible to have rough measurements of the peripheral actin thickness labelled at the edge of the cells (see Figure 5.6 for the U2OS and 3T3 cells). The average thickness of the peripheral actin was  $2.3 \pm 0.6 \mu\text{m}$  for 3T3 cells and  $0.2 \pm 0.08 \mu\text{m}$  U2OS cells.

Increasing either  $E$  of the cortex from 2 to 10 - 20 kPa or cortex thickness from 0.2 to 1  $\mu\text{m}$  computationally, matched AFM force-indentation curves of 3T3. This cortex reinforcement of 3T3 cells predicted by the current model was corroborated with microscopic images of this cell type (Figure 4.10 B), showing a higher amount of actin at the cell edge in 3T3 cells.

## 5.4 Discussion

Numerous decisions have to be made in the process of building and loading a FE model cell regarding, among other things, model geometry, material properties and boundary conditions. All these parameters affect the way in which cells respond to external forces. In order to make reliable statements based on FE analysis, it is important that input parameters introduced in the model are in relation with the biological variation found in literature for changes in cell mechanics depending on its structure and function. The sensitivity study is a crucial step in constructing an effective model and in interpreting the output results.

Mechanical properties of CSK networks characterise cells with different rigidities. Cells have a very dynamic nature and internal changes occur in specific cytoskeletal networks when cells are required to adapt to new external conditions. To ensure that a cell maintains its physiological function, the CSK filaments polymerise and depolymerise accordingly. However, the mechanical properties of the cellular components are not defined in literature for each cell type.

Material properties for the multi-structures of the FE model were assumed from literature, and the sensitivity of the results to those values was examined. Hence, sensitivity analyses were performed to understand the effect of varying the mechanical properties of the CSK components in cellular response to compression and stretching. It was shown here that the mechanical properties of the whole cell were dependent on the specific structural distribution and properties of cytoskeletal components.

The parametric study showed that for the same 50% increase of the mechanical properties of the cell components, axial force was highly sensitive to changes in cortex thickness, cortex Young's modulus, rigidity of the remain-

ing cytoplasm, and to the increased number of actin bundles in the interior of the cell. However, axial force was relatively insensitive to changes in the microtubules Young's modulus, nucleus rigidity and cytoplasm compressibility. The parameters that influences the most the changes in cell force to resist compression are cortex thickness and rigidity. This is in accordance with previous findings showing that the cortex is the major component to resist compression. Longitudinal force was sensitive to changes in the rigidity of actin bundles and increase in the number of microtubules in the cell, but relatively insensitive to changes in the mechanical properties of the remaining cell components (see Table 5.1).

Incompressibility of the cytoplasm was tested by changing the Poisson's ratio and no effect for the maintenance of cell forces in resisting different loading conditions were found. Nucleus rigidity is known to be higher than the rigidity of the surrounding cytoplasm (Caille et al., 2002; Guilak & Mow, 2000; Maniotis et al., 1997). Although the nucleus could play an important role in stabilising the cell when subjected to mechanical forces, the results of the parametrical study showed that the reaction force of the cell to different loading conditions was not affected by variation of nucleus rigidity. The material properties of the nucleus were not crucial for cell integrity in this study. Nevertheless, the spatial location of the nucleus was shown to influence cellular forces in compression. The nucleus in the current FE model is connected to the discrete fibres of the CSK by only one node representing the centrosome, where the microtubules are originated. Because the forces have been shown to propagate in a discrete manner inside the cell, and a discrete network of fibres representing the nucleoskeleton surrounding the nucleus is not considered in this model, the computational predictions may be underestimating the effect of nucleus rigidity.

Changing the interconnection of the discrete elements affected the cell response when the cell was stretched but not in compression. The decrease in the force during stretching, when the discrete components were not connected to each other or to the cortex, is because the cell loses the main structure responsible to resist this type of forces. This shows the importance of having connections between the discrete elements of the CSK for force balance. This only happens in response to shearing because the load applied in the model for compression is not sufficient to activate the response of actin bundles, using this configuration/distribution of the bundles in the interior of the cell model. For this reason, there is only a slight difference in the transference of forces between discrete components. The reaction force during compression is slightly higher in a cell with a disconnected discrete structure of the CSK. This is believed to be due to the fact that the rigid microtubules are the only structure responding to the external deformation by developing high forces that are not being counter-balanced by the actin bundles in this model. In this case, the response to compression is also mainly dependent on the mechanical properties of the cortex and not on the behaviour of the discrete components.

Furthermore, it was observed that varying the number and orientation of the actin bundles inside the cell changes the resulting compression forces obtained (Figure 5.2): the more actin bundles in the cell model, the higher the compression forces obtained. This is related with the orientation of the bundles with respect to the direction of the external indentation applied to the cell. In this new configuration, there are more actin bundles that were randomly generated inside the cell and therefore, they have a very different orientation from the initial actin bundles distribution adopted in the model. The new actin bundles configurations analysed have more fibres oriented with

respect to the bead displacement applied on the top of the cell. This suggests that for more actin fibres oriented in the direction of indentation, the compression forces obtained with the model will be higher. Moreover, the model suggests that more fibres oriented in the direction of indentation will increase the actin bundles capability of responding to compressive forces, which may be related with contractility as suggested by [Caille et al. \(2002\)](#); [Ofek et al. \(2009\)](#); [Peeters et al. \(2004\)](#); [Weafer et al. \(2013\)](#). This also suggests that the model is highly sensitive to the assumed distribution, density and orientation of truss elements representing the actin bundles.

Cell mechanics experimental techniques such as, micropipette aspiration ([Pajerowski et al., 2007](#)), AFM ([Cross et al., 2007](#)) and flow cytometry ([Rosenbluth et al., 2008b](#)) were helpful tools to assay this cellular heterogeneity and have led to findings associating cellular mechanical properties to different cell states. However, there is still no accurate technique to measure the mechanical properties of the different actin organisation in cells. This model and the sensitivity study combined with AFM force measurements and imaging was shown to be effective in providing more information on this matter. This complex material model is sensitive to the parameters mentioned above, for the different loading conditions simulated, compressing and stretching. This analysis enabled the understanding of the model predictions to assess which might be the optimum values into the biological context. Some cell modelling work published in literature have shown the effect of material properties in cell response ([Caille et al., 2002](#); [McGarry, 2009](#); [Ofek et al., 2009](#)). For this multi-structural model, the inclusion of many components brings the need to tackle the more difficult factors such as, the CSK fibres interaction and the distinction between deep and cortical actin properties.

Cell rigidity was only greatly affected for high variation of the rigidity of the CSK components, meaning that those structures are strong and stable. For these cases, the parametrical study together with the AFM force-indentation curves and optical images were used to predict possible common characteristics for cells with different rigidities. This is particularly important to understand how the mechanical properties of the distinct networks of actin CSK, actin cortex and actin bundles, affect cell force. For these two cell components, the mechanical properties were varied covering the extended range of values that are commonly reported in literature. Increasing either cortex elasticity or thickness in the FE model provided information about forces generated during compression by stiffer cells. These models showed that the whole cell rigidity is in the range found experimentally for the 3T3 fibroblasts. Models considering cells with either thicker or more rigid cortex generated more force to resist the same amount of compressive loads. Increasing both rigidity and thickness of the cortex also increases linearity in the force-indentation curves predicted by the model since it overcomes the effect of the non-linear components in the model, the prestressed actin bundles. This is in agreement with the higher amount of fibres in the cortex area of the 3T3 fibroblasts compared with the U2OS cells.

Cortex thickness is reported to be in the range of  $0.1 \mu\text{m}$  to  $2 \mu\text{m}$  (Fritzsche et al., 2013; Moreno-Flores et al., 2010; Unnikrishnan et al., 2007). Previous studies of fluorescence images of suspended cells showed that the cortical thickness of a normal NIH-3T3 or BALB-3T3 fibroblast is in the range of  $17 \pm 23\%$ , while that of malignantly transformed SV-T2 fibroblasts is in the range of  $12 \pm 15\%$  of the cell area (Ananthakrishnan et al., 2006). The authors then used theoretical models to show that actin cortical thickness is the most important determinant of the mechanical response, in the

linear regime, for those types of cells (Ananthakrishnan et al., 2006). Therefore, when the  $E$  and thickness of the cortex are increased in this study within the physiological range accepted in literature (Ananthakrishnan et al., 2006; Brugués et al., 2010), it is possible to predict forces obtained for different cell types (different rigidities and during different cell processes).

Therefore, it is important to discuss information from this sensitivity study of cell mechanical properties to understand the numerical and the biological impact for future developments at both levels. Sensitivity studies in computational predictions are as important as model validity and validation.

This study was started before validation to elucidate the model characteristics that need to be monitored during the experimental procedure for an appropriate validation. After validation, the sensitivity study was revised, as suggested in Anderson et al. (2007). In this way, the sensitivity study allowed the understanding of the differences from different experimental observations for different cell types, complementing model validation of the results obtained with the 3T3 fibroblasts in the previous chapter.

In general research, and future clinical application, understanding the changes in the mechanical properties of the structural components of cells can be used as cell identifiers, indicative of disease, to predict the degree of differentiation important for stem cells therapy or give information on the metastatic potential in cancer cells. For drug discovery, a simple measure of cytoskeletal integrity could allow screening for cytoskeletal-acting drugs or evaluation of cytoskeletal drug resistance (Tse, 2012).

### 5.4.1 Main conclusions

The sensitivity analysis predicted that cell axial and longitudinal forces are highly affected by changes in cortex thickness, cortex Young's modulus and

rigidity of the remaining cytoplasm. However, these cell forces are relatively insensitive to changes in the microtubules Young's modulus, nucleus rigidity and cytoplasm compressibility. Only longitudinal force is sensitive to changes in the rigidity of actin bundles and increase in the number of microtubules in the cell. On the other end, only axial force was sensitive to increase of actin bundles in the interior of the cell. This information helps to clarify the structure-function relationship of the cell, showing that loads are predominately carried by the cortex for the loading and boundary conditions examined, and also provided valuable guidelines in the structure of each CSK component for future cell-phenotype modelling efforts. This FE sensitivity study was used to conduct virtual experiments that can be used for further parameter optimisations to identify structural difference between several cell types or cell processes, without having to assemble large experimental samples and time.

---

# COMPUTATIONAL INVESTIGATION OF POWER-LAW BEHAVIOUR IN ADHERENT CELLS

---

## 6.1 Introduction

Rheological properties of living cells determine how cells interact with their mechanical environment and influence their physiological functions. A mechanical behaviour called power-law rheology is considered as an intrinsic feature of cell structure when responding to mechanical stimuli. Power-law together with prestress are governing principles of cell deformation over time, and the controlling physics is at the level of cytoskeletal lattice properties.

When exhibiting viscoelastic phenomena, such as creep or stress relaxation, the elastic moduli of cells show a weak-power dependence on time or frequency. This has been qualitatively and quantitatively demonstrated with several experimental techniques (Dahl et al., 2005; Desprat et al., 2005; Fabry et al., 2001; Hoffman et al., 2006; Lenormand et al., 2004). This mechanical behaviour has been studied to find more about the coordinated assembly and disassembly of cytoskeletal polymers for CSK remodelling at different time-scales and during different cellular processes. However, intrinsic mechanical material properties remain difficult to quantify due to cell heterogeneity, active cytoskeletal forces, irregular geometry and a complex viscoelasticity (Lim

et al., 2006; Zhou et al., 2012). To this end, a mathematical model must be developed that accurately describes the testing configuration and must be based on an appropriate constitutive equation, describing the power-law and cellular prestress.

To describe spatial and temporal aspects of cell response, several models have been proposed based on, and to explain, observations from MTC and micropipette aspiration experiments. The two most common models currently standing in literature include the soft glass rheology model and the tensegrity. The SGR model describes the dynamic feature of the cell mechanical properties (Bursac et al., 2005; Deng et al., 2006; Fabry et al., 2001), whereas the tensegrity model describes prestress-dependent force balances in living cells (Ingber, 2003b; Wang et al., 2001b, 2002). However, the two intrinsic features governing cell rheology have not been combined into a single model yet.

The attention that prestress and power-law behaviour of cells has lately received is, in part, due to experiments examining the behaviour of cells under cyclic-loading conditions (Bursac et al., 2005) in the frequency domain (Vaziri et al., 2007). To test different types of forces, other than sinusoidal and cyclic conditions with MTC and micropipette aspiration, AFM was further developed to allow rheologic studies, which can be used to perform standard creep but also stress-relaxation tests. The advances in AFM technology include the programming of custom load or displacement profiles, frequency variation and small horizontal movements of the cantilever. Previous AFM stress-relaxation work demonstrated the potential of the technique (Alcaraz et al., 2003; Darling et al., 2006; Moreno-Flores et al., 2010; Rosenbluth et al., 2008a) but it did not explore cytoskeletal roles in governing stress-relaxation. Thus, understanding the overall process of stress-relaxation requires identifi-

cation of the contributions of cytoskeletal components with the appropriate viscoelastic models that include the PL rheology behaviour.

More recent biomechanical models incorporating material properties associated with power-law rheology have been developed using FE method (Dailey & Ghadiali, 2010; Vaziri et al., 2007) for a deeper understanding of the rheological cell behaviour. To extend the application of the previous models from frequency to time domain, Dailey & Ghadiali (2010) applied the Prony-Dirichlet series to approximate the PL creep function to study force-induced cell injury with PL behaviour in a FE formulation. Nonetheless, this model was linear and did not account for large deformations, condition normally found in both *in vivo* and *in vitro* cell experiments. With the use of computational simulations and the FE analysis, with models that accurately describe frequency or time dependence viscoelastic response of cells, it is possible to predict absolute stiffness of cells for a single frequency or time scale.

Here, force-relaxation response of cells is investigated using the previous multi-structural FE cell model using material properties associated with power-law. The viscoelastic behaviour of cells is studied under compressive loading conditions in the time domain. This biomechanical model is used to explore the role of material constants associated with power-law rheology affecting the whole cell viscoelastic response. The goal is to explore whether the simulations with this cell model provide data that is in line with the experimental data based on force-relaxation tests performed with AFM. And therefore, presenting a novel, AFM based stress-relaxation FE model, to determine the contribution of the CSK to the viscoelastic properties of living cells.

In this study, the implementation of viscoelastic behaviour is done for the

cytoplasm and to the cortex, which is modelled as an  $\hat{\text{AI}}\text{extension}\hat{\text{AI}}$  of the continuum elements that define the cytoplasm and therefore, increase the number of viscoelastic parameters of the model. Since the model gives the possibility to study cortex mechanical response individually from other components, the viscoelastic contribution of the cortex is investigated, since changes in the viscoelastic properties of the cortex have been associated with evolution of certain diseases, including cancer.

## 6.2 Materials and methods

### 6.2.1 Power-law behaviour

The biomechanical model of the cell, composed of a nucleus, cytoplasm, cortex, microtubules, and actin bundles (presented in chapter 3) was integrated with the material law associated with PL rheology

$$G(t) = G(1)t^{-\beta} \quad (6.1)$$

where  $t$  is time in seconds,  $\beta$  is the PL exponent ( $0 < \beta < 1$ ) and  $G(t)$  is the shear modulus. Power-law behaviour is approximated by Prony-series expansion. Prony-series coefficients were used to fit the PL relationship defined in Equation 6.1 considering  $G(1) = 100$  (Zhou et al., 2012), which was used to calculate the Prony-series parameters defined in Table 6.1.

Prestress, which is related to cells stiffness and has been recently linked to the PL exponent (Kollmannsberger et al., 2011), is defined in the actin bundles of the model. The viscoelastic behaviour defined in Equation 6.1 was used for the cytoplasm, and the remaining components of the cell were defined with elastic properties as used in Table 3.2. The instantaneous modulus was considered to be the same as the Young's modulus used to describe the

elasticity of the cytoplasm  $E = 250$  Pa. A bead was modelled to apply a displacement of  $0.5 \mu\text{m}$  in compression and was held constant for 15 s, after which the bead was retracted to its original position on the top of the cell and relaxation was registered for 15 s more (Rosenbluth et al., 2008a). The loading rate is the same as the unloading rate applied and unloading does not entail a new displacement boundary condition.

### 6.2.2 Numerical implementation of viscoelasticity

Using the FE method for time-domain viscoelasticity, the software Abaqus assumes that the viscoelastic material is defined by a Prony-series expansion of the shear relaxation modulus:

$$G_R(t) = 1 - \sum_{i=1}^N g_i [1 - e^{-t/\lambda_i}] \quad (6.2)$$

Where the Prony-series coefficients  $\lambda_i$  and  $g_i$  are the material constants characterising the relaxation spectrum. These relaxation parameters of the Prony-series were obtained from fitting the PL of creep measurements in the time domain using 6.1 and from finite element simulations ((Zhou et al., 2012)) with 5-term Prony-series expansion ( $i = 1, 2, \dots, 5$ ) using a least-squares regression, which are presented in Table 6.1. This 5-term Prony-series approximation fits the relaxation modulus for  $t = 10^{-3} \sim 10^3$  s, which extends the time domain to cover the time scales used in most of cell mechanics experiments (Zhou et al., 2012). These values are used in this study to evaluate the concept of power-law governance of cellular force-relaxation behaviour.

### 6.2.3 Force-relaxation and equilibration time analysis

The power-law exponent  $\beta$  was varied from 0.1 to 0.5 to study its effect on cell relaxation. This was possible by changing  $\lambda_i$  and  $g_i$  parameters of

Table 6.1: Prony-series parameters for fitting power-law rheology model using Equation 6.1

$\beta$	0.1	0.2	0.3	0.4	0.5
$\lambda_1$ ( $10^{-3}$ s)	3.34	3.13	2.93	2.74	2.56
$\lambda_2$ ( $10^{-2}$ s)	5.61	5.25	4.91	4.60	4.31
$\lambda_3$ ( $10^{-1}$ s)	9.09	8.43	7.84	7.29	6.78
$\lambda_4$ (10s)	1.54	1.43	1.34	1.25	1.18
$\lambda_5$ ( $10^2$ s)	2.87	2.58	2.34	2.14	1.97
$g_1$	0.245	0.429	0.567	0.671	0.750
$g_2$	0.185	0.245	0.246	0.222	0.188
$g_3$	0.139	0.140	0.106	0.0722	0.0463
$g_4$	0.106	0.0801	0.0459	0.0235	0.0114
$g_5$	0.0926	0.0513	0.0216	0.00825	0.00297

the Equation 6.2, as reported in Table 6.1. The effect of the instantaneous modulus ( $E$ ) of the cytoplasm on the force-relaxation curves was analysed by increasing and decreasing the instantaneous modulus by 50%. In the same way, the effect of varying the indentation depth for analysis of larger deformations was analysed by displacing the bead 0.1, 0.25, 0.5, 1 and 1.5  $\mu\text{m}$  in the vertical direction to compress the cell. The effect of prestress in the viscous response of the cell during indentation and retraction of the bead was also analysed in the FE simulation.

Since the FE simulations in the elastic regime (performed in chapter 4) showed the major effect of the cortex in resisting compressive loads, it is hypothesised that this component will have a major contribution in the viscoelastic response of the cell during compression. To test this, force-

relaxation curves from two model simulations were obtained and compared: one model with both cortex and cytoplasm defined as viscoelastic materials; and a model with cytoplasm alone defined as a viscoelastic material. In this case, viscous properties were the same for both cortex and cytoplasm, while the instantaneous moduli defining the elastic contribution were the same values used in the static analysis. Finally, the effect of bead position on the top of the cell is also evaluated for these two models. In this way, whole cell equilibration times in different locations of the cell were evaluated. The position of the bead on the top of the cell was varied away from the nucleus (reference location, called *bead 0*),  $2\ \mu\text{m}$  (*bead 2*),  $6\ \mu\text{m}$  (*bead 6*) and  $8\ \mu\text{m}$  (*bead 8*) to the right, as represented in Figure 3.7.

## 6.3 Results

### 6.3.1 Finite element analysis of whole cell strain and force-relaxation curves

Analysis of cell deformation over time is one of the most important parameters to describe the ability of a cell to respond mechanical forces. Evaluation of strain distribution in the whole cell in different time points was possible using this FE model combined with PL behaviour to simulate AFM force-relaxation during indentation. Upon indentation, high values of minimum principal strains were located under the bead and at the end nodes of the CSK due to actin contractility, as reported in Figure 6.1. The maximum and minimum principal strain values obtained in the cell were slightly higher than the values obtained considering elastic material properties. These changes were expected since different properties were considered with the inclusion

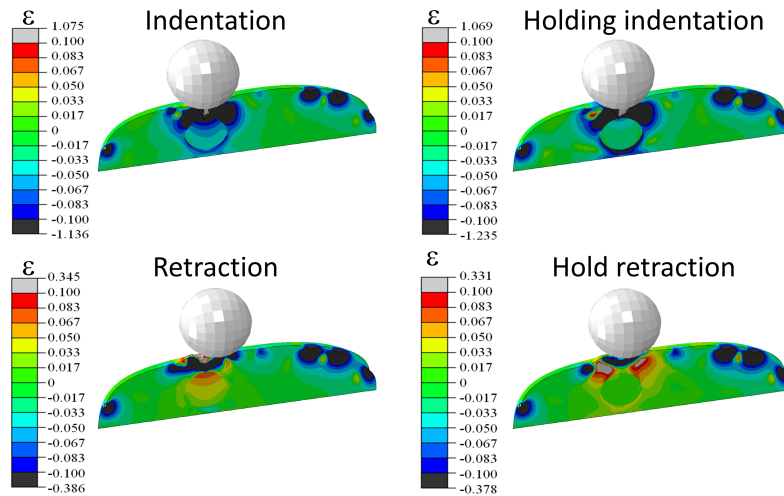


Figure 6.1: Cross-sectional view of strain distribution in the cell over time.

of viscoelastic material properties. The nucleus was mainly affected during indentation (where minimum principal strain values were concentrated under the bead and the nucleus), and during bead retraction (where maximum principal strain values were observed). The distribution of strain in the cell changes over time, mainly under the indentation zone, around the nucleus and in the end nodes of CSK (Figure 6.1).

Force versus time curves describing cell relaxation were obtained considering the different power-law exponents  $\beta$ , as presented in Figure 6.2. Force was plotted as the reaction force of the cell in the nodes that were fixed, as it is defined for the boundary conditions of the model. The initial force upon indentation was similar for the different exponents but the equilibration times increased with  $\beta$ , showing a more viscous behaviour of the cell. This observation is valid for the cell model under compression and after release of the bead.

When holding the indentation for 15 s, the force decreased about 34% (for  $\beta = 0.2$ ), showing force-relaxation (Figure 6.2). This relaxation was observed

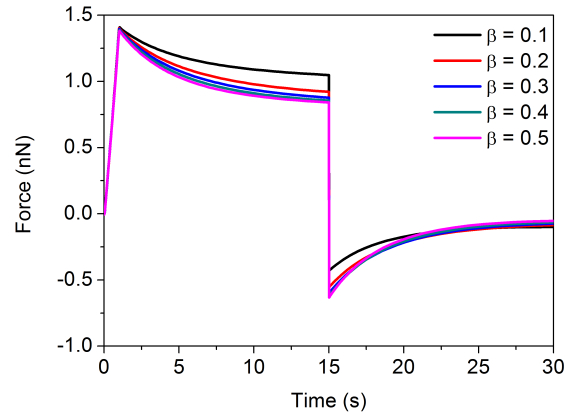


Figure 6.2: Force-relaxation curves considering different PL exponents  $\beta$ .

for all the PL exponents and the decrease is presented in Table 6.2 for the PL exponent considered in this study. For the same force obtained in the elastic response, the bigger the relaxation after 15 s (i.e., the equilibration time, which is described by the slope of the curve in the viscous regime), the more fluid-like is the cell, which corresponds to an increase in  $\beta$ .

Table 6.2: Decrease in force after 15 s of compression

$\beta$	0.1	0.2	0.3	0.4	0.5
force decrease	25.6%	34.4%	37.2%	38.5%	39.1%

To evaluate the effect of prestress during the viscoelastic response of cell in compression, force-relaxation curves with and without including prestress in the FE model were compared, as shown in Figure 6.3. The equilibration time was the same with and without prestress while the cell was being compressed and after bead retraction. However, removing prestress from the model affected the elastic response, causing a small decrease in cell rigidity.

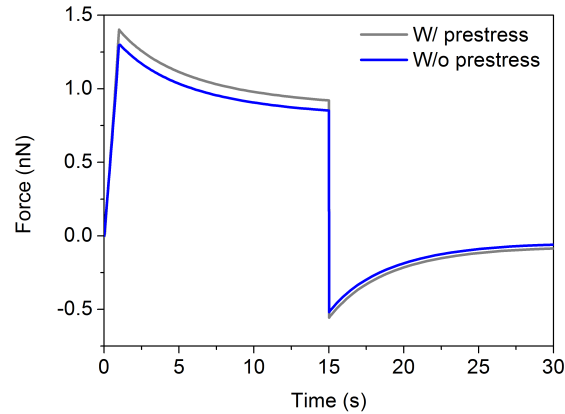


Figure 6.3: The effect of prestress in the force-relaxation curve considering  $\beta = 0.2$ .

### 6.3.2 Effect of loading and instantaneous modulus on viscoelastic response

The effect of the instantaneous modulus on the force-relaxation curve was analysed by increasing and decreasing the instantaneous modulus of the cytoplasm of the cell model by 50%, considering PL exponent  $\beta = 0.2$  (Figure 6.4 A). Both the initial force during the elastic response of the cell and the equilibration time of the cell during the viscous part increased with the instantaneous modulus, meaning that the more solid-like cells are at the beginning the more they behave as fluid-like during relaxation. The same observation was obtained for the effect of the indentation depth on the force-relaxation curves (Figure 6.4 B). This effect, observed during indentation, was also obtained when bead retraction was simulated.

The effect of these two variables, instantaneous modulus and indentation depth, in the force of the cell over time was also estimated for different PL exponents, see Figure 6.5. The initial force upon indentation was not affected

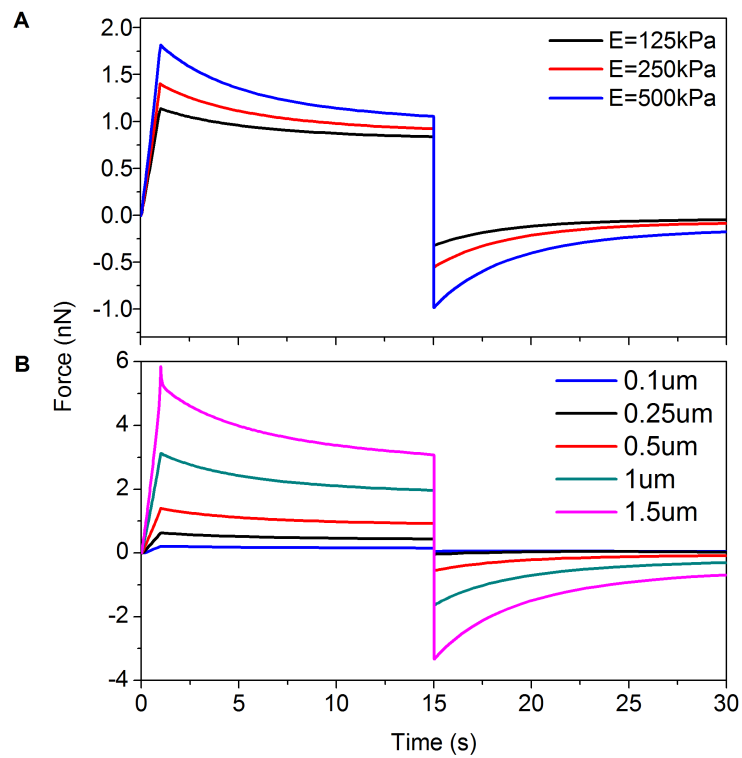


Figure 6.4: Force-relaxation curves considering variation of instantaneous moduli and indentation depths for PL exponent  $\beta = 0.2$ .

by the PL exponents, for the same indentation depth and instantaneous modulus (Figure 6.5 A and C). However, considering the same indentation depth and instantaneous modulus, a decrease in the cell force after relaxation was observed with increasing PL exponent towards a plateau (Figure 6.5 B and D). This was more evident for higher indentation depths and instantaneous moduli, which could be indicative of the departure from the theory of linear viscoelasticity at larger deformations.

### 6.3.3 Distance-dependence force propagation

The force-relaxation was analysed for  $\beta = 0.2$  considering different bead positions. Whole cell force and equilibration times depend on the position of the indenter on the top of the cell (Figure 6.6). Therefore, both elastic and viscoelastic response of the cell during compression were affected by the exact location of indentation. To know more about the effect of material properties of the different components on the viscoelastic response of cells, the bead position was varied considering two models. One where cytoplasm was the only component with viscoelastic properties in the cell (Figure 6.6 A), and the other where both cortex and cytoplasm were modelled as viscoelastic materials (Figure 6.6 B). The effect of these different material properties on the force-relaxation curve was analysed when comparing the plots in Figure 6.6. In Figure 6.6 A, only cytoplasm was modelled as viscoelastic material and the rest of the cell components were modelled as elastic. In this case, there was a decrease in the elastic response with the increase in the distance of the indentation point away from the reference position (*bead 0*), where elastic reaction force was maximum. However, a very high peak in the reaction force was obtained when the bead was in *bead 2* position, which is explained by the fact that this position coincides with the end node of one microtubule.

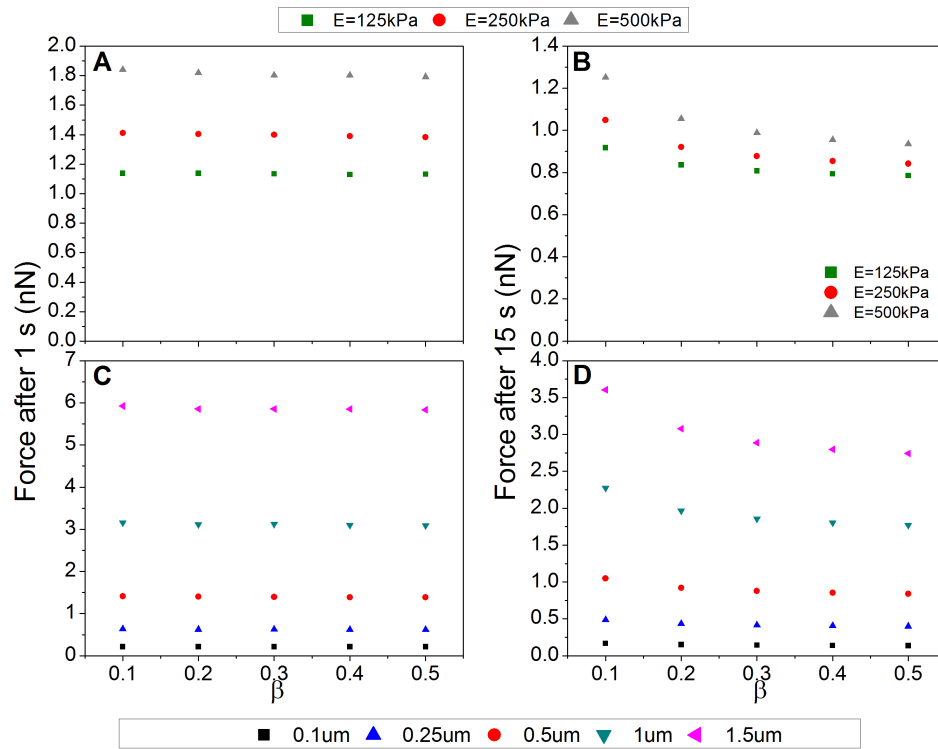


Figure 6.5: Cell forces for different PL exponents considering  $t = 1$  s (which corresponds to the time for maximum indentation), and  $t = 15$  s (which corresponds to the time of relaxation after indentation). (A) Cell force after 1 s considering different instantaneous moduli, (B) Cell force after 15 s considering different instantaneous moduli, (C) Cell force after 1 s considering different indentation depths, and (D) Cell force after 15 s considering different indentation depths.

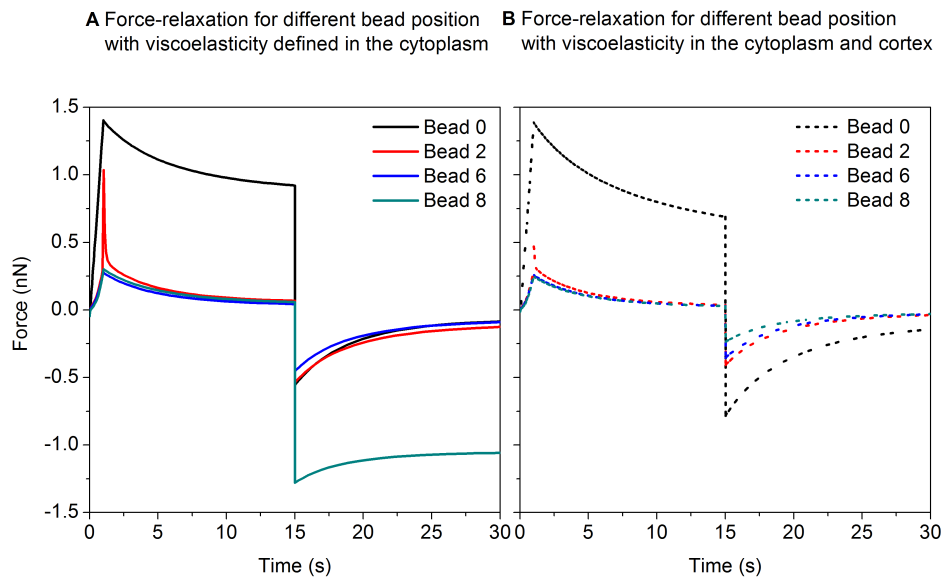


Figure 6.6: Force-relaxation curves for different bead positions: (A) considering viscoelasticity defined in the cytoplasm and elastic material properties defined for the remaining components of the cell, and (B) considering viscoelastic material properties for both cytoplasm and cortex.

No trend in the reaction force was obtained when the bead was removed from the cell. When looking at the equilibration time, the slopes of the curves in the viscous part did not change considerably with the indentation position.

When the cortex together with the cytoplasm were modelled as viscoelastic materials (Figure 6.6 B), a decrease in the elastic response with an increase in the distance of the indentation point was also observed. However, the recovery after bead retraction was smoother when the cortex was modelled as viscoelastic. Furthermore, the difference in the equilibration time during the viscous response was more pronounced than when only the cytoplasm was modelled as viscoelastic. The equilibration time decreased with the distance of the bead away from the reference position, and it was less accentuated further away from the reference position.

In Figure 6.7, the viscoelastic responses of the cell considering the different material properties were observed in detail for the bead positions represented as *bead 0* and *bead 6*. Here, for the same initial elastic response, the equilibration time during the viscous response of the cell (after 15 s) increased when cortex and cytoplasm were modelled as viscoelastic. This difference was much higher for the position represented as *bead 0* than when the bead was further away from the nucleus. No trend was observed upon bead retraction, at  $t = 30$  s. However, retraction happened more rapidly when the bead was in positions further away from the nucleus. This might be explained by the rapid release of discrete elastic elements representing the CSK back to their initial configuration, as it was observed from the results.

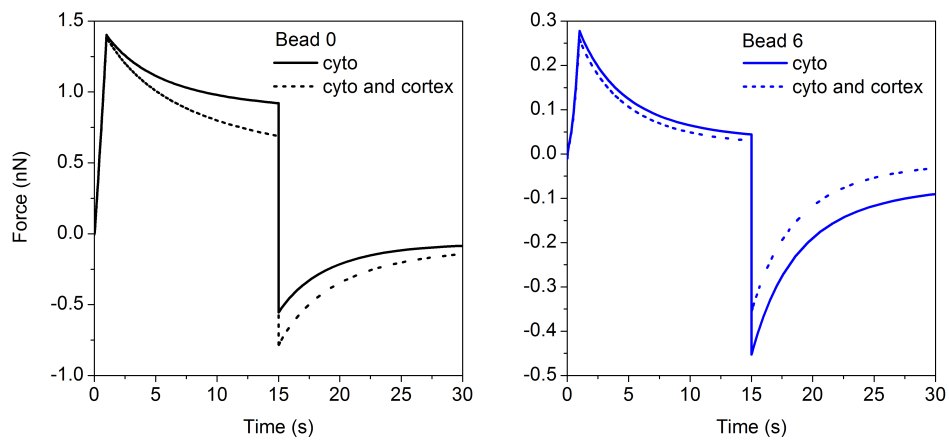


Figure 6.7: Comparing force-relaxation curves for two bead positions considering different material properties of the cell components: straight lines represent viscoelastic material properties defined for the cytoplasm of the cell and dashed lines represent the response obtained with a model considering viscoelastic properties for both cytoplasm and cortex. Bead 0 and bead 6 positions results from Figure 6.6 were selected for detailed comparison.

## 6.4 Discussion

It has been suggested that power-law behaviour is an intrinsic cellular feature that is independent of measuring technique (Desprat et al., 2005). Here, the usefulness of this model cell, incorporating the material behaviour associated with power-law to simulate force-relaxation and equilibration times, was investigated with a FE model for AFM measurements. The findings of this study showed that the viscoelastic properties of cells are well characterised by the power-law behaviour for force-relaxation for different indentations and are affected by the viscoelastic properties of the CSK networks.

By including the viscoelastic properties of the cytoplasm and/or cortex in combination with the discrete elements of the actin fibers and microtubules, the time-dependent response of a cell is modelled. Yet, CSK remodelling that is likely to happen during the time investigated, is not accounted for in this study. Nonetheless, the findings of this chapter show that the response of the model is as expected from a qualitative point of view and provide an understanding of the viscoelastic contribution of the cortex for the whole cell response. However, time-dependent experiments must be further performed to check the validity of the model in these time-dependent conditions simulated.

### 6.4.1 The parameters affecting power-law behaviour in the finite element analysis

The model reported in this chapter replicates the power-law behaviour and allows investigating the contribution of the viscous properties of the different cellular components. This was done by changing the material properties of the cellular components and to compare the equilibration times of the

force-relaxation curves upon indentation. The results showed how the equilibration times change when viscous properties were considered in the CSK components, other than in the cytoplasm. Forces relaxed to a larger extent when cortex was modelled as viscoelastic indicating that the cell behaves more as a fluid-like material under compression. This shows the viscoelastic contribution of the actin cortex. However, because in this FE analysis, discrete and continuous approaches were combined, the inclusion of viscoelastic material properties in the discrete elements of the CSK, the microtubules and actin bundles, would not affect the force-relaxation of the whole cell but would change the equilibration times of the cell locally.

Since there is still a debate regarding the timescale over which a single power-law exponent is applicable (Deng et al., 2006), the power of computational simulations was used here to predict changes on the cellular response for the different power-law exponents. The relationship between the two parameters of the power-law, stiffness and PL exponent, indicates that stiffer cells have a smaller PL exponent. This means that they are more solid-like, as long as small forces are applied to the cell, which ensure a force-independent linear response (Fabry et al., 2001; Kollmannsberger et al., 2011). However, cells are known to have non-linear responses and to sense higher stimuli. With this FE analysis, the non-linear behaviour of the cells is possible to be predicted and it was carried out in a high-force and larger-deformation regime. In this study, strain rate is varied, as the indentation is changed for the same time of analysis. For small strain rates applied, the initial predicted cell force was smaller and the equilibration time was also smaller, indicating that the cells are more solid-like in these situations (Figure 6.4). For higher applied strain rates, the opposite was observed and it is in agreement with the experimental results of Kollmannsberger et al. (2011), who observed

simultaneous stress stiffening and fluidisation.

In this study the initial rigidity of the cells was tested for different initial instantaneous moduli. It was observed that for  $0.5 \mu\text{m}$  indentation the equilibration time of stiffer cells, modelled with higher instantaneous moduli, was also higher, meaning that they also behave more as a fluid-like material. These results are in agreement with the observed paradox of stiffening and fluidisation, where more rigid cells fluidise to a larger extent, which were discussed in the literature review of chapter 2. Therefore, this shows an opposite effect to what is observed in the linear viscoelastic response. This variation of both initial rigidity and forces applied to the model cell was also observed considering different PL exponents (Figure 6.5), which is consistent with viscoelastic responses, as expected. In these cases, for cells characterised by a higher PL exponent and thus, more fluid-like, the variation of these two parameters caused a smaller variation on the observed equilibration time than for cells that have a lower PL exponent and are therefore, more solid-like. The equilibration time decreased non-linearly with the PL exponent for higher indentation depths and instantaneous modulus.

The increase of the power-law exponent and rigidity with increasing external applied stress was found to depend on the cytoskeleton, for experiments applying shearing loads with magnetic tweezers (Kollmannsberger et al., 2011). Furthermore, in this study only the viscoelastic response of the cell was not affected by variation of prestress during compressive loads. This might be related to spatial distribution of the actin bundles in this cell model. The findings presented in previous chapters in the elastic regime showed that prestress affects cell response mostly during stretching or during compression when actin bundles are distributed in the cell interior. This elastic response of the cell to prestress variation might be extrapolated to the viscoelastic

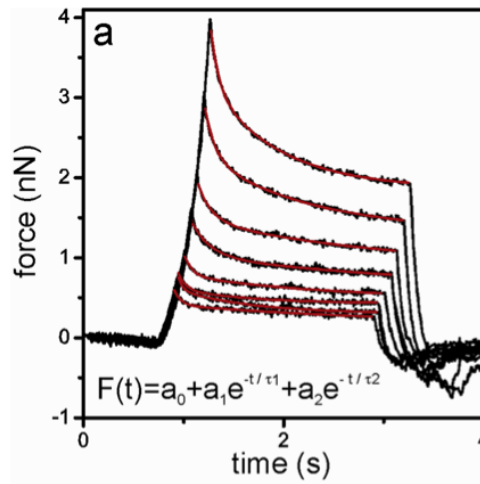


Figure 6.8: Force-relaxation curves obtained at different loads, varying from 0.5 to 4 nN, applied on the nuclear region of an MCF-7 cell by [Moreno-Flores et al. \(2010\)](#).

response.

Qualitative agreement is also obtained when force-relaxation simulated in this study is compared with the same type of curves presented in literature for different indentation depths ([Moreno-Flores et al., 2010](#)), as seen in Figure 6.8. The simulations here are performed for 15 s indentation, while the AFM force-relaxation measurements of [Moreno-Flores et al. \(2010\)](#) were performed for a shorter total time of 4 s. Therefore, the FE simulations include the time of experiments, and this latter can be used for validation of the current results for different loading conditions. These AFM experimental measurements were performed in MCF-7 cells, and for this reason quantitative analysis in terms of force-relaxation curve is not evaluated, although it is in the same range of the FE simulations of the current study.

### 6.4.2 Viscoelastic properties for different indentation positions

When comparing the force-relaxation for different bead positions, the elastic response is always higher for the *bead 0* position due to the elastic contribution of the nucleus (in *bead 0* position, the bead is on the top of the nucleus). Further away from the nucleus, the elastic contribution observed in the force-relaxation curves did not vary considerably. This happened because there is no strong influence of the other elastic components of the cell, except for the *bead 2* position, in which the end node of one microtubule is below the bead. Therefore, that microtubule contributes to the peak of elastic force observed in the force-relaxation curves for *bead 2* position. The results corroborate what was obtained in previous chapters considering elastic material properties: the physical mechanism for the different elastic response of the cell indented in different positions is related to the spatial heterogeneity of the CSK, and is dependent on the distance of the indenter to the nucleus.

When comparing viscoelastic properties in different components of the cell, the increase in the equilibration time was higher for *bead 0* position than for the other positions tested. This means that the viscous contribution of the cortex becomes more important in regions where the thickness of the cytoplasm is smaller, as it happens in *bead 0* position. These changes in cell viscosity when testing zones with different thickness shows a bimodal response from the cytoplasm to the cortex layer, which were also observed in the experimental study of [Moreno-Flores et al. \(2010\)](#) using AFM.

Furthermore, including cortex as a viscoelastic material made the variation in the force-relaxation curves for different bead positions much smoother than having only the cytoplasm as a viscoelastic material. To evaluate if this observation is not due to model singularities of the FE formulation, the

author analysed the possible presence of extreme forces, stresses or strains in one of the discrete components of the CSK, in both models of only cytoplasm and cytoplasm together with cortex modelled as viscoelastic materials. If singularities are not observed, then it is valid to consider the importance of the cortex for the viscoelastic response of the cell. And this is undoubtedly important for the understanding of the role of the cellular components for the viscoelastic response of the cell at different times. When varying bead positions, no peaks of stress, reaction force or deformation were observed in the microtubules and actin bundles structures, for the model with cytoplasm as viscoelastic. Moreover, these values were not considerably different from the model with cortex and cytoplasm modelled as viscoelastic materials. For this difference, there are no singularities in the distribution of forces and deformation in the discrete elements responsible for this difference when the bead position is varied considering the two models. Therefore, the differences are attributed to the spatial location of the discrete fibres of the CSK in the model cell. The investigation of the viscoelastic response of the cortex is key to the relationship between cell injury and the changes in the PL parameters over time, especially for modelling the failure phenomena at the cortex/membrane areas of cells. This has been done for cell injury during airway reopening (Dailey & Ghadiali, 2010) and can now be applied for different cell types and biological processes.

### 6.4.3 Main conclusions

In this study, a unified method to study the mechanical properties of cells using FE simulations of AFM combining prestress and power-law behaviour is presented. The results suggest that the origin of different relaxation times is related with the spatial arrangement of the CSK structure in the cell and

that the relationship between PL and prestress is dependent on these arrangements but also on the type of load applied to the cell. In this study, prestress does not affect cell viscoelastic response to compressive loads. Nonetheless, this cell model is capable of relating the rheology and material constants to overall cell response and is a robust tool for investigating the contribution of specific CSK networks for cell rheology.

The results reported here add to a growing body of literature pertaining to power-law behaviour of cells mainly from dynamic mechanical analyses and creep measurement (Desprat et al., 2005; Fabry et al., 2003; Hemmer et al., 2009), and now AFM stress-relaxation. This FE cell model may represent a significant contribution to the field of computational cell mechanics with insights on the dynamics of cytoskeletal viscoelasticity under mechanical perturbation.

## DISCUSSION

---

### 7.1 General discussion

Cellular deformability is largely determined by cytoskeletal structure, while force and signal transmissions resulting from an applied load are believed to involve complex interactions among integrins, cytoskeletal components and the nucleus. Therefore, detailed knowledge of the role cytoskeletal constituents play in governing cell mechanics is one necessary step in developing a comprehensive understanding of mechanotransduction in disease and tissue development. A more detailed comprehension to this knowledge required the development of a simple, yet accurate, multi-structural model to better quantify cellular viscoelastic behaviour and for an accurate description of the broad range of experimental data.

Previous studies have been carried out to investigate cellular response to mechanical stress, mainly by looking at changes in gene expression, protein synthesis patterns and signalling pathways (Chen et al., 2001; Janmey, 1998; Wasserman et al., 2002). The main objective of the research contained in this thesis was to investigate the first step of cellular mechanotransduction, which is the deformation and displacement that occur in the CSK and whole cell in response to an externally applied mechanical force. These immediate and

time-dependent changes in the intracellular architecture would consequently lead to biochemical changes that affect various aspects of cell behaviour such as growth, differentiation, motility and apoptosis. The model can also incorporate increasing levels of complexity but because it is based on physical and mechanical principles it does not *per se* explain chemical behaviour in living cells. However, the author believes it provides a framework to distribute and focus mechanical forces on specific cellular components and hence, it may help to explain how mechanical forces regulate cellular biochemistry and influence gene expression.

The major advantage of this new method of model construction is that the different CSK networks are interconnected but can move independently from each other without collapsing the cell, as opposed to what is observed in models based on the tensegrity theory. In this model, prestress is defined based on a prestrain in the actin bundles and not from the tensed interconnection between cables and struts that hold the prestressed tensegrity-based models. Therefore, when the CSK components of the current model are removed, the cell structure does not disintegrate. Another advantage is that the model of this thesis is capable of simulating the mechanical behaviour of a wide variety of cells. This potentially allows for results that may be predictive across cell types and across cellular functions. Additional advantages of this method of model construction over previous models based on tensegrity are that it allows incorporation of cytoskeletal elements in a non-arbitrary manner, following a closer similarity to the different cytoskeletal networks that can be formed in different living cells.

Prestress has been shown to play a critical role in the mechanical behaviour of actin fibers ([Kumar et al., 2006](#)). The majority of the models in literature, including the ones defined based on the tensegrity concept, account

for very small values of prestress that do not match actual values assessed by experimental work (McGarry & Prendergast, 2004; Mijailovich et al., 2002; Milner et al., 2012; Slomka et al., 2011). This is probably due to limitations of their model's construction. In this thesis however, physiological values of prestress measured for single actin fibres are incorporated by defining pre-strain values for the actin filaments in the cell through a subroutine in the FE software used, that redefines the entire stress-strain behaviour of these elements. The model defines a relation of prestress and amount of external stimuli, and a "prestress plateau" where actin bundles do not respond to compressive loads. Under these conditions, actin bundles are only activated if the external stimuli are above or below the plateau that overcomes the prestrain condition. This was observed in chapter 3 for the parametrical analysis of the effects of prestress to cell rigidity, and confirmed in chapter 5 when actin and microtubules were disconnected. These results showed that during compressive loads no changes were observed in the cell force since the microtubules were carrying all the compressive loads, considering that amount of applied compression.

This thesis also studied the individual contribution of CSK components and specific actin networks, which is better controlled computationally than experimentally. The role of microtubules in cellular mechanical behaviour is very controversial. It can depend greatly on factors such as the degree of cell spreading (Hemmer et al., 2009), and type of chemical drug used to disrupt this cellular component and the time of exposure to the drug (Pelling et al., 2007). For example, nocodazole, the same drug used in the current thesis, has been found to induce the formation of actin stress fibres via a rho signaling mechanism, which increases the cell forces when microtubules are being disrupted. Therefore, previous studies have demonstrated an increase

in cellular stiffness from microtubule disruption (Stamenović et al., 2002; Wu et al., 1998), while others have found the opposite effect (Wang, 1998). An alternative explanation is the room temperature at which the experiments are performed, where a significant depolymerisation of microtubules is induced above the near-freezing temperature of microtubules or actin, and the bending stiffness of individual microtubules may be lower at room temperature than at physiologic temperature (Hemmer et al., 2009; Kis et al., 2002). By using a computational tool to study the specific mechanical role of CSK components, it reduces the environmental variables possibly affecting the understanding of experimental results. Therefore, the model of this thesis predicts quantification on the decrease of force that is load type-dependent based only on the mechanical properties of the microtubules. The same specific contribution was, for the first time, quantified for the role of the actin cortex, separately from inner actin fibres.

Finally, this computational model explains how the CSK individual components behave and contribute to cell rigidity, and how they are affected by prestress and change their viscoelasticity over time following a weak power-law, for two different loading conditions, compression and stretching. It puts together the principles that stand for governing the mechanical behaviour of cells.

The model specifies the elementary nature of the mechanics of cell components to resist external stimuli and it is the basis to build up remodeling of the CSK during the application of forces, as a superstructure onto this model. The development of this model has been done to the extent that computational tools at the cellular level become a new way of experimentation that can be very powerful when integrated along with *in vitro* observations.

## 7.2 Limitations

### 7.2.1 Computational limitations

Although this approach has some advantages over previous models, there are inherent assumptions and simplifications. In this thesis, one cell shape was considered whereas in the organism, cells can attain different sizes and shapes. The use of image-based FE modelling, a powerful engineering analytical tool, is considered a state-of-the-art methodology for researching the mechanics of organs and tissues. However, its use for single cell mechanics research has been limited until recently (Dailey & Ghadiali, 2010; Slomka & Gefen, 2010; Weafer et al., 2013; Wood et al., 2012). This is largely due to the highly complex geometries and material nonlinearity exhibited by cells, which leads to models that are more computationally expensive and time consuming. In this thesis, cell-specific shapes are not considered, and simplification of assuming one standard cell geometry was verified to be a valid assumption for the purpose of the thesis. This justification relies on two facts, namely: an initial hypothesis of the CSK components as main contributors to cell stability was verified in this thesis, which means that the presence of these components define the shape of the cell and not the other way around; and correlation between Young's modulus and area of adhesion of living cells was not observed, emphasising the idea that the spatial distribution of the cell interior, rather than the external shape, contributes to passive cell mechanics.

Previous attempts to model the mechanical behaviour of cells have focused primarily on the material parameters of the model, rather than the arrangement of those materials to explain and fit the experimental data. In this thesis, both material and spatial distributions of the cellular components require some modelling assumptions and simplifications. The microtubules

network in living cells is highly complex, but normally with a common easily discernible pattern, typically present in cells. In the model, this was simplified by having microtubules distributed throughout the cell, starting in a common point, the centrosome, to the actin cortex.

Additionally, it is highly difficult to discern from microscopy images the number of actin fibres in each of the peripheric and inner actin networks. Furthermore, these structures are highly variable from different cell types. Therefore, it was assumed two different actin networks: one representing the actin cortex at the cell periphery; and a system of actin bundles that can assume different configurations to represent both peripheric and deeper structures of actin in the cell. The model cell does not attempt to faithfully reproduce the exact actin and microtubules networks observed in the confocal images, but rather to generate a spatial representation of them with discrete elements. This was sufficient to show the importance of incorporating such geometries for cell integrity.

Material properties for the cellular components of the FE model of this thesis are taken from both experimental data and FE model predictions, from literature. These properties rely on the geometric arrangement of the structural components of the simulated cell, to provide the model with realistic results. These parameters are therefore material constants in the model that are assigned to the finite elements.

Another limitation of this study is the type of elements that were used to represent the continuum elements of the cell model. The author used reduced integrated continuum elements to represent the cytoplasm, nucleus and cortex. However, full integration elements are more accurate than the reduced integrated elements used in this thesis. The reduced integration elements use less number of Gaussian (integration) points through the element

when solving the integral in the FE analysis, and for this reason are less accurate than the full integrated elements. Reduced integration elements have only one integration point while in full integration, there are four integration points where the stress results are calculated and the output displayed at these integration points. But this has to be weighed up against the cost of computation time and this was the reason for using reduced integrated elements. Furthermore, because there is a large number of elements to define in the cell model, the differences in the results should not be significant. Nonetheless, the time of computational analysis is considerably reduced.

Cells are known to have a non-linear response to mechanical loads, as reviewed in chapter. However, linear elastic properties were assumed for all the cell components, except for the actin bundles that were modelled with a non-linear behaviour due to the inclusion of prestress and the fact that these elements only resist tensile forces. Nonetheless, several non-linear behaviours can be implemented in Abaqus, including the hyperelastic material models to represent the non-linearity of cells, mostly by defining neo-Hookean models with few parameters or Mooney-Rivlin models. Hyperelastic models could be another option to define the non-linear behaviour of cells, which could have been interesting to evaluate especially for the understanding of the contribution of the cortex behaviour. However, a multi-structural cell model was developed in this thesis and therefore, it was quite difficult to find the appropriate parameters needed to define hyperelasticity in the different cell components. Using linear elastic assumptions it is possible to have a better control over the variables of the model.

Another model assumption is the use of an infinitesimal strain analysis for the results presented in this thesis despite the possibility of having large deformation, as it was previously analysed and discussed. In linear

geometry analysis, the geometric dimensions are not updated as the load changes. On the other hand, in a large deformation analysis, the effect of geometric nonlinearity can be significant. This could have been accounted for in the simulations in Abaqus by using "NLGEOM" in the step analyses, to take into account the changes in geometry. When large deformations are expected, nonlinear geometry updates the element geometry at each increment of analysis and has the ability to recognise that the element shape is very different than when the analysis started, meaning that the stiffness matrix is calculated using the current position of the nodes in the model.

In this study, the author assumes a rigid bonding of the cell to the substrate, where all the nodes of the basal part of the cell are fully constrained. However, this is a simplification of modelling the contact that the cells establish with the ECM. It is known that the cells attach to the ECM through FAs, which could have been modelled as local points of contact between the cell and the substrate by defining that only the end nodes of the CSK at the basal part of the cell would be constrained. This would have been of particular importance to understand how the forces are transmitted from the exterior on the top of the cell, through the CSK to the underlying substrate, which if modelled, could have assumed different rigidities.

The assumption associated with the CSK in this study is that the actin networks and microtubules are sufficient to represent the mechanical response of the cytoskeleton and the class of intermediate filaments is neglected. When large loads are applied, the role of the intermediate filaments in tension-bearing becomes more crucial, while under small loads their contribution is negligible (Maniotis et al., 1997; Wang & Stamenović, 2000). More recent studies on the mechanics of intermediate filaments showed a different picture, especially for force transmission between ECM and nucleus, important for cell

signalling and mechanotransduction. The keratin intermediate filaments of epithelial cells showed a network that is largely responsible for the capacity of epithelial cells to sustain mechanical stress (Coulombe & Wong, 2004). As a consequence, this CSK network needs to be included in the interplay that takes place between actin-mediated cell stiffness and ECM rigidity in simple epithelial cells (Bordeleau et al., 2012). When mechanically tested with optical tweezers combined with microscopic imaging, results showed that intermediate filaments modulate both cell and ECM stiffness, through actin organisation (Bordeleau et al., 2012). Especially in tissue cells, their shape and mechanical properties depend largely on the cytoskeleton and on the ECM to which the cells are anchored. The three filamentous systems of the CSK are not only believed to maintain the mechanical stability of the cell but also to provide mechanical interactions all the way from the membrane and cell cortex down to the nucleus (Dowling et al., 2012; Ingber, 1993; Wang, 1998).

Finally, the most important limitation of a finite element model of this type is that cells are living systems capable of active responses. Although the study of dynamic analysis of cell response to mechanical forces over time was simulated, the actin and microtubules remodelling was not included in this thesis. This multi-structural model, explaining the passive mechanical behaviour of cells, may be further used to distinguish the difference between the active and passive responses of cells important in mechanotransduction and remodelling processes at tissue level.

## 7.2.2 Experimental limitations

Atomic force microscopy is an attractive tool for investigating the mechanical behaviour of cells. It has the ability to be used as a high precision indenter

to measure the mechanical properties of living cells in their physiological conditions. In comparison to the magnetic bead methods to apply force onto cells, the use of AFM in this thesis has several advantages: first, the force is well-defined and highly localised; the AFM applies a static load, in comparison to the oscillating loads applied by a magnetic bead; and third, there is no specific molecular linking between the probe and the cell surface, as in the case of magnetic bead experiments, which could independently modify cell behaviour. Furthermore, the ability to combine the use of the AFM with simultaneous optical and fluorescence observations, allows real-time visualisation of changes in the intracellular architecture that follows an externally applied stress.

The FE predictions for the study of CSK-disruption for the application of compressive loads were corroborated in this thesis with AFM force-measurements performed in two cell types, NIH-3T3 fibroblasts and U2OS osteosarcoma cells. However, predictions of the CSK-disruption after stretching were only validated with results from literature using MTC. Validation of the results from the inclusion of frequency-dependence following power-law behaviour was also obtained with results published in literature. It would have been particularly interesting to corroborate the predictions presented in chapter 6 showing that prestress does not affect the stress-relaxation curves simulated following power-law during compressive loads; as opposing to the documented results during stretching, where it was demonstrated that cell contractility affects the stress-relaxation curves ([Kollmannsberger et al., 2011](#); [Krishnan et al., 2009](#)). Until the date, to the author's knowledge, experimental validation of this prediction relating prestress and frequency-dependence for compressive loads does not exist in literature.

During the experiments presented in chapter 4, microscopic images of the

actin structure, before and after drug treatment, were taken for visualisation of the effect of cytochalasin-D in the actin networks. The same protocol could have been used to see the effect of nocodazole in the two cell types, not only affecting the microtubules structure but also the actin networks. This is of particular interest since nocodazole might have an indirect effect in increase force of cell by inducing actin formation. Therefore, it might be the explanation for the small decrease in cell force observed in the U2OS cells.

Finally, during the sensitivity analysis presented in chapter 5, measurements of the height of living cells before force measurements with AFM were not possible due to AFM limitations. These measurements would be interesting for the calculation of cell volume and correlate with cell's rigidity, to discuss a possible effect of cell geometries in the FE model. The limitations include the fact that AFM is very sensitive to both thermal noise and vibrations affecting the first moments of contact of the cantilever. The moments of contact are first with the surface and then with the cell, when the positions of the piezo should be recorded and subtracted in order to get the value of cell height. The differences in the piezo position from the surface to the cell are small and therefore, even very small AFM noise affects accurate measurements. Accurate measurements of cell height could have been achieved for example, by reconstructing confocal images of cells, which unfortunately was not available in the AFM used.

---

## CONCLUSIVE REMARKS

---

### 8.1 Main results and contributions

The present thesis was focused on the biomechanical study of the mechanical properties of human cells and its cytoskeleton. A computational approach for the study of passive cell behaviour focusing on the cytoskeletal mechanics, in response to static and dynamic conditions under two loads, compression and stretching, has been presented. This general multi-structural finite element model of a single adherent cell accounts for the physical and mechanistic fundamental principles to describe cell mechanics according to the universal aspects in the field. The model also incorporates the required high complexity of its components. The mechanical role of CSK components was investigated under these conditions to predict the passive cell responses to external forces. The findings of this thesis explain and predict how complex cellular behaviours observed at different time scales and under different experimental conditions emerge from collective interactions among specific cytoskeletal components. Therefore, the main findings of this thesis may be built up as follows:

- The model predicts force and strain distribution in the CSK components and whole cell under different external loads, compression and

stretching. It also provides quantitative predictions of adherent cell's structural behaviour that is mainly attributed to the cytoskeleton components. This study shows that considering one elasticity to describe cellular mechanical properties on a whole cell basis is not sufficient, but it is also needed to consider variations of specific intracellular mechanical properties.

- The cell model defines a relationship between cell force and prestress depending on the specific loading conditions, which is in good agreement with *in vitro* experiments. The model predicts that variation in the amount of prestress affects mainly the response of cells under shear loads.
- The key features of this mechanical model keep fundamental principles governing cell behaviour, including prestress and interplay of the discrete components, with a more accurate morphological representation of the CSK, where they are free to move independently of each other, as opposite to the tensegrity theory. Therefore, this thesis opens new perspectives in studying the correlation of cellular mechanical properties and stress distribution within particular CSK components across different cell types.
- The model predicts the role of specific CSK components for force transmission through the cell, which is dependent on the external force. Actin cortex and microtubules are targeted to respond to compressive loads, while actin bundles and microtubules are major components to maintain cell integrity during cell stretching. This explains the previously reported differences for the mechanical role of each CSK component for the diverse experimental single-cell stimulation techniques.

More importantly, using this numerical cell model, isolating the specific contribution of the actin cortex for cell integrity from the remaining CSK networks was achieved for the first time.

- Cell force was highly affected by changes in cortex thickness, cortex Young's modulus and rigidity of the remaining cytoplasm. Changes in the rigidity of actin bundles and increase of the number of microtubules influenced the cell response to stretching. Finally, increasing the number of actin bundles in the interior of the cell affected cell response to compression.
- The finite element sensitivity analysis of the material properties in the model cell allows classification of the cellular mechanical behaviour for further identification of which biological parameters in cells influence tissue mechanics the most. This will inform the search for new experimental methodologies to measure cortex thickness and other changes in the material properties of the cytoskeleton during specific cellular processes. The author believes that the sensitivity analysis provides valuable guidelines about the structure of each CSK component for future cell-phenotype modelling efforts.
- The findings of this study show that the viscoelastic properties of cells are well characterised by the power-law behaviour for force-relaxation indentation. The results suggest that the origin of different relaxation times may be due to the complex structural architecture of the cell. For this reason, it is important to consider the viscoelastic properties of the actin cortex other than the cytoplasm.
- This approach clarifies the effects of cytoskeletal heterogeneity and regional variations on the interpretation of force-deformation measure-

ments.

- The model includes the three parameters defining the universal laws of cell mechanics, rigidity, prestress and time-dependence deformation following a power-law behaviour, that are in this finite element model associated with the mechanics of the cytoskeleton components.

The development of this computational model is interesting for cell mechanics research as it helps researchers to better understand the passive mechanisms involving the cytoskeleton. This passive mechanics underly the active processes of cytoskeleton remodelling. This FE cell model represents a significant contribution to the field of computational cell mechanics for describing quantitatively the biological processes involving a mechanical interaction between cells and their mechanical environment, such as matrix remodelling, mechanotransduction or tissue development.

## 8.2 Future prospects

Some of the previous limitations of the computational model are the ground basis for model further developments that were not accomplished in this thesis. The following are recommended to be incorporate in the multi-structural cell model of this thesis and are directed toward simulations of active dynamics behaviour of cells:

- As mechanical connections have previously been shown to exist between cytoskeletal filaments and the nucleus ([Maniotis et al., 1997](#)), this multi-structural model might be further used to explain the mechanical cues for force transduction directly to the nucleus, that are known to affect gene transcription ([Chen et al., 2001](#); [Ingber, 1993](#)). The inclusion of a nucleoskeleton structure, integrated with the cytoskeleton as

well as the inclusion of a network of intermediate filaments to make the connection between the cell periphery, the CSK and the nucleus, are proposed.

- Following the approach from [Maurin et al. \(2008\)](#), could also be useful to consider the centrosome in the cell model. Because of the relations where only intermediate filaments hold the nucleus and only microtubules are connected with the centrosome, and assuming that these interactions stabilise the cell, the centrosome might be an important link between nucleus and microtubules. However, little is known about the mechanics of the centrosome to define realistic constitutive properties for the model. A computational study considering or not the centrosome to know if it is mechanically important and in which loading conditions, could be a first step to investigate the mechanics of this cellular component.
- Eventually, the methods described in this study could also be incorporated into multi-scale models, providing a key link between the prediction of mechanical responses of cells to pathological conditions and the development of new medical treatments from the tissue level down to the molecular level.
- The current model has been further used to investigate the mechanisms of cell mechanosensation during perfusion fluid flow ([Khayyeri et al., 2013](#)). Although it is well established that the mechanical environment modulates biological tissue and cell responses, the central mechanisms with which cells sense their environment are still unclear. Cells sense their environment through focal adhesions ([Pelham & Wang, 1999](#)), network of microtubules and actins ([Stamenović et al., 2002](#)), stretch-

activated channels (Chen et al., 2001) as well as primary cilia (Hoey et al., 2012; Malone et al., 2007). However, whether all these mechanisms play an equally important role for signal mechanosensation is under investigation. To test this, a primary cilia has been included to the model to investigate its role as a mechanoreceptor for simulation of *in vitro* experiments on perfusion chambers and to investigate how forces are transferred to the CSK structure (Khayyeri et al., 2013). Controlling the way cells mechanically interact with their physiological environment to further extend the knowledge on mechanotransduction could help to effectively treat diseases such as cancer and osteoporosis.

- The multi-structural cell model of this thesis specifies the elementary nature of the mechanical components to resist different external stimuli and is the basis to build up remodeling of the CSK during application of forces as a superstructure onto this model. This general model accounts for the physical and mechanistic aspects to describe cell contractility, stiffening and fluidisation and frequency-dependent following a power-law. Active responses could be incorporated in the future as the cell's cytoskeletal arrangement could be made to change with time and in response to specific external stimuli. This may be done by incorporating a similar description of CSK remodelling proposed by Deshpande et al. (2006) following the approach of Dowling et al. (2013). In these cases, the remodelling process is based on an activation signal that triggers actin polymerisation and myosin phosphorylation, the tension-dependent assembly of the actin and myosin into stress fibers, and the cross-bridge cycling between the actin and myosin filaments that generates the tension. The model is capable of predicting key experimentally established characteristics including the decrease in the forces

generated by the cell with increasing substrate compliance and the formation of high concentration of the stress fibres at the focal adhesions (Deshpande et al., 2006). Another way of including the remodelling process could be by proposing simple relations to model these coupled phenomena based on the principal of minimum energy a cell would spend in terms of stress and strain to change the configuration of each CSK element in each iteration for load adaptation.

The author believes the work presented in the current thesis represents an important step toward the ability to use finite element models for the construction of highly representative cell geometries and to accurately predict the mechanical response of living cells. This thesis provides a solid foundation from which to build even more representative models of living cells and biological processes. Such model could potentially be utilised to elucidate the mechanisms of cell signalling and mechanotransduction. An integrated model of cell physiology that incorporates the high complexity of its components is the basis for understanding adaptive responses and to be used for research in areas of immediate concern, such as drug development, tissue engineering, cancer and regenerative medicine therapies.

# Bibliography

- Alberts, B., Johnson, A., Lewis, J., Raff, M., Roberts, K., & Walter, P. (2002). *Molecular biology of the cell*. *Garland Science, 4th edn*, New York.
- Alcaraz, J., Buscemi, L., Grabulosa, M., Trepas, X., Fabry, B., Farre, R., & Navajas, D. (2003). Microrheology of Human Lung Epithelial Cells Measured by Atomic Force Microscopy. *Biophys J*, *84*, 2071–2079.
- Ananthakrishnan, R., Guck, J., Wottawah, F., Schinkinger, S., Lincoln, B., Romeyke, M., Moon, T., & Käs, J. (2006). Quantifying the contribution of actin networks to the elastic strength of fibroblasts. *J Theor Biol*, *242*, 502–16.
- Anderson, A. E., Ellis, B. J., & Weiss, J. A. (2007). Verification, validation and sensitivity studies in computational biomechanics. *Comput Meth Biomech Biomed Eng*, *3*, 171–184.
- Azeloglu, E. U., Bhattacharya, J., & Costa, K. D. (2008). Atomic force microscope elastography reveals phenotypic differences in alveolar cell stiffness. *J App Physiol*, *105*, 652–61.
- Balaban, N. Q., Schwarz, U. S., Riveline, D., Goichberg, P., Tzur, G., Sabanay, I., Mahalu, D., Safran, S., Bershadsky, A., Addadi, L., & Geiger,

- B. (2001). Force and focal adhesion assembly: a close relationship studied using elastic micropatterned substrates. *Nature Cell Biol*, *3*, 466–72.
- Bao, G., & Suresh, S. (2003). Cell and molecular mechanics of biological materials. *Nature Mater*, *2*, 715–25.
- Bausch, A. R., Hellerer, U., Essler, M., Aepfelbacher, M., & Sackmann, E. (2001). Rapid stiffening of integrin receptor-actin linkages in endothelial cells stimulated with thrombin: a magnetic bead microrheology study. *Biophys J*, *80*, 2649–57.
- Bausch, A. R., Ziemann, F., Boulbitch, A. A., Jacobson, K., & Sackmann, E. (1998). Local measurements of viscoelastic parameters of adherent cell surfaces by magnetic bead microrheometry. *Biophys J*, *75*, 2038–49.
- Beningo, K. A., & Wang, Y. L. (2002). Flexible substrata for the detection of cellular traction forces. *Trends Cell Biol*, *12*, 79–84.
- Besser, A., & Safran, S. A. (2006). Force-induced adsorption and anisotropic growth of focal adhesions. *Biophys J*, *90*, 3469–84.
- Binnig, G., Quate, C. F., & Gerber, C. (1986). Atomic force microscopy. *Phys Rev Lett*, *50*, 715–725.
- Bischofs, I. B., Schmidt, S. S., & Schwarz, U. S. (2009). Effect of adhesion geometry and rigidity on cellular force distributions. *Phys Rev Lett*, *103*, 048101.
- Blumenfeld, R. (2006). Isostaticity and controlled force transmission in the cytoskeleton: A model awaiting experimental evidence. *Biophys J*, *91*, 1970–83.

- Bordeleau, F., Myrand Lapierre, M. E., Sheng, Y., & Marceau, N. (2012). Keratin 8/18 regulation of cell stiffness-extracellular matrix interplay through modulation of Rho-mediated actin cytoskeleton dynamics. *PLoS one*, *7*, e38780.
- Brangwynne, C. P., MacKintosh, F. C., Kumar, S., Geisse, N. A., Talbot, J., Mahadevan, L., Parker, K. K., Ingber, D. E., & Weitz, D. A. (2006). Microtubules can bear enhanced compressive loads in living cells because of lateral reinforcement. *J Cell Biol*, *173*, 733–41.
- Brenner, B. (2006). The stroke size of myosins: a reevaluation. *J Muscle Res Cell Motil.*, *27*, 173–87.
- Brown, M. J., Hallam, J. A., Colucci-Guyon, E., & Shaw, S. (2001). Rigidity of circulating lymphocytes is primarily conferred by vimentin intermediate filaments. *J Immunol.*, *166*, 6640–6.
- Brown, R. A., Talas, G., Porter, R. A., McGrouther, D. A., & Eastwood, M. (1996). Balanced mechanical forces and microtubule contribution to fibroblast contraction. *J Cell Physiol*, *169*, 439–47.
- Brugués, J., Maugis, B., Casademunt, J., Nassoy, P., Amblard, F., & Sens, P. (2010). Dynamical organization of the cytoskeletal cortex probed by micropipette aspiration. *Proc Natl Acad Sci U S A*, *107*, 15415–20.
- Bursac, P., Lenormand, G., Fabry, B., Oliver, M., Weitz, D. A., Viasnoff, V., Butler, J. P., & Fredberg, J. J. (2005). Cytoskeletal remodelling and slow dynamics in the living cell. *Nature Mater*, *4*, 557–61.
- Butt, H. J., & Jaschke, M. (1995). Calculation of thermal noise in atomic force microscopy. *Nanotechnology*, *6*, 1–7.

- Byrne, D. P., Lacroix, D., & Prendergast, P. J. (2011). Simulation of fracture healing in the tibia: mechanoregulation of cell activity using a lattice modeling approach. *J Orthop Res*, *29*, 1496–503.
- Cañadas, P., Laurent, V. M., Oddou, C., Isabey, D., & Wendling, S. (2002). A cellular tensegrity model to analyse the structural viscoelasticity of the cytoskeleton. *J Theor Biol*, *218*, 155–173.
- Caille, N., Thoumine, O., Tardy, Y., & Meister, J. J. (2002). Contribution of the nucleus to the mechanical properties of endothelial cells. *J Biomech*, *35*, 177–87.
- Callies, C., Fels, J., Liashkovich, I., Kliche, K., Jeggle, P., Kusche-Vihrog, K., & Oberleithner, H. (2011). Membrane potential depolarization decreases the stiffness of vascular endothelial cells. *J Cell Sci*, *124*, 1936–42.
- Charras, G., & Horton, M. A. (2002a). Single cell mechanotransduction and its modulation analyzed by atomic force microscope indentation. *Biophys J*, *82*, 2970–2981.
- Charras, G. T., & Horton, M. A. (2002b). Determination of cellular strains by combined atomic force microscopy and finite element modeling. *Biophys J*, *83*, 858–79.
- Chaudhuri, O., Parekh, S. H., Lam, W. A., & Fletcher, D. A. (2009). Combined atomic force microscopy and side-view optical imaging for mechanical studies of cells. *Nat Methods*, *6*, 383–388.
- Chen, C. S., Alonso, J. L., Ostuni, E., Whitesides, G. M., & Ingber, D. E. (2003). Cell shape provides global control of focal adhesion assembly. *Biochem Biophys Res Commun*, *307*, 355–361.

- Chen, J., Fabry, B., Schiffrin, E. L., & Wang, N. (2001). Twisting integrin receptors increases endothelin-1 gene expression in endothelial cells. *Am J Physiol Cell Physiol*, *280*, C1475–C1484.
- Chicurel, M. E., Chen, C. S., & Ingber, D. E. (1998). Cellular control lies in the balance of forces. *Curr Opin Cell Biol*, *10*, 232–9.
- Collinsworth, A. M., Torgan, C. E., Nagda, S. N., Rajalingam, R. J., Kraus, W. E., & Truskey, G. A. (2000). Orientation and length of mammalian skeletal myocytes in response to a unidirectional stretch. *Cell and Tissue Res*, *302*, 243–251.
- Collinsworth, A. M., Zhang, S., Kraus, W. E., & Truskey, G. A. (2002). Apparent elastic modulus and hysteresis of skeletal muscle cells throughout differentiation. *Am J Physiol Cell Physiol*, *283*, C1219–27.
- Cooper, J. (1987). Effects of cytochalasin and phalloidin on actin. *J Cell Biol*, *105*, 1473–1478.
- Coulombe, P. A., & Wong, P. (2004). Cytoplasmic intermediate filaments revealed as dynamic and multipurpose scaffolds. *Nat Cell Biol*, *6*, 699–706.
- Cross, S. E., Jin, Y. S., Rao, J., & Gimzewski, J. K. (2007). Nanomechanical analysis of cells from cancer patients. *Nat Nanotechnol*, *2*, 780–3.
- Dahl, K. N., Engler, A. J., Pajeroski, J. D., & Discher, D. E. (2005). Power-law rheology of isolated nuclei with deformation mapping of nuclear substructures. *Biophys J*, *89*, 2855–64.
- Dailey, H. L., & Ghadiali, S. N. (2010). Influence of power-law rheology on cell injury during microbubble flows. *Biomech Model Mechanobiol*, *9*, 263–79.

- Darling, E. M., Zauscher, S., & Guilak, F. (2006). Viscoelastic properties of zonal articular chondrocytes measured by atomic force microscopy. *Osteoarthritis Cartilage*, *14*, 571–9.
- De Santis, G., Lennon, A. B., Boschetti, F., Verheghe, B., Verdonck, P., & Prendergast, P. J. (2011). How can cells sense the elasticity of a substrate? An analysis using a cell tensegrity model. *Eur Cell Mater*, *22*, 202–13.
- Deguchi, S., Ohashi, T., & Sato, M. (2005). Evaluation of tension in actin bundle of endothelial cells based on preexisting strain and tensile properties measurements. *Mol Cell Biomech*, *2*, 125–33.
- Deguchi, S., Ohashi, T., & Sato, M. (2006). Tensile properties of single stress fibers isolated from cultured vascular smooth muscle cells. *J Biomech*, *39*, 2603–10.
- Deguchi, S., & Sato, M. (2009). Biomechanical properties of actin stress fibers of non-motile cells. *Biorheology*, *46*, 93–105.
- Dembo, M., & Wang, Y. L. (1999). Stresses at the cell-to-substrate interface during locomotion of fibroblasts. *Biophys J*, *76*, 2307–16.
- Deng, L., Treppe, X., Butler, J. P., Millet, E., Morgan, K. G., Weitz, D. A., & Fredberg, J. J. (2006). Fast and slow dynamics of the cytoskeleton. *Nature Mater*, *5*, 636–40.
- Deshpande, V. S., McMeeking, R. M., & Evans, A. G. (2006). A bio-chemo-mechanical model for cell contractility. *Proc Natl Acad Sci U S A*, *103*, 14015–20.
- Deshpande, V. S., McMeeking, R. M., & Evans, A. G. (2007). A model

- for the contractility of the cytoskeleton including the effects of stress-fibre formation and dissociation. *Proc R Soc A*, *463*, 787–815.
- Desprat, N., Richert, A., Simeon, J., & Asnacios, A. (2005). Creep function of a single living cell. *Biophys J*, *88*, 2224–33.
- Diz-Muñoz, A., Fletcher, D. A., & Weiner, O. D. (2013). Use the force: membrane tension as an organizer of cell shape and motility. *Trends Cell Biol.*, *23*, 47–53.
- Dong, C., Skalak, R., & Sung, K. L. (1988). Passive deformation analysis of human leukocytes. *Biorheology*, *110*, 27–36.
- Dong, C., Skalak, R., Sung, K. L., Schmid-Schonbein, G. W., & Chien, S. (1991). Cytoplasmic rheology of passive neutrophils. *J Biomech Eng*, *28*, 557–67.
- Dowling, E. P., Ronan, W., & McGarry, J. P. (2013). Computational investigation of in situ chondrocyte deformation and actin cytoskeleton remodelling under physiological loading. *Acta Biomater*, *9*, 5943–55.
- Dowling, E. P., Ronan, W., Ofek, G., Deshpande, V. S., McMeeking, R. M., Athanasiou, K. A., & x, J. P. (2012). The effect of remodelling and contractility of the actin cytoskeleton on the shear resistance of single cells: a computational and experimental investigation. *J R Soc Interface*, *9*, 3469–79.
- Drury, J. L., & Dembo, M. (1999). Hydrodynamics of micropipette aspiration. *Biophys J*, *76*, 110–28.
- Eghiaian, F., & Schaap, I. A. T. (2011). Single Molecule Enzymology. *Methods Mol Biol*, *778*, 71–95.

- Engler, A. J., Sen, S., Sweeney, H. L., & Discher, D. E. (2006). Matrix elasticity directs stem cell lineage specification. *Cell*, *126*, 677–89.
- Ethier, C. R., & Simmons, C. A. (2007). Introductory biomechanics. *Cambridge University Press, 1st edn*, New York.
- Fabry, B., Maksym, G., Butler, J., Glogauer, M., Navajas, D., & Fredberg, J. (2001). Scaling the Microrheology of Living Cells. *Phys Rev Lett*, *87*, 148102.
- Fabry, B., Maksym, G., Butler, J., Glogauer, M., Navajas, D., Taback, N., Millet, E., & Fredberg, J. J. (2003). Time scale and other invariants of integrative mechanical behavior in living cells. *Phys Rev E Stat Nonlin Soft Matter Phys*, *68*, 041914.
- Fletcher, D. A. (2010). On force and function. *Mol Biol Cell*, *21*, 3795–6.
- Fletcher, D. A., & Mullins, R. D. (2010). Cell mechanics and the cytoskeleton. *Nature*, *463*, 485–92.
- Fritzsche, M., Lewalle, A., Duke, T., Kruse, K., & Charras, G. (2013). Analysis of turnover dynamics of the submembranous actin cortex. *Mol Biol Cell*, *24*, 757–67.
- Fudge, D. S., Gardner, K. H., Forsyth, V. T., Riekel, C., & Gosline, J. M. (2003). The mechanical properties of hydrated intermediate filaments: insights from hagfish slime threads. *Biophys J*, *85*, 2015–27.
- Galbraith, C. G., & Sheetz, M. P. (1998). Forces on adhesive contacts affect cell function. *Curr Opin Cell Biol*, *10*, 566–71.

- Gardel, M., Nakamura, F., Hartwig, J., Crocker, J., Stossel, T., & Weitz, D. (2006). Stress-Dependent Elasticity of Composite Actin Networks as a Model for Cell Behavior. *Physical Rev Lett*, *96*, 12–15.
- Gardel, M. L., Shin, J. H., MacKintosh, F. C., Mahadevan, L., Matsudaira, P., & Weitz, D. A. (2004). Elastic behavior of cross-linked and bundled actin networks. *Science*, *304*, 1301–5.
- Geiger, B., & Bershadsky, A. (2002). Exploring the neighborhood: adhesion-coupled cell mechanosensors. *Cell*, *110*, 139–42.
- Gordon, A. M., Huxley, A., & Julian, F. J. (1966). The variation in isometric tension with sarcomere length in vertebrate muscle fibres. *J Physiol*, *184*, 1706–92.
- Guilak, F., & Mow, V. C. (2000). The mechanical environment of the chondrocyte: a biphasic finite element model of cell-matrix interactions in articular cartilage. *J Biomech*, *33*, 1663–1673.
- Hamill, O. P., & Martinac, B. (2001). Molecular basis of mechanotransduction in living cells. *Physiol Rev*, *81*, 685–740.
- Han, S. J., Bielawski, K. S., Ting, L. H., Rodriguez, M. L., & Sniadecki, N. J. (2012). Decoupling substrate stiffness, spread area, and micropost density: a close spatial relationship between traction forces and focal adhesions. *Biophys J*, *103*, 640–8.
- Han, Y., Cowin, S. C., Schaffler, M. B., & Weinbaum, S. (2004). Mechanotransduction and strain amplification in osteocyte cell processes. *Proc Natl Acad Sci U S A*, *101*, 16689–94.

- Harris, A. K., Wild, P., & Stopak, D. (1980). Silicone rubber substrata: a new wrinkle in the study of cell locomotion. *Science*, *208*, 177–9.
- Hawkins, T., Mirigian, M., Selcuk Yasar, M., & Ross, J. L. (2010). Mechanics of microtubules. *J Biomech*, *43*, 23–30.
- Heidemann, S. R., & Wirtz, D. (2004). Towards a regional approach to cell mechanics. *Trends Cell Biol*, *14*, 160–6.
- Hemmer, J. D., Nagatomi, J., Wood, S. T., Vertegel, A. A., Dean, D., & Laberge, M. (2009). Role of cytoskeletal components in stress-relaxation behavior of adherent vascular smooth muscle cells. *J Biomech Eng*, *131*, 041001.
- Hill, A. V. (1938). The heat of shortening and the dynamic constants of muscle. *Proc R Soc Lond. B*, *126*, 136–195.
- Hochmuth, R. M. (2000). Micropipette aspiration of living cells. *J Biomech*, *33*, 15–22.
- Hoey, D. A., Tormey, S., Ramcharan, S., O'Brien, F. J., & Jacobs, C. R. (2012). Primary cilia-mediated mechanotransduction in human mesenchymal stem cells. *Stem Cells*, *30*, 2561–70.
- Hoffman, B. D., & Crocker, J. C. (2009). Cell mechanics: dissecting the physical responses of cells to force. *Ann Rev Biomed Eng*, *11*, 259–88.
- Hoffman, B. D., Massiera, G., Van Citters, K. M., & Crocker, J. C. (2006). The consensus mechanics of cultured mammalian cells. *Proc Natl Acad Sci U S A*, *103*, 10259–64.

- Hu, S., Chen, J., Fabry, B., Numaguchi, Y., Gouldstone, A., Ingber, D. E., Fredberg, J. J., Butler, J. P., & Wang, N. (2003). Intracellular stress tomography reveals stress focusing and structural anisotropy in cytoskeleton of living cells. *Am J Physiol Cell Physiol*, *285*, C1082–90.
- Hu, S., Eberhard, L., Chen, J., Love, J. C., Butler, J. P., Fredberg, J. J., Whitesides, G. M., & Wang, N. (2004). Mechanical anisotropy of adherent cells probed by a three-dimensional magnetic twisting device. *Am J Physiol Cell Physiol*, *287*, C1184–91.
- Huang, H., Kamm, R. D., & Lee, R. T. (2004). Cell mechanics and mechanotransduction: pathways, probes, and physiology. *A J Physiol Cell Physiol*, *287*, C1–11.
- Huang, H., Sylvan, J., Jonas, M., Barresi, R., So, P. T. C., Campbell, K. P., & Lee, R. T. (2005). Cell stiffness and receptors: evidence for cytoskeletal subnetworks. *Am J Physiol Cell Physiol*, *288*, C72–80.
- Huxley, A. F. (1957). Muscle structure and theories of contraction. *Prog Biophys Biophys Chem*, *8*, 255–318.
- Huxley, H. E. (2004). Fifty years of muscle and the sliding filament hypothesis. *Eur J Biomech*, *271*, 1403–15.
- Ingber, D. E. (1993). Cellular tensegrity: defining new rules of biological design that govern the cytoskeleton. *J Cell Sci*, *104*, 613–27.
- Ingber, D. E. (1997). Tensegrity: the architectural basis of cellular mechanotransduction. *Ann Rev Physiol*, *59*, 575–99.
- Ingber, D. E. (2003a). Mechanobiology and diseases of mechanotransduction. *Ann Med*, *35*, 564–577.

- Ingber, D. E. (2003b). Tensegrity I. Cell structure and hierarchical systems biology. *J Cell Sci*, *116*, 1157–1173.
- Ingber, D. E., Heidemann, S. R., Lamoureaux, P., & Buxbaum, R. E. (2000). Opposing views on tensegrity as a structural framework for understanding cell mechanics. *J App physiology*, *89*, 1670–1678.
- Janmey, P. A. (1998). The cytoskeleton and cell signaling: component localization and mechanical coupling. *Physiol Rev*, *78*, 763–81.
- Janmey, P. A., Euteneuer, U., Traub, P., & Schliwa, M. (1991). Viscoelastic properties of vimentin compared with other filamentous biopolymer networks. *J Cell Biol*, *113*, 155–60.
- Janmey, P. A., & Weitz, D. A. (2004). Dealing with mechanics: mechanisms of force transduction in cells. *Trends Biochem Sci*, *29*, 364–70.
- Jonas, M., Huang, H., Kamm, R. D., & So, P. T. C. (2008). Fast fluorescence laser tracking microrheometry. I: instrument development. *Biophys J*, *94*, 1459–69.
- Jonas, O., & Duschl, C. (2010). Force propagation and force generation in cells. *Cytoskeleton*, *67*, 555–63.
- Karcher, H., Lammerding, J., Huang, H., Lee, R. T., Kamm, R. D., & Kaazempur-Mofrad, M. R. (2003). A three-dimensional viscoelastic model for cell deformation with experimental verification. *Biophys J*, *85*, 3336–49.
- Kardas, D., Nackenhorst, U., & Balzani, D. (2012). Computational model for the cell-mechanical response of the osteocyte cytoskeleton based on self-stabilizing tensegrity structures. *Biomec Model Mechanobio*, *12*, 167–83.

- Kasas, S., Wang, X., Hirling, H., Marsault, R., Huni, B., Yersin, A., Regazzi, R., Grenningloh, G., Riederer, B., Forrò, L., Dietler, G., & Catsicas, S. (2005). Superficial and deep changes of cellular mechanical properties following cytoskeleton disassembly. *Cell Motil Cytoskeleton*, *62*, 124–32.
- Kasza, K. E., Rowat, A. C., Liu, J., Angelini, T. E., Brangwynne, C. P., Koenderink, G. H., & Weitz, D. A. (2007). The cell as a material. *Curr Opin Cell Biol*, *19*, 101–7.
- Kaunas, R., & Hsu, H. J. (2009). A kinematic model of stretch-induced stress fiber turnover and reorientation. *J Theor Biol*, *257*, 320–30.
- Kaunas, R., Hsu, H. J., & Deguchi, S. (2011). Sarcomeric model of stretch-induced stress fiber reorganization. *Cell Health CSK*, *3*, 13–22.
- Kaunas, R., Usami, S., & Chien, S. (2006). Regulation of stretch-induced JNK activation by stress fiber orientation. *Cell Signal*, *18*, 1924–31.
- Kaverina, I., Rottner, K., & Small, J. V. (1998). Targeting, capture, and stabilization of microtubules at early focal adhesions. *J Cell Biol*, *142*, 181–90.
- Kearney, E. M., Prendergast, P. J., & Campbell, V. A. (2008). Mechanisms of strain-mediated mesenchymal stem cell apoptosis. *J Biomech Eng*, *130*, 061004.
- Khayyeri, H., Barreto, S., & Lacroix, D. (2013). A computational investigation of the mechanisms behind cell mechanosensation. *Proceedings of the 19th annual conference of the section of Bioengineering of the Royal Academy of Medicine in Ireland, Dublin, 19th*.

- Kis, A., Kasas, S., Babić, B., Kulik, A., Benoît, W., Briggs, G., Schönenberger, C., Catsicas, S., & Forró, L. (2002). Nanomechanics of microtubules. *Phys Rev Lett.*, *89*, 1–4.
- Kollmannsberger, P., & Fabry, B. (2011). Linear and nonlinear rheology of living Cells. *Annual Rev Mater Research*, *41*, 75–97.
- Kollmannsberger, P., Mierke, C. T., & Fabry, B. (2011). Nonlinear viscoelasticity of adherent cells is controlled by cytoskeletal tension. *Soft Matter*, *7*, 3127.
- Kolodney, M. S., & Elson, E. L. (1995). Contraction due to microtubule disruption is associated with increased phosphorylation of myosin regulatory light chain. *Proc Natl Acad Sci U S A*, *92*, 10252–6.
- Kolodney, M. S., & Wysolmerski, R. B. (1992). Isometric contraction by fibroblasts and endothelial cells in tissue culture: a quantitative study. *J Cell Biol*, *117*, 73–82.
- Krishnan, R., Park, C. Y., Lin, Y.-C., Mead, J., Jaspers, R. T., Trepap, X., Lenormand, G., Tambe, D., Smolensky, A. V., Knoll, A. H., Butler, J. P., & Fredberg, J. J. (2009). Reinforcement versus fluidization in cytoskeletal mechanoresponsiveness. *PloS one*, *4*, e5486.
- Kroy, K., & Glaser, J. (2007). The glassy wormlike chain. *New J Phys*, *9*, 1–12.
- Kumar, S., Maxwell, I. Z., Heisterkamp, A., Polte, T. R., Lele, T. P., Salanga, M., Mazur, E., & Ingber, D. E. (2006). Viscoelastic retraction of single living stress fibers and its impact on cell shape, cytoskeletal organization, and extracellular matrix mechanics. *Biophys J*, *90*, 3762–73.

- Kurpinski, K., Chu, J., Hashi, C., & Li, S. (2006). Anisotropic mechanosensing by mesenchymal stem cells. *Proc Natl Acad Sci U S A*, *103*, 16095–100.
- Lacroix, D., & Prendergast, P. J. (2002). Three-dimensional simulation of fracture repair in the human tibia. *Comp Methods Biomech Biomedl Eng*, *5*, 369–376.
- Lam, W. A., Chaudhuri, O., Crow, A., Webster, K. D., Li, T.-D., Kita, A., Huang, J., & Fletcher, D. A. (2011). Mechanics and contraction dynamics of single platelets and implications for clot stiffening. *Nat Mater*, *10*, 61–6.
- Lang, T., Wacker, I., Wunderlich, I., Rohrbach, A., Giese, G., Soldati, T., & Almers, W. (2000). Role of actin cortex in the subplasmalemmal transport of secretory granules in PC-12 cells. *Biophys J*, *78*, 2863–77.
- Laurent, V. M., Planus, E., Fodil, R., & Isabey, D. (2003). Mechanical assessment by magnetocytometry of the cytosolic and cortical cytoskeletal compartments in adherent epithelial cells. *Biorheology*, *40*, 235–40.
- Lee, J., Leonard, M., Oliver, T., Ishihara, A., & Jacobson, K. (1994). Traction forces generated by locomoting keratocytes. *J Cell Biol*, *127*, 1957–64.
- Lenormand, G., Millet, E., Fabry, B., Butler, J. P., & Fredberg, J. J. (2004). Linearity and time-scale invariance of the creep function in living cells. *J R Soc Interface*, *22*, 91–7.
- Lim, C. T., Zhou, E. H., & Quek, S. T. (2006). Mechanical models for living cells—a review. *J Biomech*, *39*, 195–216.
- Mahaffy, R. E., Park, S., Gerde, E., Käs, J., & Shih, C. K. (2004). Quantitative analysis of the viscoelastic properties of thin regions of fibroblasts using atomic force microscopy. *Biophys J*, *86*, 1777–93.

- Mahaffy, R. E., Shih, C. K., MacKintosh, F. C., & Käs, J. (2000). Scanning probe-based frequency-dependent microrheology of polymer gels and biological cells. *Physic rev Lett*, *85*, 880–3.
- Malone, A. M., Anderson, C. T., Tummala, P., Kwon, R. Y., Johnston, T. R., Stearns, T., & Jacobs, C. R. (2007). Primary cilia mediate mechanosensing in bone cells by a calcium-independent mechanism. *Proc Natl Acad Sci U S A*, *104*, 061004.
- Mandadapu, K. K., Govindjee, S., & Mofrad, M. R. K. (2008). On the cytoskeleton and soft glassy rheology. *J Biomech*, *41*, 1467–78.
- Maniotis, A. J., Chen, C. S., & Ingber, D. E. (1997). Demonstration of mechanical connections between integrins, cytoskeletal filaments, and nucleoplasm that stabilize nuclear structure. *Proc Natl Acad Sci U S A*, *94*, 849–54.
- Mathur, A. B., Collinsworth, A. M., Reichert, W. M., Kraus, W. E., & Truskey, G. A. (2001). Endothelial, cardiac muscle and skeletal muscle exhibit different viscous and elastic properties as determined by atomic force microscopy. *J Biomech*, *34*, 1545–53.
- Mathur, A. B., Truskey, G. A., & Reichert, W. M. (2004). Atomic force and total internal reflection fluorescence microscopy for the study of force transmission in endothelial cells. *Biophys J*, *78*, 1725–35.
- Matthews, B. D., Overby, D. R., Mannix, R., & Ingber, D. E. (2006). Cellular adaptation to mechanical stress: role of integrins, Rho, cytoskeletal tension and mechanosensitive ion channels. *J Cell Sci*, *119*, 508–18.
- Maurin, B., Cañadas, P., Baudriller, H., Montcourrier, P., & Bettache, N.

- (2008). Mechanical model of cytoskeleton structuration during cell adhesion and spreading. *J Biomech*, *41*, 2036–41.
- McCreadie, B. R., & J, H. S. (1997). Strain concentrations surrounding an ellipsoid model of lacunae and osteocytes. *Comput Methods Biomech Biomed Engin*, *1*, 61–68.
- McGarry, J. G., Klein-Nulend, J., Mullender, M. G., & Prendergast, P. J. (2005a). A comparison of strain and fluid shear stress in stimulating bone cell responses—a computational and experimental study. *FASEB J*, *19*, 482–4.
- McGarry, J. G., & Prendergast, P. J. (2004). A three-dimensional finite element model of an adherent eukaryotic cell. *Eur Cell Mater*, *7*, 27–33.
- McGarry, J. P. (2009). Characterization of Cell Mechanical Properties by Computational Modeling of Parallel Plate Compression. *Ann Biomed Eng*, *37*, 2317–2325.
- McGarry, J. P., Fu, J., Yang, M. T., Chen, C. S., McMeeking, R. M., Evans, A. G., & Deshpande, V. S. (2009). Simulation of the contractile response of cells on an array of micro-posts. *Philos Trans A Math Phys Eng Sci*, *1902*, 3477–97.
- McGarry, J. P., Murphy, B. P., & McHugh, P. E. (2005b). Computational mechanics modelling of cell-substrate contact during cyclic substrate deformation. *J Mech Physics Solids*, *53*, 2597–2637.
- Mijailovich, S. M., Kojic, M., Zivkovic, M., Fabry, B., & J, F. J. (2002). A finite element model of cell deformation during magnetic bead twisting. *J Applied Physiol*, *93*, 1429–1436.

- Milner, J. S., Grol, M. W., Beaucage, K. L., Dixon, S. J., & Holdsworth, D. W. (2012). Finite element modeling of viscoelastic cells during high-frequency cyclic strain. *J Funct Biomater*, *3*, 209–224.
- Moeendarbary, E., Valon, L., Fritzsche, M., Harris, A. R., Moulding, D. A., Thrasher, A. J., Stride, E., Mahadevan, L., & Charras, G. T. (2013). The cytoplasm of living cells behaves as a poroelastic material. *Nat Mater*, *12*, 1–9.
- Mofrad, M. R. (2009). Rheology of the cytoskeleton. *Annual Rev Fluid Mech*, *41*, 433–453.
- Moreno-Flores, S., Benitez, R., dM Vivanco, M., & Toca-Herrera, J. L. (2010). Stress relaxation and creep on living cells with the atomic force microscope: a means to calculate elastic moduli and viscosities of cell components. *Nanotechnology*, *21*, 445101.
- Nagayama, K., & Matsumoto, T. (2008). Contribution of actin filaments and microtubules to quasi-in situ tensile properties and internal force balance of cultured smooth muscle cells on a substrate. *Am J Physiol Cell Physiol*, *295*, C1569–78.
- Nawaz, S., Sánchez, P., Bodensiek, K., Li, S., Simons, M., & Schaap, I. A. T. (2012). Cell visco-elasticity measured with AFM and optical trapping at sub-micrometer deformations. *PLoS ONE*, *7*, e45297.
- Nguyen, B. V., Wang, Q. G., Kuiper, N. J., ElHaj, A. J., Thomas, C. R., & Zhang, Z. (2010). Biomechanical properties of single chondrocytes and chondrons determined by micromanipulation and finite-element modelling. *J R Soc Interface*, *7*, 1723–33.

- Oberleithner, H., Callies, C., Kusche-Vihrog, K., Schillers, H., Shahin, V., Riethmüller, C., Macgregor, G. A., & de Wardener, H. E. (2009). Potassium softens vascular endothelium and increases nitric oxide release. *Proc Natl Acad Sci U S A*, *106*, 2829–34.
- Ofek, G., Natoli, R. M., & Athanasiou, K. A. (2009). In situ mechanical properties of the chondrocyte cytoplasm and nucleus. *J Biomech*, *42*, 873–7.
- Ohayon, J., & Tracqui, P. (2005). Computation of adherent cell elasticity for critical cell-bead geometry in magnetic twisting experiments. *Ann Biomed Eng*, *33*, 131–141.
- Or-Tzadikario, S., & Gefen, A. (2011). Confocal-based cell-specific finite element modeling extended to study variable cell shapes and intracellular structures: The example of the adipocyte. *J Biomech*, *44*, 567–73.
- Overby, D. R., Matthews, B. D., Alsberg, E., & Ingber, D. E. (2005). Novel dynamic rheological behavior of individual focal adhesions measured within single cells using electromagnetic pulling cytometry. *Acta biomater*, *1*, 295–303.
- Pajerowski, J. D., Dahl, K. N., Zhong, F. L., Sammak, P. J., & Discher, D. E. (2007). Physical plasticity of the nucleus in stem cell differentiation. *Proc Natl Acad Sci U S A*, *40*, 15619–24.
- Pampaloni, F., & Florin, E. L. (2008). Microtubule architecture: inspiration for novel carbon nanotube-based biomimetic materials. *Trends Biotechnol*, *26*, 302–10.
- Peeters, E. A., Bouten, C. V., Oomens, C. W., Bader, D. L., Snoeckx, L. H.,

- & Baaijens, F. P. (2004). Anisotropic, three-dimensional deformation of single attached cells under compression. *Ann Biomed Eng.*, *32*, 1443–52.
- Peeters, E. A., Oomens, C. W., Bouten, C. V., Bader, D. L., & Baaijens, F. P. (2005). Viscoelastic properties of single attached cells under compression. *J Biomech Eng.*, *127*, 237–43.
- Pelham, R. J., & Wang, Y. L. (1999). High resolution detection of mechanical forces exerted by locomoting fibroblasts on the substrate. *Mol Biol Cell*, *10*, 935–45.
- Pelling, A. E., Dawson, D. W., Carreon, D. M., Christiansen, J. J., Shen, R. R., Teitell, M. A., & Gimzewski, J. K. (2007). Distinct contributions of microtubule subtypes to cell membrane shape and stability. *Nanomedicine*, *3*, 43–52.
- Picart, C., Dalhaimer, P., & Discher, D. E. (2000). Actin protofilament orientation in deformation of the erythrocyte membrane skeleton. *Biophys J*, *79*, 2987–3000.
- Pourati, J., Maniotis, A., Spiegel, D., Schaffer, J. L., Butler, J. P., Fredberg, J. J., Ingber, D. E., Stamenovic, D., & Wang, N. (1998). Is cytoskeletal tension a major determinant of cell deformability in adherent endothelial cells? *Am J Physiol*, *274*, C1283–9.
- Prendergast, P. J. (2007). Computational modelling of cell and tissue mechanoresponsiveness. *Gravit Space Biol*, (pp. 43–50).
- Pullarkat, P., Fernandez, P., & Ott, A. (2007). Rheological properties of the eukaryotic cell cytoskeleton. *Phys Reports*, *449*, 29–53.

- Radmacher, M. (1997). Measuring the elastic properties of biological samples with the AFM. *IEEE Eng Med Biol Mag*, *2*, 47–57.
- Ramaekers, F. C. S., & Bosman, F. T. (2004). The cytoskeleton and disease. *The Journal of pathology*, *204*, 351–4.
- Rehfeldt, F., & Discher, D. E. (2007). Cell dipoles feel their way Quantum to classical and back. *Nature Phys*, *3*, 592–593.
- Ronan, W., Deshpande, V. S., McMeeking, R. M., & McGarry, J. P. (2012). Numerical investigation of the active role of the actin cytoskeleton in the compression resistance of cells. *J Mech Behav Biomed Mater.*, *14*, 1143–57.
- Rosenblatt, N., Alencar, A., Majumdar, A., Suki, B., & Stamenović, D. (2006). Dynamics of prestressed semiflexible polymer chains as a model of cell rheology. *Physic Rev Letters*, *97*, 168101.
- Rosenbluth, M. J., Crow, A., Shaevitz, J. W., & Fletcher, D. A. (2008a). Slow stress propagation in adherent cells. *Biophys J*, *95*, 6052–9.
- Rosenbluth, M. J., Lam, W. A., & Fletcher, D. A. (2006). Force microscopy of nonadherent cells: a comparison of leukemia cell deformability. *Biophys J*, *90*, 2994–3003.
- Rosenbluth, M. J., Lam, W. A., & Fletcher, D. A. (2008b). Analyzing cell mechanics in hematologic diseases with microfluidic biophysical flow cytometry. *Lab Chip*, *8*, 1062–70.
- Rotsch, C., Jacobson, K., & Radmacher, M. (1999). Dimensional and mechanical dynamics of active and stable edges in motile fibroblasts investigated by using atomic force microscopy. *Proc Natl Acad Sci USA*, *96*, 921–6.

- Rotsch, C., & Radmacher, M. (2000). Drug-induced changes of cytoskeletal structure and mechanics in fibroblasts: an atomic force microscopy study. *Biophys J*, *78*, 520–35.
- Satcher, R. L., & Dewey, C. F. (1996). Theoretical estimates of mechanical properties of the endothelial cell cytoskeleton. *Biophys J*, *71*, 109–18.
- Schaap, I. A. T., Carrasco, C., de Pablo, P. J., MacKintosh, F. C., & Schmidt, C. F. (2006). Elastic response, buckling, and instability of microtubules under radial indentation. *Biophys J*, *91*, 1521–31.
- Schwarz, U. S., Balaban, N. Q., Rivelino, D., Bershadsky, A., Geiger, B., & Safran, S. A. (2002). Calculation of forces at focal adhesions from elastic substrate data: the effect of localized force and the need for regularization. *Biophys J*, *83*, 1380–94.
- Seifriz, W. (1937). Methods of research on the physical properties of the protoplasm. *Plan Physiol*, *12*, 99–116.
- Shafir, Y., & Forgacs, G. (2002). Mechanotransduction through the cytoskeleton. *Am J Physiol Cell Physiol*, *282*, C479–86.
- Simon, A., Cohen-Bouhacina, T., PortÓ, M. C., AimÓ, J. P., AmÓdÓe, J., Bareille, R., & Baquey, C. (2003). Characterization of dynamic cellular adhesion of osteoblasts using atomic force microscopy. *Cytometry A*, *54*, 36–47.
- Sims, J. R., Karp, S., & Ingber, D. E. (1992). Altering the cellular mechanical force balance results in integrated changes in cell, cytoskeletal and nuclear shape. *J Cell Sci*, *103 ( Pt 4)*, 1215–22.

- Slomka, N., & Gefen, A. (2010). Confocal microscopy-based three-dimensional cell-specific modeling for large deformation analyses in cellular mechanics. *J Biomech*, *43*, 1806–16.
- Slomka, N., Oomens, C. W. J., & Gefen, A. (2011). Evaluating the effective shear modulus of the cytoplasm in cultured myoblasts subjected to compression using an inverse finite element method. *J Mech Behav Biomed Mater*, *4*, 1559–66.
- Smith, B. A., Tolloczko, B., Martin, J. G., & Grütter, P. (2005). Probing the viscoelastic behavior of cultured airway smooth muscle cells with atomic force microscopy: stiffening induced by contractile agonist. *Biophys J*, *88*, 2994–3007.
- Sniadecki, N. J., Anguelouch, A., Yang, M. T., Lamb, C. M., Liu, Z., Kirschner, S. B., Liu, Y., Reich, D. H., & Chen, C. S. (2007). Magnetic microposts as an approach to apply forces to living cells. *Proc Natl Acad Sci USA*, *104*, 14553–8.
- Sniadecki, N. J., Desai, R. A., Ruiz, S. A., & Chen, C. S. (2006). Nanotechnology for cell-substrate interactions. *Ann Biomed Eng*, *34*, 59–74.
- Sollich, P. (1998). Rheological constitutive equation for a model of soft glassy materials. *Phys Rev E*, *58*, 738–759.
- Sollich, P., Lequeux, F., Hébraud, P., & Cates, M. (1997). Rheology of soft glassy materials. *Phys Rev Lett*, *78*, 2020.
- Stamenović, D. (2006). Two regimes, maybe three. *Nature Mater*, *5*, 597–598.

- Stamenović, D., & Coughlin, M. F. (1999). The role of prestress and architecture of the cytoskeleton and deformability of cytoskeletal filaments in mechanics of adherent cells: a quantitative analysis. *J Theor Biol*, *201*, 63–74.
- Stamenović, D., Fredberg, J. J., Wang, N., Butler, J. P., & Ingber, D. E. (1996). A microstructural approach to cytoskeletal mechanics based on tensegrity. *J Theor Biol*, *181*, 125–36.
- Stamenović, D., & Ingber, D. E. (2009). Tensegrity-guided self assembly: from molecules to living cells. *Soft Matter*, *5*, 1137.
- Stamenović, D., Mijailovich, S. M., Tolić-Nørrelykke, I. M., Chen, J., & Wang, N. (2002). Cell prestress. II. Contribution of microtubules. *Am J Physiol Cell Physiol*, *282*, C617–24.
- Stamenović, D., Rosenblatt, N., Montoya-Zavala, M., Matthews, B. D., Hu, S., Suki, B., Wang, N., & Ingber, D. E. (2007). Rheological behavior of living cells is timescale-dependent. *Biophys J*, *93*, L39–41.
- Stamenovic, D., Suki, B., Fabry, B., Wang, N., & Fredberg, J. J. (2004). Rheology of airway smooth muscle cells is associated with cytoskeletal contractile stress. *J Appl Physiol*, *96*, 1600–5.
- Stops, A. J. F., McMahon, L. A., O’Mahoney, D., Prendergast, P. J., & McHugh, P. E. (2008). A finite element prediction of strain on cells in a highly porous collagen-glycosaminoglycan scaffold. *J Biomech Eng*, *130*, 061001.
- Stricker, J., Falzone, T., & Gardel, M. L. (2010). Mechanics of the F-actin cytoskeleton. *Journal of biomechanics*, *43*, 9–14.

- Sunyer, R. (2008). *Contribution of active processes to the cytoskeleton dynamics of living cells.* Ph.D. thesis Facultat de Medicina, Universitat de Barcelona.
- Suresh, S. (2007). Biomechanics and biophysics of cancer cells. *Acta Biomater*, *3*, 413–438.
- Takai, E., Costa, K. D., Shaheen, A., Hung, C. T., & Guo, X. E. (2005). Osteoblast elastic modulus measured by atomic force microscopy is substrate dependent. *Ann Biomed Eng*, *33*, 963–971.
- Tan, J. L., Tien, J., Pirone, D. M., Gray, D. S., Bhadriraju, K., & Chen, C. S. (2003). Cells lying on a bed of microneedles: an approach to isolate mechanical force. *Proc Natl Acad Sci U S A*, *100*, 1484–9.
- Tapley, E. C., & Starr, D. A. (2013). Connecting the nucleus to the cytoskeleton by SUN-KASH bridges across the nuclear envelope. *Curr Opin Cell Biol*, *25*, 57–62.
- Thompson, D. A. W. (1917). On the growth and form. *Cambridge University Press, 1st edn*, Cambridge, England.
- Trepat, X., Deng, L., An, S. S., Navajas, D., Tschumperlin, D. J., Gerthoffer, W. T., Butler, J. P., & Fredberg, J. J. (2007). Universal physical responses to stretch in the living cell. *Nature*, *447*, 592–5.
- Trepat, X., Grabulosa, M., Puig, F., Maksym, G. N., Navajas, D., & Farré, R. (2004). Viscoelasticity of human alveolar epithelial cells subjected to stretch. *Am J Physiol Lung Cell Mol Physiol*, *287*, L1025–34.
- Trepat, X., Lenormand, G., & Fredberg, J. J. (2008). Universality in cell mechanics. *Soft Matter*, *4*, 1750.

- Trichet, L., Le Digabel, J., Hawkins, R. J., Vedula, S. R. K., Gupta, M., Ribault, C., Hersen, P., Voituriez, R., & Ladoux, B. (2012). Evidence of a large-scale mechanosensing mechanism for cellular adaptation to substrate stiffness. *Proc Natl Acad Sci U S A*, *109*, 6933–8.
- Tsai, M. A., Frank, R. S., & Waugh, R. E. (1993). Passive mechanical behavior of human neutrophils: power-law fluid. *Biophys J*, *65*, 2078–88.
- Tse, T. (2012). *The study of mechanical properties of cells as a biomarker for cancer diagnostics..* Ph.D. thesis University of California, Los Angeles.
- Ujihara, Y., Nakamura, M., Miyazaki, H., & Wada, S. (2010). Proposed spring network cell model based on a minimum energy concept. *Ann Biomed Eng*, *38*, 1530–8.
- Unnikrishnan, G. U., Unnikrishnan, V. U., & Reddy, J. N. (2007). Constitutive material modeling of cell: a micromechanics approach. *J Biomech Eng*, *129*, 315–23.
- van Citters, K. M., Hoffman, B. D., Massiera, G., & Crocker, J. C. (2006). The role of F-actin and myosin in epithelial cell rheology. *Biophys J*, *91*, 3946–56.
- Vasquez, R. J., Howell, B., Yvon, A. M., Wadsworth, P., & Cassimeris, L. (1997). Nanomolar concentrations of nocodazole alter microtubule dynamic instability in vivo and in vitro. *Molecular biology of the cell*, *8*, 973–85.
- Vaziri, A., & Gopinath, A. (2008). Cell and biomolecular mechanics in silico. *Nature Mater*, *7*, 15–23.

- Vaziri, A., Xue, Z., Kamm, R. D., & Kaazempur Mofrad, M. R. (2007). A computational study on power-law rheology of soft glassy materials with application to cell mechanics. *Computer Meth App Mech Eng*, *196*, 2965–2971.
- Vereney, F. J., & Farsad, M. (2011). A constrained mixture approach to mechano-sensing and force generation in contractile cells. *J Mech Behav Biomed Mater.*, *4*, 1683–99.
- Viens, D., & Brodland, G. W. (2007). A three-dimensional finite element model for the mechanics of cell-cell interactions. *J Biomech Eng*, *129*, 651–7.
- Wang, J. H., Goldschmidt-Clermont, P., Wille, J., & Yin, F. C. (2001a). Specificity of endothelial cell reorientation in response to cyclic mechanical stretching. *J Biomech*, *34*, 1563–72.
- Wang, N. (1998). Mechanical interactions among cytoskeletal filaments. *Hypertension*, *32*, 162–5.
- Wang, N., & Ingber, D. E. (1994). Control of cytoskeletal mechanics by extracellular matrix, cell shape, and mechanical tension. *Biophys J*, *66*, 2181–2189.
- Wang, N., Naruse, K., Stamenović, D., Fredberg, J. J., Mijailovich, S. M., Tolić-Nørrelykke, I. M., Polte, T., Mannix, R., & Ingber, D. E. (2001b). Mechanical behavior in living cells consistent with the tensegrity model. *Proc Natl Acad Sci U S A*, *98*, 7765–70.
- Wang, N., & Stamenović, D. (2000). Contribution of intermediate filaments to cell stiffness, stiffening, and growth. *Am J Physiol Cell Physiol*, *279*, C188–94.

- Wang, N., & Suo, Z. (2005). Long-distance propagation of forces in a cell. *Biochem Biophys Res Commun*, *328*, 1133–8.
- Wang, N., Tolić-Nørrelykke, I. M., Chen, J., Mijailovich, S. M., Butler, J. P., Fredberg, J. J., & Stamenović, D. (2002). Cell prestress. I. Stiffness and prestress are closely associated in adherent contractile cells. *Am J Physiol Cell Physiol*, *282*, C606–16.
- Wang, N., Tytell, J. D., & Ingber, D. E. (2009). Mechanotransduction at a distance: mechanically coupling the extracellular matrix with the nucleus. *Nat Rev Mol Cell Biol*, *10*, 75–82.
- Wasserman, S. M., Mehraban, F., Komuves, L. G., Yang, R.-B., Tomlinson, J. E., Zhang, Y., Spriggs, F., & Topper, J. N. (2002). Gene expression profile of human endothelial cells exposed to sustained fluid shear stress. *Physiol Genomics*, *12*, 13–23.
- Weaver, P., Ronan, W., Jarvis, S. P., & McGarry, J. P. (2013). Experimental and computational investigation of the role of stress fiber contractility in the resistance of osteoblasts to compression. *Bull Math Biol*, *75*, 1284–303.
- Webster, K. D., Crow, A., & Fletcher, D. A. (2011). An AFM-based stiffness clamp for dynamic control of rigidity. *PLoS one*, *6*, e17807.
- Wolff, L., Kroy, K., & Fernandez, P. (2012). Resolving the Stiffening-Softening Paradox in Cell Mechanics. *PLoS one*, *7*, e40063.
- Wood, S. T., Dean, B. C., & Dean, D. (2012). A computational approach to understand phenotypic structure and constitutive mechanics relationships of single cells. *Ann Biome Eng*, *41*, 630–40.

- Wu, H. W., Kuhn, T., & Moy, V. T. (1998). Mechanical properties of L929 cells measured by atomic force microscopy: effects of anticytoskeletal drugs and membrane crosslinking. *Scanning*, *20*, 389–97.
- Xu, W., Mezencev, R., Kim, B., Wang, L., McDonald, J., & Sulchek, T. (2012). Cell stiffness is a biomarker of the metastatic potential of ovarian cancer cells. *PloS one*, *7*, e46609.
- Yeung, A., & Evans, E. (1989). Cortical shell-liquid core model for passive flow of liquid-like spherical cells into micropipets. *Biophys J*, *56*, 139–49.
- Yu, H., Mouw, J. K., & Weaver, V. M. (2011). Forcing form and function: biomechanical regulation of tumor evolution. *Trends Cell Biol.*, *21*, 47–56.
- Zemel, A., & Safran, S. (2007). Active self-polarization of contractile cells in asymmetrically shaped domains. *Phys Rev E Stat Nonlin Soft Matter Phys*, *76*, 021905.
- Zhou, E. H., Xu, F., Quek, S. T., & Lim, C. T. (2012). A power-law rheology-based finite element model for single cell deformation. *Biomech Model Mechanobiol*, *11*, 1075–84.
- Zhu, C., Bao, G., & Wang, N. (2000). Mechanical response, cell adhesion, and molecular deformation. *Annu. Rev. Biomed. Eng.* (pp. 189–226).

SUBROUTINE TO CALCULATE PRESTRESS

---

---

This appendix is the subroutine that was used in Abaqus (Simulia, USA) to implement prestress in the actin bundles through the modification of the Abaqus subroutine UMAT

```

*USER SUBROUTINES
SUBROUTINE UMAT(STRESS,STATEV,DDSDDE,SSE,SPD,SCD,
1 RPL,DDSDDT,DRPLDE,DRPLDT,
2 STRAN,DSTRAN,TIME,DTIME,TEMP,DTEMP,PREDEF,DPRED,CMNAME,
3 NDI,NSHR,NTENS,NSTATEV,PROPS,NPROPS,COORDS,DROT,PNEWDT,
4 CELENT,DFGRD0,DFGRD1,NOEL,NPT,LAYER,KSPT,KSTEP,KINC)

INCLUDE 'ABA_PARAM.INC'

CHARACTER*8 CMNAME
DIMENSION STRESS(NTENS),STATEV(NSTATEV),
1 DDSDDE(NTENS,NTENS),DDSDDT(NTENS),DRPLDE(NTENS),
2 STRAN(NTENS),DSTRAN(NTENS),TIME(2),PREDEF(1),DPRED(1),
3 PROPS(NPROPS),COORDS(3),DROT(3,3),DFGRD0(3,3),DFGRD1(3,3)

PARAMETER (ZERO=0.0D0, ONE=1.0D0, TWO=2.0D0)
E=PROPS(1)
ANU=PROPS(2)
ALAMDA=ANU*E/(ONE+ANU)/(ONE-TWO*ANU)
AMU=E/TWO/(ONE+ANU)
DO I=1,NTENS
DO J=1,NTENS
DDSDDE(I,J)=0.0D0
ENDDO
ENDDO
DDSDDE(1,1)=ALAMDA+TWO*AMU
DDSDDE(2,2)=DDSDDE(1,1)
DDSDDE(3,3)=DDSDDE(1,1)
DDSDDE(4,4)=AMU
DDSDDE(5,5)=AMU
DDSDDE(6,6)=AMU
DDSDDE(1,2)=ALAMDA
DDSDDE(1,3)=ALAMDA
DDSDDE(2,3)=ALAMDA
DDSDDE(2,1)=DDSDDE(1,2)
DDSDDE(3,1)=DDSDDE(1,3)
DDSDDE(3,2)=DDSDDE(2,3)

IF (KSTEP.EQ.1.AND.KINC.EQ.1) THEN
DO I=1,NTENS
STRESS(I)=0.082
ENDDO
END IF
TOMAS=STRAN(1)+DSTRAN(1)
IF (TOMAS.LE.-0.24) THEN
DO J=1,NTENS
STRESS(J)=0
ENDDO
ELSE
DO I=1,NTENS
DO J=1,NTENS
STRESS(I)=STRESS(I)+DDSDDE(I,J)*DSTRAN(J)
ENDDO
ENDDO
ENDIF
RETURN
END
=====

```

SUBROUTINE TO CALCULATE MAJOR PRINCIPAL  
STRAINS

---

---

This appendix is the subroutine that was used in Abaqus (Simulia, USA) calculate the major principal strains in the different elements of the model, and to plot this new variable in the visualisation output of the software, through the use of the subroutine UVARM

```
*USER SUBROUTINES
SUBROUTINE UVARM(UVAR,DIRECT,T,TIME,DTIME,CMNAME,ORNAME,
1 NUVARM,NOEL,NPT,LAYER,KSPT,KSTEP,KINC,NDI,NSHR,COORD,
2 JMAC,JMATYP,MATLAYO,LACCFLA)
```

```
INCLUDE 'ABA_PARAM.INC'
```

```
integer nf,ip,i,iuvar
```

```
CHARACTER*80 CMNAME,ORNAME
CHARACTER*3 FLGRAY(15)
DIMENSION UVAR(NUVARM),DIRECT(3,3),T(3,3),TIME(2)
DIMENSION ARRAY(15),JARRAY(15),JMAC(*),JMATYP(*),COORD(*)
DIMENSION elogstr(3)
```

```
c -----
c  Subroutine to define user output variables
c
c  UVARM2    Deviatoric octahedral strain [-]
c  elogstr   Principal Green strains [-]
c  fv       Fluid velocity [mm.s-1]
c  ss       Deviatoric octahedral strain [-]
c -----
```

```
REAL*8 major
```

```
CALL GETVRM ('EP',ARRAY,JARRAY,FLGRAY,JRCD
1,JMAC,JMATYP,MATLAYO,LACCFLA)
```

```
EP1=ARRAY(1)
EP3=ARRAY(3)
  if (ABS(EP1).GE.ABS(EP3)) then
    major=EP1
  else
    major=EP3
  end if
```

```
UVAR(1)=major
```

```
RETURN
END
```

---